INTERNAL MODES IN

HIGH TEMPERATURE PLASMAS

by

GEOFFREY BENNETT CREW

A.B.   Dartmouth College
(1978)

Submitted to the Department of
Physics
in Partial Fulfillment of the
Requirements of the
Degree of

DOCTOR OF PHILOSOPHY

at the

MASSACHUSETTS INSTITUTE OF TECHNOLOGY

February 1983

© Massachusetts Institute of Technology, 1983

Signature of Author_____
Department of Physics
January 7, 1983

Certified by_____
Prof. Bruno Coppi
Thesis Supervisor

Accepted by_____
Prof. George F. Koster
Chairman, Physics Department Graduate Committee

Archives

MASSACHUSETTS INSTITUTE
OF TECHNOLOGY

MAR 24 1983

LIBRARIES

INTERNAL MODES IN

HIGH TEMPERATURE PLASMAS

by

GEOFFREY BENNETT CREW

Submitted to the Department of Physics
on January 7, 1983 in partial fulfillment of the
requirements for the Degree of Doctor of Philosophy in
Physics

ABSTRACT

The linear stability of current-carrying toroidal plamsas is
examined to determine the possibility of exciting global
internal modes. The ideal magnetohydrodynamic (MHD) theory
provides a useful framework for the analysis of these modes,
which involve a kinking of the central portion of the plasma
column. Non-ideal effects can also be important, and these
are treated for high temperature regimes where the plasma is
collisionless.

The ideal MHD analysis assumes an equilibrium plasma confine-
ment configuration in which the nested magnetic flux surfaces
are circular in cross section. In the limit of a large aspect
ratio torus, this is an exact solution for the hydromagnetic
force balance in low-beta regimes, where the poloidal beta is
of order unity, and a reasonable model in finite-beta regimes,
where the poloidal beta is on the order of the aspect ratio.
Poloidal beta refers to the ratio of the plasma pressure to
the energy density of the magnetic field generated by the
toroidal current. The ideal MHD energy principle is applied
to study the stability of these internal kink modes, whose
dependence on the poloidal angle is dominated by an $m=1$
harmonic. In particular, the analysis demonstrates that
these modes, which may be excited above a low-beta threshold,
are stable above a second threshold at finite beta.

Non-ideal effects are then considered within a narrow layer
about the mode resonant surface. The plasma response, deter-
mined from a collisionless kinetic calculation, includes
finite electron conductivity and the non-adiabatic ion response.
Since the layer width is assumed on the order of the ion gyro-
radius, the mode structure is given by an integro-differential
system of equations. In the MHD stable region, this system is
solved in a low-beta limit to yield an unstable reconnecting
mode. Numerical evaluation of the stability criteria shows
that this mode stabilizes with increasing temperature gradient
or decreasing magnetic shear. This mode transforms into a
collisionless modification of the ideal internal kink mode

which at low beta has a positive growth rate where the ideal
MHD theory predicts stability. However, an approximate solu-
tion, valid for arbitrary beta, indicates that stability is
restored for plasmas above a finite-beta threshold. Finally,
for plasmas well within the MHD instability region, the
collisionless effects are negligible, and the results of the
ideal analysis are recovered.

Thesis Supervisor: Dr. Bruno Coppi

          Title: Professor of Physics

to Harriet Schwartz Crew

ACKNOWLEDGEMENTS

TABLE OF CONTENTS

LIST OF FIGURES

CHAPTER 1

Introduction

In this thesis we examine the linear stability of high temperature plasmas against the onset of a certain class of internal modes. By "internal" we refer to those instabilities which do not induce appreciable displacements at the plasma surface. In fact these instabilities may exist even though the surface of the plasma is held fixed, which may be physically accomplished with a conducting wall. Our analysis assumes a toroidal plasma configuration typical of many current tokamak experiments, although we consider a temperature regime which is hopefully characteristic of the next generation of experiments. Nevertheless, some of the effects we discuss are common to other plasma configurations both in the laboratory and in nature.

It is well known[1] that with one important exception, internal modes in tokamaks tend to be localized near a mode resonant surface. The exception, which is the principal subject of this thesis, is the internal kink mode. This mode is nonlocal in nature and may be excited if the value of q, the inverse rotational transform, falls below unity at the magnetic axis. An understanding of the internal kink mode is important, especially in finite-beta regimes, because it is hoped that thermonuclear plasma confinement devices will operate with low values of q.

Our approach to the internal kink begins within the framework of the ideal magnetohydrodynamic (MHD) theory. For reference, we recall the familiar equations

$$\frac{\partial \rho}{\partial t} + \underline{\nabla} \cdot (\rho \underline{v}) = 0 \tag{1.1}$$

$$(\frac{\partial}{\partial t} + \underline{v} \cdot \underline{\nabla}) (p\rho^{-\Gamma}) = 0 \tag{1.2}$$

$$\rho(\frac{\partial}{\partial t} + \underline{v} \cdot \underline{\nabla}) v = - \underline{\nabla}p + \frac{1}{c} \underline{J} \times \underline{B} \tag{1.3}$$

$$\underline{E} + \frac{1}{c} \underline{v} \times \underline{B} = 0 \tag{1.4}$$

$$\underline{\nabla} \times \underline{B} = \frac{4\pi}{c} \underline{J} \tag{1.5}$$

$$\underline{\nabla} \times \underline{E} + \frac{1}{c} \frac{\partial \underline{B}}{\partial t} = 0 \ , \tag{1.6}$$

which describe the plasma mass density ρ, velocity $\underline{v}$, pressure p, current $\underline{J}$, in relation to the electromagnetic fields $\underline{E}$ and $\underline{B}$. The first two equations are fluid equations, where Γ is the ratio of specific heats, and the last two are Ampère's and Faraday's laws, with c equal to the speed of light. The remaining two equations couple the plasma to the field through force balance and the so-called "frozen-in law."

For the limiting case of a large aspect ratio torus, it is convenient to approximate a torus with major radius

R by a straight cylinder of length $2\pi R$ having periodic boundary conditions. Since the equilibrium is independent of the poloidal angle and the longitudinal (toroidal) coordinate, the plasma perturbations can then be analayzed in terms of uncoupled m and n modes, where m is the poloidal wave number and n is the longitudinal (toroidal) wave number. Then the internal kinks are the $m = 1$ modes, distinguished by differing values of n. An internal kink is known[2] to be unstable whenever its mode rational surface lies within the plasma. The instability can be roughly visualized as a rigid helical displacement of the plasma within this surface, that is, plasma with radius less than r_1, where $q(r_1) = m/n$. This instability is driven by both the plasma current density and pressure gradients. We can form a simple physical picture of this instability[3] by considering a current I flowing in a wire aligned with a homogeneous magnetic field B. Then if the wire is given a helical perturbation with the proper helicity (right- or left-handed depending on whether the current and field are parallel or antiparallel), the $I \times B$ force acts to reinforce the displacement, and the perturbation grows.

In the case of toroidal plasma, the analysis is more involved. In the first place, the two-dimensional equilibrium equation is more difficult to solve. Then, due to the fact that the equilibrium configuration depends on the poloidal variable, a decomposition of the perturbation into independent

m modes is no longer possible. In other words, different m harmonics are now coupled. The internal kink has now primarily an $m = 1$ component with an admixture of other m harmonics. The toroidal angle remains ignorable, and we may continue to identify different n modes. Analytic progress on the stability properties of this mode can be made using asymptotic methods for large aspect ratio tori. This will be the approach we follow in this thesis.

For large aspect ratio, low-beta tokamaks, i.e. $\varepsilon \ll 1$, $\beta_p \sim 1$, a tractable equilibrium solution is available[4,5] in terms of an expansion in powers of ε. Here ε is the inverse aspect ratio and β_p is the ratio of the plasma pressure to the poloidal magnetic pressure. In this solution, the magnetic flux surfaces are essentially circular in cross section, while their centers are slightly shifted away from the magnetic axis on the equatorial plane of the torus. An analytic stability criterion against internal kink modes in these low-beta configurations has been derived[6] by expanding the ideal MHD energy functional, retaining consistently terms to order $\varepsilon^2 \sim (\varepsilon\beta_p)^2$. This theory shows that modes with $n \geq 2$ behave essentially as in the cylindrical case, that is, they are always unstable when their mode resonant surface is within the plasma. On the other hand, the behavior of the $n = 1$ mode is significantly altered by the toroidal effects. For usual q profiles that fall below unity within the plasma, this mode is found to be stable at sufficiently low β_p but it becomes unstable as β_p exceeds some threshold

value. Its growth rate in the unstable regime increases parabolically with β_p. This behavior has also been observed numerically[7,8].

We note that in its unstable regime the internal kink becomes mostly driven by the pressure gradient, as is the case for ballooning modes. The latter modes have been shown to have a "second stability region" at still higher beta, due to the crowding of the magnetic surfaces at the outer side of the torus.[9] We should expect a similar stabilization also to occur for the internal kinks. An attempt to incorporate higher beta effects into the internal kink stability criterion was made[10] by considering the limit of small current density gradients and retaining some terms of order $(\epsilon\beta_p)^4$ under the assumptions $\epsilon\beta_p \ll 1$ but $\beta_p \gg 1$. The ensuing correction turned out to be stabilizing as opposed to the standard destabilizing contribution of order $(\epsilon\beta_p)^2$.

In order to investigate the stability properties of internal kinks in the $\epsilon\beta_p \sim 1$ regime, we have developed a method which still assumes a large aspect ratio but does not involve expansions in powers of $\epsilon\beta_p$. For this approach we have adopted an equilibrium model that retains the strong outward shift of the magnetic axis characteristic of high-beta flux-conserving configurations, while neglecting effects due to the deformation of the shape of the magnetic surfaces. Using this model equilibrium we have been able to prove[11] that at sufficiently high $\epsilon\beta_p$, the internal kink instability is suppressed, independent of the toroidal mode number n.

This "second stability region" has recently been observed for finite aspect ratio numerical equlibria using the ERATO code.[12]

Having identified these two regions of stability, we must now ask if additional, non-ideal effects can further destabilize the plasma. For example, with the introduction of the slightest amount of resistivity η, Eq. (1.4) must be modified. The new equation

$$\underline{E} + \frac{1}{c} \underline{v} \times \underline{B} = \eta \underline{J} \, , \tag{1.7}$$

allows the plasma motion to decouple from that of the magnetic field lines. The original theories[13,14] considered a collisional resistivity and found a new set of modes, the tearing modes. Characteristic of these modes is the existence of a reconnection layer in which the field lines are broken and rejoined in a new topology by the mode. In collisional regimes of current experiments, modes of this type can produce the so-called sawtooth oscillations of the soft X-ray emissions. These oscillations are due to a thermal instability of the central plasma column held in check by the excitation of reconnecting modes which redistribute the thermal energy of the center of the plasma towards the surface.

At higher temperatures, however, collisional resistivity is no longer the most important non-ideal effect, and the analysis of these modes must be modified. Kinetic theories

in which finite electron inertia is responsible for the de-
coupling of plasma and field lines have been formulated[14-16].
However, these treatments considered only the limit where
the spatial variations of the reconnection layer occured on
scale lengths greater than the ion gyro-radius. This resulted
in the use of two second order differential equations to des-
cribe the mode structure. It was observed[16] that under real-
istic conditions (comparable electron and ion temperatures,
and an electron temperature gradient at least as steep as
the density gradient) this limit was invalid. This led to
the reformulation of the problem in terms of an integral
equation[17], which was valid to all orders of the ion gyro-
radius.

Some of these effects have been incorporated into the
analysis of m=1 modes[18-21]. The analysis of this case differs
from those with m>1 (the standard assumption for tearing modes)
since a) the boundary conditions on the layer are different,
and b) the ideal internal kink mode exists in the absence of
these effects. The main consequence of the first point is
that the conventional stability parameter of tearing modes, Δ'
(studied in Ref. 22 for the cylindrical case) is replaced by
a quantity λ_H which may be identified from our MHD results.
The second point implies that non-ideal effects modify the
existing internal kink (when destabilized) rather than intro-
duce a new mode. The first treatment of the resistive case[18]
was extended[19] with a moment equation approach to include a
full set of non-ideal effects, including finite electrical
resistivity, ion gyro-radius, electron drift wave frequency

and ion-ion collisions. The problem has also been examined in low-beta, arbitrary collisionality regimes[20], and discussed for finite-beta in the collisionless regime[21].

We shall investigate the behavior of these modes in collisionless, finite ion gyro-radius regimes where the use of the integral equation is indicated. In the low-beta, ideal internal kink stable regime, the solution[23] of the integral formulation of the reconnecting mode is in fact applicable to the m=1 case. For the finite-beta regime, however, we must adopt a model equation for the description of the mode. Then we can show that the mode stabilizes above a finite-beta threshold.

This thesis is organized in the following manner. In Chapter 2, we review the ideal MHD theory[6,24] that applies to the low-beta ($\varepsilon\beta_p<<1$) regime. This is appropriate since the same techniques will be applied in Chapter 3 for the discussion of the finite-beta case. Our approach resembles that of Ref. 24, however we use the coordinate system of Ref. 5. The analysis of the ideal internal kink modes in finite-beta ($\varepsilon\beta_p\sim1$) regimes is presented in Chapter 3. Here we introduce the finite-beta equilibrium model and demonstrate in several ways the stabilization of the modes at sufficiently high beta. The asymptotic matching that exists between these two regimes is presented in Chapter 4. There we present the complete picture of the stability of the ideal mode at arbitrary beta.

Our discussion of non-ideal effects begins in Chapter 5.

The problem is formulated in terms of a boundary layer analysis in which the external MHD solution is matched to the solution within the layer via the quantity λ_H. The integro-differential set of equations describing the solution within the layer are then derived using collisionless kinetic theory. The solutions to these equations for $\lambda_H < 0$ are reconnecting modes, which we anaylze in Chapter 6. Modifications of the ideal internal kink for $\lambda_H \geq 0$ are discussed in Chapter 7 for finite-beta regimes. Here we find it useful to neglect the effects of temperature gradients to simplify the analysis. Finally we are able to summarize all results in Chapter 8. There we complete the picture of m=1 modes and identify directions for future analyses.

CHAPTER 2

We begin by reviewing the theory of internal kink modes in the standard low-beta, large aspect ratio tokamak[6,24]. This theory is based on an asymptotic expansion of the ideal MHD energy functional in powers of the inverse aspect ratio ε. The fluid displacement is assumed to be dominated by a poloidal harmonic with wavenumber $m = 1$. This couples, through the poloidal modulation of the equilibrium, to $m = 0$ and $m = 2$ sidebands whose amplitudes are one order in ε smaller than the fundamental one. The Euler equations for minimization of the energy functional are solved perturbatively about the well-known circular cylinder solution[2,25]. This perturbative solution must be consistently carried out to order ε^2 because the mode is marginally stable in zeroth and first orders. Therefore an equilibrium is needed correct to order ε^2.

2.1 Low-beta confinement configuration

We begin by identifying an axisymmetric equilibrium solution to the hydromagnetic force balance equation

$$\Delta^* \psi = - T \frac{dT}{d\psi} - 4\pi R^2 \frac{dp}{d\psi} \qquad , \qquad (2.1)$$

where in cylindrical coordinates (R,ζ,z) the Grad-Shafranov operator is defined

$$\Delta^* \psi \equiv R \frac{\partial}{\partial R}\left(\frac{1}{R} \frac{\partial \psi}{\partial R}\right) + \frac{\partial^2 \psi}{\partial z^2} \qquad (2.2)$$

and gives the toroidal current in terms of the poloidal flux $2\pi\psi$. The other terms in Eq. (2.1) represent forces due to the poloidal current $cT/2 = cRB_t/2$ (B_t is the toroidal magnetic field), and the gradient of the plasma pressure p. To order ε^2, a solution of the hydromagnetic force balance equation in large aspect ratio, low-beta, nearly circular tokamaks is described by the following mapping between cylindrical and flux coordinates[5]:

$$R = R_0 + \Delta(r) + r[1 + e(r)]\cos\theta \ , \tag{2.3a}$$

$$z = r[1 - e(r)]\sin\theta \ , \tag{2.3b}$$

$$\zeta = \zeta \ . \tag{2.3c}$$

The geometry is indicated in Fig. 1. The coordinate r represents a flux variable that equals the approximate radius of the nearly circular magnetic surfaces. The displacement of their centers from the magnetic axis is given by $\Delta(r)$, and the elliptical distortion needed to satisfy the equilibrium equation in order ε^2 is measured by e(r). Other magnetic surface functions like the poloidal flux $2\pi\psi$, the poloidal current $cT/2$, the plasma pressure p and the inverse rotational transform q will be regarded as functions of r; primes will denote differentiation with respect to r throughout this paper. Since we are interested in the stability of internal modes, we assume that the plasma extends up to a perfectly conducting wall at $r = a$. The inverse aspect ratio is defined as $\varepsilon \equiv a/R_0$.
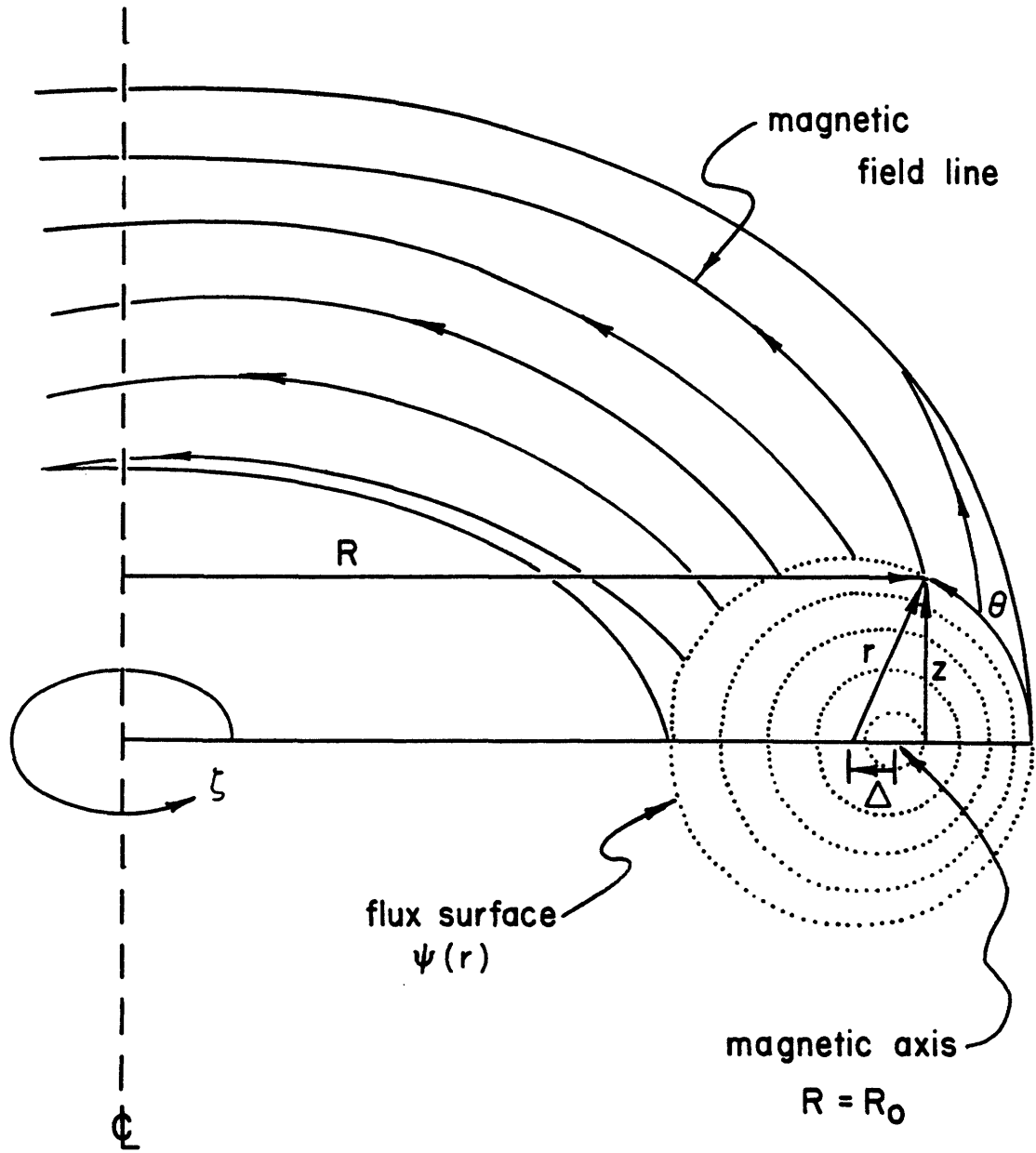
Figure 1: Coordinate systems for toroidal geometry.

The large aspect ratio, low-beta $(\varepsilon\beta_p \sim \varepsilon \ll 1)$, circular tokamak ordering implies:

$$\Delta/r \sim \Delta' \sim r\,\Delta'' \sim r/R_0 \sim \varepsilon , \qquad (2.4a)$$

$$e \sim r\,e' \sim r^2\,e'' \sim \varepsilon^2 . \qquad (2.4b)$$

For convenience we define the following dimensionless variables of order ε:

$$\eta \equiv -\Delta/r, \qquad \alpha \equiv -\Delta', \qquad \rho \equiv r/R_0 . \qquad (2.5)$$

Assuming the geometry (2.3) and the orderings (2.4), the Grad-Shafranov equation is expanded in powers of ε. Retaining terms to order ε^2, the expanded equilibrium equation is of the form:

$$\sum_{m=0}^{2} A_m(r)\,\cos m\theta = O(\varepsilon^3) , \qquad (2.6)$$

and the three radial coefficients $A_m(r)$ vanish for a suitable choice of the functions $\psi(r)$, $\Delta(r)$ and $e(r)$. If we also recall the definition of the inverse rotational transform $q(r)$, we obtain the following relationships[5]:

$$\frac{rT}{R_0\psi'} \equiv \hat{q} = q\left[1 - \frac{1}{2}\,\alpha\rho - \eta\rho - \frac{1}{2}\,\rho^2 + O(\varepsilon^4)\right] , \qquad (2.7)$$

$$T = R_0 B_0 \left[1 + \frac{4\pi(p_0 - p)}{B_0^2} - \int_0^r \frac{\hat{r}(2-s)}{R_0^2 q^2} \, d\hat{r} + O(\varepsilon^4) \right] , \qquad (2.8)$$

$$\alpha = \frac{r}{R_0} \left[\beta_p(r) + \frac{1}{2} \ell_i(r) \right] + O(\varepsilon^3) , \qquad (2.9)$$

$$r^2 e'' + 5r\, e' - 2s(re' + e)$$

$$= \frac{3}{2}\, r\alpha'\, \alpha + \frac{3}{2}\, (1-s)\alpha^2 - \frac{1}{4}\, r\alpha'\rho + \frac{2s-5}{4}\, \alpha\rho + \frac{3}{4}\, \rho^2 + O(\varepsilon^4) , \quad (2.10)$$

where zero subscripts denote quantities evaluated at the magnetic axis. We have defined the radially dependent poloidal beta:

$$\beta_p(r) \equiv - \frac{8\pi R_0^2 q^2}{B_0^2 r^4} \int_0^r p'\, \hat{r}^2 \, d\hat{r} , \qquad (2.11)$$

the internal inductance:

$$\ell_i(r) \equiv \frac{2q^2}{r^4} \int_0^r \frac{\hat{r}^3}{q^2} \, d\hat{r} , \qquad (2.12)$$

and the magnetic shear:

$$s(r) \equiv \frac{d \ln q}{d \ln r} . \qquad (2.13)$$

The equilibrium relationships (2.7-10) allow us to relate all magnetic surface functions to the pressure $p(r)$ and inverse rotational transform $q(r)$. Thus we shall use these two profiles to characterize equilibrium states.

2.2 Energy principle

The stability analysis of the internal kink mode will be based upon the ideal MHD energy principle. The increment of potential energy associated with a fixed boundary plasma displacement $\underline{\xi}(r,\theta,\zeta)$ is[26]:

$$W[\underline{\xi}] = \frac{1}{2} \int dV \left\{ \frac{1}{4\pi} \left| \underline{\nabla} \times (\underline{\xi} \times \underline{B}) \right|^2 + \frac{1}{c} \left[\underline{\nabla} \times (\underline{\xi} \times \underline{B}) \right] \cdot (\underline{J} \times \underline{\xi}) \right.$$

$$\left. + (\underline{\xi} \cdot \underline{\nabla} p)(\underline{\nabla} \cdot \underline{\xi}) + \Gamma p(\underline{\nabla} \cdot \underline{\xi})^2 \right\} , \qquad (2.14)$$

where $\underline{B}$ and $\underline{J}$ are the equilibrium magnetic field and current density respectively, and Γ is the ratio of specific heats. We minimize W with respect to $\underline{\xi} \cdot \underline{B}$ by taking the plasma displacement to be divergenceless ($\underline{\nabla} \cdot \underline{\xi} = 0$). Since the equilibrium configuration is axisymmetric it is sufficient to consider a single toroidal harmonic with wavenumber n:

$$\underline{\xi}(r,\theta,\zeta) = \text{Re} \left[\underline{\Xi}(r,\theta) \exp(-in\zeta) \right]. \qquad (2.15)$$

After substituting the equilibrium solution of Section 2.1 in Eq. (2.14) and integrating over the toroidal angle, the potential energy functional reads:

$$W[X,Y] = \frac{1}{8R_0^{\,3}} \int_0^a dr \; rT^2 \int_{-\pi}^{\pi} d\theta \left\{ \frac{R_0 R}{r^2 D} \; \left| \frac{\partial Y}{\partial \theta} - \left(r\frac{\partial}{\partial r} - \alpha\sin\theta \frac{\partial}{\partial \theta} + D \right) X \right|^2 \right.$$

$$+ \frac{R}{R_0 \hat{q}^2 D^3} \left| \frac{in\hat{q}DR_0}{R} \, Y - \left[r\frac{\partial}{\partial r} - \alpha\sin\theta \frac{\partial}{\partial \theta} - D\left(1 - \frac{2r}{R}\cos\theta \right) \right] X \right|^2$$

$$+ \frac{R}{R_0 \hat{q}^2 D^3} \left| \left[\frac{in\hat{q}D^2 R_0}{R} + (\alpha+\rho)\sin\theta - D\frac{\partial}{\partial \theta} \right] X \right|^2$$

$$+ \; 2 \left[\frac{4\pi R_0 R^3 p'}{r \, T^2} + \frac{R_0^{\,2} \, T'}{r \, T} (1 - n\rho) \right] |X|^2 \left. \right\} \;, \qquad (2.16)$$

where

$$D \equiv 1 - \alpha \cos\theta \;, \qquad (2.17)$$

and the components of the fluid displacement perpendicular to the magnetic field are given by:

$$X(r,\theta) \equiv \underline{\Xi}(r,\theta) \cdot \underline{\nabla} r \, D \, R_0 \, R^{-1} \;, \qquad (2.18a)$$

$$Y(r,\theta) \equiv \underline{\Xi}(r,\theta) \cdot (\underline{B} \times \underline{\nabla} r) \, D^2 \, R_0 \, T^{-1} \qquad (2.18b)$$

In the equilibrium coefficient functions of Eq. (2.16) we have dropped terms of the form $O(\epsilon^2)\exp(im\theta)$ with $m \neq 0$, because, as we shall see, they will not contribute to the leading increment of potential energy for $m=1$ dominated

internal kink modes. In particular, the small ellipticity
e(r) can be disregarded throughout the stability analysis
for this reason.

The Euler equation for the minimization of W with respect
to Y is:

$$
\frac{inr^2}{\hat{q}D^2R_0{}^2}\left[\frac{in\hat{q}DR_0}{R}Y - \frac{\partial(rX)}{\partial r} + \frac{\partial(\alpha\sin\theta X)}{\partial\theta} + \frac{2DR_0(1-\eta\rho)}{R}\right]X
$$

$$
+ \frac{\partial}{\partial\theta}\left[\frac{R}{R_0 D}\left(\frac{\partial Y}{\partial\theta} - \frac{\partial(rX)}{\partial r} + \frac{\partial(\alpha\sin\theta X)}{\partial\theta}\right)\right] = 0 \ . \qquad (2.19)
$$

Since we want both X and Y to be periodic functions of θ,
they must satisfy the constraint:

$$
\int_{-\pi}^{\pi} d\theta\left[\frac{in\hat{q}R_0}{D\,R}Y - \frac{1}{D^2}\frac{\partial(rX)}{\partial r} + \frac{1}{D^2}\frac{\partial(\alpha\sin\theta X)}{\partial\theta} + \frac{2R_0(1-\eta\rho)}{D\,R}X\right] = 0 \qquad (2.20)
$$

We are interested in modes whose poloidal variation is domin-
ated by the m=1 harmonic. However the mode eigenfunctions
must contain a mixture of poloidal harmonics because the
equilibrium is not independent of the poloidal angle. The
standard, large aspect ratio, low-beta tokamak equilibrium
functions can be analyzed as:

$$
f(r,\theta) = \sum_{m=-\infty}^{\infty} \exp(im\theta)\left[\sum_{k=0}^{\infty} f_{mk}(r)\right] \ , \qquad (2.21)
$$

where

$$f_{mk}(r) = O(\varepsilon^{|m|+2k}) \quad , \tag{2.22}$$

and the term of order unity, $f_{00}(r)$, corresponds to the long circular cylinder solution. Consistent with this perturbative expansion we take a representation identical to (2.21) for the mode eigenfunctions, with the exception that now it is centered around the $m = 1$ harmonic:

$$\tilde{f}_{mk} = O(\varepsilon^{|m-1|+2k}) \quad , \tag{2.23}$$

where the tilde indicates a component of the plasma displacement. Since in the long cylinder approximation (i.e. keeping only f_{00} and $\tilde{f}_{10}$) the mode is marginally stable[27], and the contribution to the potential energy functional in order ε vanishes due to orthogonality, the stability of the mode will be determined by the contribution of order ε^2. To compute this we need to keep only the f_{00}, f_{01}, f_{10} and f_{-10} terms in the equilibrium, and the $\tilde{f}_{10}$, $\tilde{f}_{11}$, $\tilde{f}_{20}$ and $\tilde{f}_{00}$ terms in the displacement. We shall disregard all other terms, as we have already done in the equilibrium coefficient functions of Eq. (2.16). Accordingly, we introduce the representations:

$$X(r,\theta) = x_0(r) + x_1(r) \exp(i\theta) + x_2(r) \exp(2i\theta), \tag{2.24a}$$

$$Y(r,\theta) = -i \left[y_0(r) + y_1(r) \exp(i\theta) + y_2(r) \exp(2i\theta) \right] , \tag{2.24b}$$

where the radial amplitudes are:

$$x_1 \sim y_1 = O(1) + O(\epsilon^2) \ , \tag{2.25a}$$

$$x_0 \sim y_0 \sim x_2 \sim y_2 = O(\epsilon) \ . \tag{2.25b}$$

We are concerned with the stability of fixed boundary modes, so that these radial amplitudes are subject to the boundary conditions that they vanish at $r = a$, besides being regular at $r = 0$. Finally, they can be taken to be purely real without loss of generality, because their real and imaginary parts yield uncoupled contributions to the energy functional. Within these assumptions we rewrite the Euler equation (2.19) as:

$$\frac{\partial}{\partial \theta} \left[\frac{R}{R_0 D} \left(\frac{\partial Y}{\partial \theta} - \frac{\partial (rX)}{\partial r} + \frac{\partial (\alpha \sin\theta \ X)}{\partial \theta} \right) \right]$$

$$+ \frac{in\rho^2}{q} (nq \ y_1 - rx_1' + x_1) \ e^{i\theta} = 0 \ , \tag{2.26}$$

which can be integrated once to yield:

$$\frac{\partial Y}{\partial \theta} - \frac{\partial (rX)}{\partial r} + \frac{\partial (\alpha \sin\theta \ X)}{\partial} + \frac{n\rho^2}{q} (nqy_1 - rx_1' + x_1) e^{i\theta}$$

$$+ (r \ x_0)' \ [1 - (\alpha + \rho)\cos\theta] = 0 \ . \tag{2.27}$$

The integration constant $(r \ x_0)'$ has been determined in such a way that Eq.(2.27) will admit periodic solutions. Taking Eq.(2.27) to the expression for the potential energy (2.16)

we observe that, from its first positive definite term, there remains a stabilizing contribution of the form $\rho^{-2} |(r \, x_0)'|^2$ which is $O(\epsilon^{-2})$ larger than any other term involving x_0. Thus minimization of W with respect to x_0 will require the latter to be at least of order ϵ^2. For our purposes we can take

$$x_0 = 0 \; . \tag{2.28}$$

Now we integrate Eq.(2.27) to get:

$$y_1 = (1 - \rho^2 n^2)(r x_1' + x_1) + \frac{\rho^2 n}{q}(r x_1' - x_1) + \frac{1}{2} \alpha x_2 , \tag{2.29a}$$

$$y_2 = \frac{1}{2}(r x_2' + x_2 - \alpha x_1) . \tag{2.29b}$$

Finally we determine the integration constant y_0 from the periodicity constraint (2.20):

$$y_0 = \frac{1}{2}(\rho - \alpha)(r x_1' + x_1) + \frac{1}{nq}(\alpha r x_1' + \rho x_1) . \tag{2.29c}$$

We take the results of the minimizations carried out so far (2.28-29), to the potential energy functional (2.16). Then, keeping only terms up to order ϵ^2, we perform the integration over the poloidal angle. The result is a quadratic form of x_1, x_2 and their derivatives. This radial functional can be cast in a more convenient form by making the change of variable

$$x_2 \to x_2 - \rho x_1 / 2 \qquad (2.30)$$

and integrating by parts the terms involving $x_1' x_1$, $x_2' x_1$ and $x_2' x_2$. As a result the $x_1 x_2$ term also drops out. After using the equilibrium relationships (2.7-10) to simplify the coefficient functions, we obtain:

$$W[x_1, x_2] = \frac{\pi B_0^2 n^2}{4R_0} \int_0^a dr \; r \left(W_0 x_1^2 + W_1 r^2 x_1'^2 \right.$$

$$\left. + W_2 r^2 x_1' x_2' + W_3 r x_1' x_2 + W_4 r^2 x_2'^2 + W_6 x_2^2 \right) , \qquad (2.31)$$

where:

$$W_0 = \frac{1}{r} \left[r^2 \left(\frac{1}{4} - \frac{1}{2}\mu + \frac{1}{2}\mu^2 - n^2\mu^2 \right) \alpha\rho \right.$$

$$\left. + r^2 \left(-\frac{3}{16} - \mu + \frac{1}{2}\mu^2 + \frac{3}{4}n^2 \right) \rho^2 \right]'$$

$$+ \left(2\mu + \frac{1}{2}\mu^2 - 2n^2\mu \right) \rho^2 \qquad (2.32a)$$

$$W_1 = (1-\mu)^2 \left(T^2 R_0^{-2} B_0^{-2} + n\rho - n^2\rho^2 \right) + \left(\frac{1}{4} - 2\mu + 2\mu^2 \right) \alpha^2$$

$$+ \left(-\frac{1}{4} - \frac{1}{2}\mu + \mu^2 \right) \alpha\rho + \left(\frac{9}{16} - \frac{5}{4}\mu + \frac{3}{4}\mu^2 \right) \rho^2 , \qquad (2.32b)$$

$$W_2 = \left(\frac{1}{2} - 3\mu + 3\mu^2 \right) \alpha + \left(-\frac{3}{4} + \mu \right) \rho , \qquad (2.32c)$$

$$W_3 = 3 \left(\frac{1}{2} - \mu + \mu^2 \right) \alpha + \left(\frac{1}{4} - 2\mu + \mu^2 \right) \rho \quad , \tag{2.32d}$$

$$W_4 = \left(\frac{1}{2} - \mu \right)^2 \quad , \tag{2.32e}$$

$$W_6 = 3 \left(\frac{1}{2} - \mu \right)^2 \quad , \tag{2.32f}$$

and

$$\mu \equiv \frac{1}{nq} \quad . \tag{2.32g}$$

The functional $W[\underline{\xi}]$ is to be minimized subject to a normalization constraint $N[\underline{\xi}]$ = constant. If we take this normalizing functional to be proportional to the kinetic energy of the mode, the associated Lagrange multiplier equals the squared mode growth rate. In this work we shall neglect the kinetic energy associated with the fluid motion parallel to the equilibrium magnetic field. This results in an over-estimated growth rate but does not alter the marginal stability points. We shall also assume a constant plasma mass density. It turns out that, in the low-beta regime, inertial effects are significant only within a narrow layer around the $m = 1$ mode resonant surface. Therefore, in this regime, the constant mass density approximation yields the proper growth rate provided we take that constant to be equal to the value at the $\mu = 1$ magnetic surface. Given these assumptions we write:

$$N[\underline{\xi}_\perp] = \frac{1}{2\pi^2 R_0} \int dV \, |\underline{\xi}_\perp|^2 \, , \qquad (2.33)$$

where $\underline{\xi}_\perp$ is the fluid displacement perpendicular to the equilibrium magnetic field. Minima of W subject to our normalizing constraint are obtained by varying the total energy functional

$$E = \frac{4WR_0}{\pi B_0^2 n^2} + \hat{\gamma}^2 N \, . \qquad (2.34)$$

The dimensionless Lagrange multiplier $\hat{\gamma}^2$ is such that

$$\hat{\gamma} = \frac{\gamma R_0}{n \, v_{Al}} \, , \qquad (2.35)$$

where γ is the (perpendicular) growth rate of the mode and v_{Al} is the Alfvén velocity at the $m = 1$ mode resonant surface. We anticipate that $\hat{\gamma}^2$ will be a quantity of order ε^4. Thus the minimization of W carried out so far to order ε^2 is not affected by the introduction of the normalization constraint. Also, because of the smallness of $\hat{\gamma}^2$, we need only the leading contribution to N which corresponds to the cylindrical approximation:

$$N[x_1] = \int_0^a dr \, r \left[x_1^2 + (r \, x_1)'^2 \right] = \int_0^a dr \, r^3 \, x_1'^2 \, . \qquad (2.36)$$

From (2.31), (2.34) and (2.36) we obtain the Euler equations to be solved for the radial amplitudes x_1 and x_2:

$$\left(2(W_1 + \hat{\gamma}^2) r^3 x_1' \right)' - 2W_0 r \, x_1 = -\left(W_2 r^3 x_2' + W_3 r^2 x_2 \right)' \quad , \qquad (2.37)$$

$$L(r) x_2 \equiv \left(2W_4 r^3 x_2' \right)' - 2W_6 r \, x_2 = -\left(W_2 r^3 x_1' \right)' + W_3 r^2 x_1'. \qquad (2.38)$$

The solution of the equation for x_2 can be expressed in terms of the Green's function $G(r,\hat{r})$ which satisfies

$$L(r) G(r,\hat{r}) = -\hat{r}^3 \, W_2(\hat{r}) \, \frac{\partial \delta (r-\hat{r})}{\partial r} + \hat{r}^2 \, W_3(\hat{r}) \, \delta (r-\hat{r}), \qquad (2.39)$$

$$G(0,\hat{r}) = G(a,\hat{r}) = 0, \qquad (2.40)$$

where δ is the Dirac delta function. Once this Green's function has been found, we immediately write down

$$x_2(r) = \int_0^a d\hat{r} \, G(r,\hat{r}) \, x_1'(\hat{r}) \quad , \qquad (2.41)$$

and observe that by (2.39) and (2.40) x_2 satisfies its Euler equation (2.38) as well as its boundary conditions at the origin and the wall. We now insert the solution (2.41) for x_2 into the Euler equation (2.37) for x_1. Then we integrate once and take into account the regularity condition for x_1 at $r = 0$, to get:

$$\left[W_1(r) + \hat{\gamma}^2\right] r^3 x_1'(r) = \int_0^r d\hat{r}\, W_0(\hat{r})\, \hat{r}x_1(\hat{r})$$

$$-\frac{1}{2} \int_0^a d\hat{r}\, x_1'(\hat{r}) \left[W_2(r)r^3\, \frac{\partial G(r,\hat{r})}{\partial r} + W_3(r)\, r^2 G(r,\hat{r})\right]. \qquad (2.42)$$

The solution for the Green's function $G(r,\hat{r})$ is detailed in Appendix A. Taking the results of Eqs.(A.4, A.12) to Eq.(2.42) and integrating the $\delta(r-\hat{r})$ term from $\partial G(r,\hat{r})/\partial r$, we obtain:

$$\left[W_1(r) - \frac{W_2(r)^2}{4W_4(r)} + \hat{\gamma}^2\right] r^3 x_1'(r) = \int_0^r d\hat{r}\, \hat{r}\, W_0(\hat{r})\, x_1(\hat{r})$$

$$+4\, r_1^2\, W_4(r_1)(b+1-c) \int_0^a d\hat{r}\, x_1'(\hat{r}) \sum_{+,-} G_\pm(\hat{r}) G_{\underset{+}{-}}(r)\, \theta(\pm r \mp \hat{r}), \qquad (2.43)$$

where θ is the unit step function, r_1 is the radius of the $m = 1$ mode resonant surface, i.e. $\mu(r_1) = 1$, and the functions $G_\pm$ as well as the parameters b and c are defined in Eqs. (A.11, A.12) of Appendix A.

From here on we can follow a procedure analogous to that used to solve the radial Euler equation for the $m = 1$ mode in a cylinder[25]. Recalling the expressions (2.32b,c,e) for the radial functions W_1, W_2 and W_4, we obtain the following structure for the coefficient of $r^3 x_1'(r)$ on the left hand side of (2.43):

$$W_1 - \frac{W_2^2}{4W_4} + \hat{\gamma}^2 = (1-\mu)^2 \left[1 + O(\epsilon^2)\right] + \hat{\gamma}^2 , \qquad (2.44)$$

where $\hat{\gamma}$ is of order ϵ^4 as will be later verified. On the other hand, the right hand side of (2.43) is of order ϵ^2 because $W_0 \sim \epsilon^2$ and $G_\pm \sim \epsilon$. From (2.44) it is clear that a perturbative solution of Eq. (2.43) in powers of ϵ will give rise to a boundary layer type of problem in the vicinity of $\mu = 1$. We shall consider two asymptotic regions in the radial variable, depending on how $|1-\mu|$ is ordered.

The first, the outer region, corresponds to values of r away from the $m = 1$ mode resonant surface, so that $|1-\mu| \gg \epsilon^2$. In this region Eq. (2.43) reads:

$$(1-\mu)^2 \, r^3 \, x_1^{(out)'}(r) = O(\epsilon^2) . \qquad (2.45)$$

Therefore we can try a solution of the form:

$$x_1^{(out)}(r) = x_{10} \, \theta(r_1 - r) + x_{1s}(r) , \qquad (2.46)$$

where

$$x_{1s}(r)/x_{10} \ll 1 . \qquad (2.47)$$

In what follows, we shall need to evaluate the integrals of the right hand side of Eq. (2.43) only to leading order in ϵ. For this purpose we can approximate $x_1(\hat{r})$ by $x_{10}\theta(r_1 - \hat{r})$

in the first integral. This only amounts to the neglect of higher order corrections coming from the contribution of $x_{1s}(\hat{r})$ in the outer region, and from the integration of the whole integrand, which is a bounded function of r, over a narrow layer around $\hat{r} = r_1$. On the other hand, the main contribution to the second integral comes from the layer $|\hat{r} - r_1|/r_1 \sim \epsilon^2$ where $x_1'(\hat{r})$ is not negligible. Since the factor that multiplies $x_1'(\hat{r})$ in the integrand is a continuous function of $\hat{r}$, it can be approximated by its value at $\hat{r} = r_1$ and taken out of the integral when evaluating the latter to leading order in ϵ. Taking these remarks into consideration, we obtain from Eq. (2.43) to leading order in ϵ:

$$\frac{x_{1s}'(r)}{x_{10}} \doteq \frac{1}{r^3(1-\mu)^2}\left[\int_0^r d\hat{r}\ \hat{r}\ W_0(\hat{r})\theta(r_1-\hat{r})\right.$$

$$\left. - r_1^2(b+1-c)\sum_{+,-} G_\pm(r_1)G_\mp(r)\theta(\pm r \mp r_1)\right]. \tag{2.48}$$

Therefore $x_{1s}'(r)$ and consequently $x_1^{(out)'}(r)$ behave symmetrically at both sides of $r = r_1$. If we now recall

$$1 - \mu \underset{r \to r_1}{\simeq} s_1 \frac{r-r_1}{r_1} \tag{2.49}$$

where $s_1 \equiv s(r_1)$, and define the parameter

$$\lambda_H \equiv \frac{\pi}{s_1^2} \left[(b+1-c)G_+(r_1)G_-(r_1) - \frac{1}{r_1^2} \int_0^{r_1} dr \, r \, W_0(r) \right] , \quad (2.50)$$

we obtain the behavior of $x_1^{(out)}(r)$ near the resonant surface:

$$\frac{x_1^{(out)\prime}(r)}{x_{10}} = \frac{x_{1s}'(r)}{x_{10}} \underset{r \to r_1 \pm 0}{\simeq} - \frac{\lambda_H r_1}{\pi (r-r_1)^2} . \quad (2.51)$$

The solution we have just derived in the outer region breaks down when $|1-\mu| \sim |r-r_1|/r_1 \sim \epsilon^2$. Therefore we consider an inner region where the latter ordering holds. Here we approximate the coefficient functions of Eq.(2.43) by the leading terms of their Taylor expansions about $r = r_1$. We also use arguments identical to those of the previous paragraph to evaluate the leading contributions to the integrals of the right hand side. Thus, to leading order in ϵ, we obtain the following equation:

$$\left[\left(\frac{r-r_1}{r_1} \right)^2 + \left(\frac{\hat{\gamma}}{s_1} \right) \right]^2 \frac{x_1^{(in)\prime}(r)}{x_{10}} = - \frac{\lambda_H}{\pi r_1} \quad (2.52)$$

Notice that all terms of Eq.(2.52) are consistently ordered in this inner layer if $\hat{\gamma}^2 \sim \epsilon^4$. This equation is easily integrated. The integration constant can be adjusted so that $x_1^{(in)}(r)$ matches $x_1^{(out)}(r)$, provided the following eigenvalue condition holds:

$$\hat{\gamma}/s_1 = \lambda_H > 0 \quad , \tag{2.53}$$

the eigenfunction being

$$\frac{x_1^{(in)}(r)}{x_{10}} = \frac{1}{2} - \frac{1}{\pi} \arctan\left(\frac{r-r_1}{\lambda_H r_1}\right). \tag{2.54}$$

For $\lambda_H < 0$, no matching eigenfunction can be constructed so that no internal kink mode exists. For $\lambda_H > 0$, an unstable mode with growth rate given by Eq.(2.53) is excited.

It is useful to point out that $\lambda_H = 0$ is the marginal stability condition we would obtain from the potential energy functional $W[x_1, x_2]$ alone, by inserting there $x_1 = x_{10}\theta(r_1-r)$ as a trial function and minimizing with respect to x_2. To see this, we take the solution (2.41) of the Euler equation (2.38) for x_2 to the functional (2.31) $W[x_1, x_2]$. After some standard manipulations we get:

$$W[x_1] = \frac{\pi B_0^2 n^2}{4R_0} \int_0^a dr \left\{ W_0(r) r \, x_1(r)^2 + \left[W_1(r) - \frac{W_2(r)^2}{4W_4(r)} \right] r^3 x_1'(r)^2 \right.$$

$$\left. - x_1'(r) r_1^2 (b+1-c) \int_0^a d\hat{r} \, x_1'(\hat{r}) \sum_{+,-} G_{\pm}(\hat{r}) G_{\mp}(r) \theta(\pm r \mp \hat{r}) \right\}. \tag{2.55}$$

If we now set $x_1(r) = x_{10}\theta(r_1-r)$ and $x_1'(r) = -x_{10}\delta(r-r_1)$, we realize that the second term in the integrand will not contribute because the coefficient of $x_1'(r)^2$ has a double

zero at $r = r_1$. The other terms yield:

$$W[x_1 = x_{10}\theta(r_1 - r)] = -\frac{1}{4}B_0^2 R_0^{-1} n^2 r_1^2 s_1^2 x_{10}^2 \lambda_H. \qquad (2.56)$$

In order to explicitly evaluate λ_H in terms of equilibrium quantities, we take the values of $G_{\pm}(r_1)$ as well as the expression (2.32a) for W_0 to Eq.(2.50). After making use of the equilibrium relationship (2.9) we obtain :

$$\lambda_H = \frac{\pi r_1^2}{R_0^2 s_1^2} \left\{ \frac{1}{b+1-c} \left[(b+1)c \left(\beta_{p1} + \frac{1}{2}\ell_{i1} - \frac{1}{4} \right)^2 \right. \right.$$

$$+ \frac{3}{2} bc \left(\beta_{p1} + \frac{1}{2}\ell_{i1} - \frac{1}{4} \right) + \frac{9}{16} b(c-1) - \frac{1}{4} \left(\ell_{i1} - \frac{1}{2} \right) \Bigg]$$

$$+ (n^2 - 1) \left[\beta_{p1} + \frac{1}{r_1^4} \int_0^{r_1} dr\ r^3 (\mu + 3)(\mu - 1) \right] \Bigg\} \quad , \qquad (2.57)$$

where $\beta_{p1} \equiv \beta_p(r_1)$ and $\ell_{i1} \equiv \ell_i(r_1)$. This expression for λ_H is the sum of two terms. The second is equal to $(1 - n^{-2})$ times the cylindrical result[2] and dominates for $n \geq 2$. The first terms contains toroidal modifications and is entirely determined by the parameters b, c and ℓ_{i1} which depend only on q(r), and by β_{p1} which also depends on p(r). For usual tokamak profiles the n = 1 mode is stable provided β_{p1} is sufficiently small[6]. For large β_{p1} and r_1 not too close to the conducting wall, Eq.(2.57) predicts the mode to be unstable with a growth rate increasing quadratically with β_{p1}. This result is

modified by the analysis of Chapter 3, where we consider regimes with $\beta_{pl} \sim \varepsilon^{-1}$. The overall stability picture for arbitrary beta will be presented in Chapter 4.

CHAPTER 3

A stability analysis of the internal kink requires knowledge of a global equilibrium solution because of the inherently non-local nature of the mode. This poses a significant difficulty to an analytical study of this instability in the finite-beta regime where $\epsilon \beta_p$ is of the order of unity. As a matter of fact the analysis of the previous section cannot be applied to the finite-beta regime, because α must attain values comparable to $\epsilon \beta_p$ and the perturbative equilibrium solution (2.7-10) that requires α to be a small expansion parameter breaks down.

Arbitrarily large values of $\epsilon \beta_p$ can be reached by means of flux conserving sequences of equilibria, but no global analytic solutions of the flux conserving tokamak equilibrium equations at finite-beta are available. In order to study analytically the stability of these configurations against internal kinks, we shall adopt an approximate equilibrium model which, although not fully consistent, encompasses some of the relevant features of finite-beta confinement configurations.

3.1 Equilibrium model for finite-beta plasma

Our finite-beta equilibrium model assumes a large aspect ratio toroidal configuration whose magnetic surfaces are circular in cross section, strongly shifted from the magnetic axis. Accordingly, the mapping between cylindrical and flux coordinates is simply:

$$R = R_0 + \Delta(r) + r\cos\theta \quad , \tag{3.1a}$$

$$z = r\sin\theta \quad , \tag{3.1b}$$

$$\zeta = \zeta \quad . \tag{3.1c}$$

Again the plasma is limited by a perfectly conducting wall at $r = a$. The inverse aspect ratio is assumed small, i.e. $\varepsilon \equiv a/R_0 \ll 1$, but the poloidal beta is assumed large, of order ε^{-1}. Therefore $\alpha \sim \varepsilon\beta_p$ is of order unity and we shall not make small α expansions but shall retain complete functional dependence on α. On the other hand, in terms not involving β_p, it is now sufficient to take the limit $\varepsilon \to 0$ because nontrivial results are already obtained to leading order in ε. Thus we write the volume element as

$$dV = dr \, d\theta \, d\zeta \, R_0 \, r \, D \, [1 + 0(\varepsilon)] \tag{3.2}$$

and the poloidal field as

$$B_p = \psi' R_0^{-1} D^{-1} [1 + 0(\varepsilon)] \tag{3.3}$$

where $D = |\nabla r|^{-1}$ is defined as in Eq.(2.17). This model involves two free radial functions, namely $\psi(r)$ and $\alpha(r)$, which we relate to the pressure $p(r)$ and inverse rotational transform $q(r)$ by taking the first two moments of the hydromagnetic force balance equation[28,29]. This equation reads:

$$\psi' \Delta^* \psi = - (T\, T' + 4\pi R^2\, p') \tag{3.4}$$

where Δ^* is the elliptic operator defined in Eq. (2.2), and primes continue to denote differentiation with respect to r. Assuming the geometry (3.1) and the large aspect ratio, large poloidal beta ordering, we have:

$$\psi' \Delta^* \psi = \left\{ \frac{\psi'\, \psi''}{D^2} + \frac{\psi'^2}{rD^3} \left[1 + \alpha^2 + (r\alpha' - 2\alpha)\cos\theta \right] \right\} \left[1 + O(\epsilon) \right] \quad , \tag{3.5}$$

$$- (TT' + 4\pi R^2 p') =$$

$$- [TT' + 4\pi R_0^2 p'\, (1 + \frac{2\Delta}{R_0}) + 8\pi R_0\, r\, p'\, \cos\theta][1 + O(\epsilon)]. \tag{3.6}$$

Notice in Eq. (3.6) the $\beta_p \sim \epsilon^{-1}$ ordering:

$$TT' + 4\pi R_0^2\, p' \sim 4\pi\epsilon\, R_0^2\, p' \quad . \tag{3.7}$$

Without expanding in powers of α, the functional dependence of Eqs. (3.5) and (3.6) on the poloidal angle θ cannot be matched. This reflects the fact that our model is inconsistent with a true solution of the equilibrium equation at finite beta. We choose to truncate the Fourier expansion of Eq. (3.5) after its second $\cos m\theta$ harmonic:

$$\psi' \Delta^* \psi = \frac{1}{r} \left\{ \frac{\psi'^2}{2(1-\alpha^2)^{1/2}} + \left(\frac{r\psi'^2}{2(1-\alpha^2)^{3/2}} \right)' \right. +$$

$$+ \left(\frac{\alpha r \psi'^2}{(1-\alpha^2)^{3/2}} \right)' \cos\theta + \sum_{m=2}^{\infty} a_m \cos m\theta \Bigg\} [1+O(\varepsilon)] , \qquad (3.8)$$

and equate the $m = 0$ and $m = 1$ harmonics of Eq.(3.8) to those of Eq.(3.6). Recalling also the definition of the inverse rotational transform we obtain:

$$\frac{rT}{R_0 \psi'} = q + O(\varepsilon) , \qquad (3.9)$$

$$T = R_0 B_0 \left(1 + \frac{4\pi(p_0 - p)}{B_0^2} + O(\varepsilon^2) \right) , \qquad (3.10)$$

$$\alpha(1-\alpha^2)^{-3/2} = \frac{r}{R_0} \beta_p(r) + O(\varepsilon) \qquad (3.11)$$

where $\beta_p(r)$ is defined in Eq.(2.11). For the usual monotonically decreasing $p(r)$ profiles, $\beta_p(r) \geq 0$ and $\alpha \geq 0$. Also from Eq.(3.11) we see that $\alpha < 1$ so that no equilibrium limit exists[29]. The value of α increases with the pressure gradient and approaches its upper bound in the extreme high-beta limit ($\alpha \to 1$ for $\varepsilon \beta_p \gg 1$), as a result of the crowding of magnetic surfaces in the outer part of the torus. This equilibrium model clearly emphasizes the effects associated with the strong outward shift of the magnetic axis in deeply diamagnetic plasmas, while neglecting those associated with finite aspect ratios and noncircularity of the magnetic surfaces. The extent to which it fails to represent a consistent solution of the hydromagnetic

equilibrium equation is measured by the magnitude of the un-
balanced a_m ($m \geq 2$) terms of Eq.(3.8) which happen to be propor-
tional to α^m. Therefore the model can be expected to yield
reliable results if the numerical value of α is reasonably
small. In practice this happens up to moderate values of
$\epsilon \beta_p$, typically $\epsilon \beta_p \lesssim 1$ for which $\alpha \lesssim 1/2$. Within these limits
the assumed circular magnetic surface configuration is in good
quantitative agreement with full numerical solutions of the
equilibrium equation.[30,31] Finally we note that, within $O(\epsilon)$,
the $\epsilon \beta_p \sim \alpha \ll 1$ limit of our model matches asymptotically the
$\beta_p \gg 1$ limit of the standard low-beta equilibrium [4,5] used in
Chapter 2.

3.2 Stability Analysis

As in the low-beta theory, we base our stability analysis
on the ideal MHD energy principle. We proceed in the same
fashion, noting however that now α is $O(1)$ and that it is
now consistent with our ordering to drop terms of order ϵ
compared to terms of order unity. The plasma displacement $\underline{\xi}$
is again taken divergenceless, and the analogue of Eq.(2.16) is:

$$W[X,Y] = \frac{B_0^2}{8R_0} \int_0^a dr\, r \int_{-\pi}^{\pi} d\theta \left\{ \frac{R_0^2}{r^2 D} \left| \frac{\partial Y}{\partial \theta} - \left(r \frac{\partial}{\partial r} - \alpha \sin\theta \frac{\partial}{\partial \theta} + D \right) X \right|^2 \right.$$

$$+ \frac{1}{q^2 D^3} \left| i\,n\,q\,D\,Y - \left(r \frac{\partial}{\partial r} - \alpha \sin\theta \frac{\partial}{\partial \theta} - D \right) X \right|^2$$

$$+ \frac{1}{q^2 D^3} \left| \left(i\, n\, q\, D^2 + \alpha \sin\theta - D\, \frac{\partial}{\partial\theta} \right) X \right|^2$$

$$+ 2 \left(\frac{4\pi R_0 p'}{B_0^2}\, q^2 D^3 \cos\theta + \frac{r}{q}\, \frac{\partial(qD)}{\partial r} - (2 - 3\alpha\cos\theta + \alpha^2) \right) |X|^2 \Bigg\} \quad , \quad (3.12)$$

where X and Y are as defined in Eq. (2.18). Likewise, W is minimized with respect to Y via the Euler equation:

$$\frac{i\, n\, r^2}{q D^2 R_0^2} \left[i\, n\, q\, DY - \frac{\partial(rX)}{\partial r} + \frac{\partial(\alpha\sin\theta\, X)}{\partial\theta} + 2\, D\, X \right]$$

$$+ \frac{\partial}{\partial\theta} \left\{ \frac{1}{D} \left[\frac{\partial Y}{\partial\theta} - \frac{\partial(rX)}{\partial r} + \frac{\partial(\alpha\sin\theta\, X)}{\partial\theta} \right] \right\} = 0 \quad , \qquad (3.13)$$

subject to the periodicity constraint

$$\int_\pi^\pi d\theta \left[\frac{i\, n\, q}{D}\, Y - \frac{1}{D^2}\, \frac{\partial(rX)}{\partial r} + \frac{1}{D^2}\, \frac{\partial(\alpha\sin\theta\, X)}{\partial\theta} + \frac{2}{D}\, X \right] = 0. \quad (3.14)$$

Integrating Eq. (3.13) once, we obtain to leading order in ϵ:

$$\frac{\partial Y}{\partial\theta} - \frac{\partial(rX)}{\partial r} + \frac{\partial(\alpha\sin\theta\, X)}{\partial\theta} + D\, \frac{\partial}{\partial r} \left[\frac{r}{2\pi} \int_{-\pi}^\pi d\theta\, X \right] = 0 \quad (3.15)$$

where the integration constant is fixed by periodicity. From Eq. (3.15) we see that the large, stabilizing first term in

$W[X,Y]$ can be suppressed if $\int_{-\pi}^{\pi} d\theta\ X = 0$. Thus we introduce the trial function

$$X(r,\theta) = x_1(r)\ \exp(i\theta) + x_2(r)\exp(2i\theta)\ , \qquad (3.16)$$

where x_1 and x_2 are now of the same order in ϵ. Ideally we should allow for higher poloidal harmonics in the trial expression for X. However we can expect the internal kink mode to be dominated by its $m = 1$ and $m = 2$ Fourier components, and all other harmonics to be numerically small. Besides, our model potential energy functional (3.12) is only competent to calculate reliably the coupling between adjacent harmonics in X because only the $m = 0$ and $m = \pm 1$ Fourier components of the instability driving term are consistent with the hydromagnetic equilibrium condition. Given the explicit representation (3.16) for X, Eq.(3.15) can be integrated to yield

$$Y(r,\theta) = -\ i\ \sum_{m=0}^{3}\ Y_m(r)\exp(im\theta), \qquad (3.17)$$

where

$$y_1 = rx_1' + x_1 + \frac{1}{2}\ \alpha x_2\ , \qquad (3.18a)$$

$$y_2 = \frac{1}{2}\ (rx_2' + x_2 - \alpha x_1)\ , \qquad (3.18b)$$

$$y_3 = -\ \frac{1}{2}\ \alpha x_2\ . \qquad (3.18c)$$

The integration constant y_0 is then determined by the periodicity constraint (3.14):

$$y_0 = \frac{1}{2\alpha^2\sigma^2}\left\{2\alpha r x_1'\left[\mu - (1+\mu)\sigma^2 + \sigma^3\right]\right.$$

$$+ \alpha\ x_1\left[-\sigma^2+\sigma^4\right]+rx_2'\left[2\mu-(1+6\mu)\sigma^2 + 2(1+2\mu)\sigma^3 - \sigma^4\right]$$

$$\left. + x_2\left[-(1-6\mu)\sigma^2 - 12\mu\sigma^3 + 3(1+2\mu)\sigma^4 - 2\sigma^5\right]\right\}, \qquad (3.18d)$$

where we have introduced $\sigma \equiv (1-\alpha^2)^{1/2}$.

The angular integrals in the periodicity constraint (3.14) and the potential energy functional (3.12) are of the form $\int_{-\pi}^{\pi}d\theta\ \exp(im\theta)/(1-\alpha\cos\theta)^\ell$, where m and ℓ are integers. In the low-beta theory it was sufficient to expand the denominators in power of α. Here, however, we must perform the integration exactly so that W retains the complete functional dependence on α. Although tedious, this can be done in general. The result is[11]:

$$\dot{W}[x_1,x_2] = \frac{\pi B_0^2 n^2}{4R_0}\int_0^a dr\ r\left(W_1\ r^2\ x_1'^2\right.$$

$$\left. + W_2r^2x_1'x_2' + W_3rx_1'x_2 + W_4r^2x_2'^2 + W_5rx_2'x_2 + W_6\ x_2^2\right), \qquad (3.19)$$

where

$$W_1 = \frac{1}{2\sigma^5\alpha^2} \left(\mu^2 - 4\mu\sigma^3 - \mu^2\sigma^4 + 4(1+\mu)\sigma^5 - 4\sigma^6 \right) , \qquad (3.20a)$$

$$W_2 = \frac{1}{2\sigma^5\alpha^3} \left(2\mu^2 + 4\mu^2\sigma^2 - 8(\mu+\mu^2)\sigma^3 - 6\mu^2\sigma^4 \right.$$

$$\left. + 4(1+6\mu+2\mu^2)\sigma^5 - 8(1+2\mu)\sigma^6 + 4\sigma^7 \right) , \qquad (3.20b)$$

$$W_3 = \frac{1}{2\sigma^5\alpha^3} \left(-6\mu^2\sigma^2 + 24\mu^2\sigma^3 - 12\mu^2\sigma^4 + 4(1-6\mu-6\mu^2)\sigma^5 \right.$$

$$\left. + 6(8\mu+3\mu^2)\sigma^6 - 12(1+2\mu)\sigma^7 + 8\sigma^8 \right) , \qquad (3.20c)$$

$$W_4 = \frac{1}{2\sigma^5\alpha^4} \left(\mu^2 + 5\mu^2\sigma^2 - 4(\mu+2\mu^2)\sigma^3 - 13\mu^2\sigma^4 + 2(1+8\mu+12\mu^2)\sigma^5 \right.$$

$$\left. - (4+16\mu+9\mu^2)\sigma^6 + 2(1+2\mu)\sigma^7 \right) , \qquad (3.20d)$$

$$W_5 = \frac{1}{2\sigma^5\alpha^4} \left(-12\mu^2\sigma^2 + 24\mu^2\sigma^3 + 24\mu^2\sigma^4 + 2(1-8\mu-48\mu^2)\sigma^5 \right.$$

$$\left. +12(4\mu+7\mu^2)\sigma^6 - 8(1+6\mu+3\mu^2)\sigma^7 + 8(1+2\mu)\sigma^8 - 2\sigma^9 \right) , \qquad (3.20e)$$

$$W_6 = \frac{1}{2\sigma^5\alpha^4} \left(3\mu^2\sigma^2 - 21\mu^2\sigma^4 + 4(1-3\mu+18\mu^2)\sigma^5 - 111\mu^2\sigma^6 \right.$$

$$\left. -2(5-24\mu-36\mu^2)\sigma^7 - 3(16\mu+5\mu^2)\sigma^8 + 2(5+6\mu)\sigma^9 - 4\sigma^{10} \right) . \qquad (3.20f)$$

In arriving at these coefficient functions (3.20), we have made use of the fact that, after integrating over θ and using the equilibrium relationship (3.11), the instability driving term in W may be written:

$$\frac{1}{2\pi} \int_{-\pi}^{\pi} d\theta \; 2 \left(\frac{4\pi R_0 p'}{B_0^2} q^2 D^3 \cos\theta + \frac{r}{q} \frac{\partial(qD)}{\partial r} - (2-3\alpha\cos\theta+\alpha^2) \right) |X|^2$$

$$= - \left[\frac{1}{q^2\sigma} + \frac{1}{r^2}\left(\frac{r^3}{q^2\sigma^3}\right)' \right] \left(x_1^2 + x_2^2 \right) - \frac{3}{r^2}\left(\frac{r^3\alpha}{q^2\sigma^3}\right)' x_1 x_2 . \qquad (3.21)$$

The derivatives of equilibrium quantities can then be eliminated by partial integration, and as a result, the coefficients (3.20) are functions of μ and α alone. In addition, the x_1^2 and $x_1' x_1$ terms exactly cancel following another integration by parts, and the $x_1 x_2'$ and $x_1 x_2$ terms vanish identically. Thus the expression (3.19) for W is free of x_1 and involves only x_1', x_2 and x_2'.

As in the low-beta theory, we shall use a perpendicular kinetic energy as a normalization constraint in order to make an estimate of the growth rate. Moreover, we now introduce a further simplification in the normalizing functional, to make it depend only on the radial amplitudes x_1 and x_2. In so doing, the previous minimization of W remains unconstrained. Thus we take:

$$N[x_1,x_2] = \frac{1}{2\pi^2 R_0} \int dV \left| \underset{\sim}{\xi}_\perp [X(x_1,x_2), Y(x_1,x_2)] \right|^2 , \qquad (3.22)$$

where X and Y depend only on $x_1(r)$ and $x_2(r)$ through Eqs. (3.16, 17, 18a-d). The price we pay for not carrying out a complete minimization of the total energy with respect to $\underset{\sim}{\xi}_1$ is only a slight underestimate of the growth rate because the Lagrange multiplier $\hat{\gamma}^2$, although formally of order unity, turns out to be numerically small ($\hat{\gamma}^2 \sim 10^{-2}$). The points of marginal stability are of course unchanged. Again we have taken the mass density to be a constant, equal to its value at the $\mu = 1$ magnetic surface. This is consistent with our expectation that, even at finite beta, inertial effects are most important in the vicinity of the $m = 1$ mode resonant surface. After we perform the angular integrations, we eventually find:

$$N[x_1, x_2] = \int_0^a dr\ r \left(N_1 r^2 x_1'^2 + N_2 r^2 x_1' x_2' + N_2 r x_1' x_2 \right.$$

$$\left. + N_4 r^2 x_2'^2 + N_5 r x_2' x_2 + N_6 x_2^2 \right) . \tag{3.23}$$

Terms in x_1 were again eliminated by partial integration. The coefficients in this expression are given by:

$$N_1 = \frac{1}{\sigma^5 (1+\sigma)^2} [\mu^2 + 2\mu^2\sigma - 2\mu^2\sigma^3 - \mu^2\sigma^4 + 2\sigma^5 + 2\sigma^6] , \tag{3.24a}$$

$$N_2 = \frac{\alpha}{\sigma^5 (1+\sigma)^2} [2\mu^2 + 4\mu^2\sigma - 2\mu^2\sigma^2 - 4\mu^2\sigma^3 + 2\sigma^5] , \tag{3.24b}$$

$$N_3 = \frac{\alpha}{\sigma^5(1+\sigma)^2} [6\mu^2\sigma^2 - 6\mu^2\sigma^4 + 2\sigma^5 + 4\sigma^6] \ , \tag{3.24c}$$

$$N_4 = \frac{1}{\sigma^5(1+\sigma)^2} [\mu^2 + 2\mu^2\sigma - 3\mu^2\sigma^2 - 4\mu^2\sigma^3 + 4\mu^2\sigma^4 + \sigma^5] \ , \tag{3.24d}$$

$$N_5 = \frac{1}{\sigma^5(1+\sigma)^2} [6\mu^2\sigma^2 - 18\mu^2\sigma^4 + (1+12\mu^2)\sigma^5 + 2\sigma^6 - \sigma^7] \ , \tag{3.24e}$$

$$N_6 = \frac{1}{\sigma^5(1+\sigma)^2} [9\mu^2\sigma^4 + 2(1-9\mu^2)\sigma^5 + (4+9\mu^2)\sigma^6 + \sigma^7 - 2\sigma^8] . \tag{3.24f}$$

We now have to minimize a total energy functional

$$E[x_1,x_2] = \int_0^a dr \ r \left(E_1 r^2 x_1'^2 + E_2 r^2 x_1' x_2' + E_3 r x_1' x_2 \right.$$

$$\left. + E_4 r^2 x_2'^2 + E_5 r x_2' x_2 + E_6 x_2^2 \right) \ , \tag{3.25}$$

where E is defined as in Eq.(2.34) so that $E_i = W_i + \hat{\gamma}^2 N_i$ for $1 \le i \le 6$. The Euler equations for x_1 and x_2,

$$(2E_1 \ r^3 \ x_1')' = - \ (E_2 \ r^3 \ x_2' + E_3 \ r^2 \ x_2)' \ , \tag{3.26}$$

$$L(r)x_2 \equiv (2E_4 r^3 x_2' + E_5 r^2 x_2)' - (E_5 r^2 x_2' + 2E_6 r x_2)$$

$$= - \ (E_2 r^3 x_1')' + E_3 r^2 x_1' \ , \tag{3.27}$$

are then solved to determine the growth rate. We observe at this point that the eigenvalue $\hat{\gamma}$ depends on the equilibrium and the toroidal mode number n only through the functions $\alpha(r)$ and $\mu(r)$. Recalling the definition of μ, we see that it is sufficient to consider a single value of n. The results for other modes follow immediately from the invariance of $\hat{\gamma}$ under the transformation $n \rightarrow \hat{n}$, $q \rightarrow q n/\hat{n}$ at fixed $\alpha(r)$.

The solution of the radial Euler equations (3.26-27) is more difficult to obtain than in the low-beta case, owing both to the greater complexity of the E_i's and to the fact that we are no longer free to use α as an $O(\epsilon)$ expansion parameter. In particular the boundary layer solution for the growth rate is no longer possible. Nevertheless, at the end of this section we shall consider a variational procedure which yields a closed form estimate for $\hat{\gamma}$. On the other hand we can make further progress with the observation that, since there is no x_1 term in E, Eq. (3.26) can be integrated:

$$r\, x_1' = -\frac{E_2}{2E_1}\, r\, x_2' - \frac{E_3}{2E_1}\, x_2 \, , \tag{3.28}$$

where the constant of integration must vanish to ensure regularity of x_1 at $r = 0$. If we take this solution back to Eq. (3.25), we can express E as a functional of x_2 alone:

$$E[x_2] = \int_0^a dr\, r \left(C_1 r^2 x_2'^2 + C_2 r x_2' x_2 + C_3 x_2^2 \right) \, , \tag{3.29}$$

where

$$C_1 = \frac{4E_1 E_4 - E_2^2}{4E_1} \quad , \tag{3.30a}$$

$$C_2 = \frac{2E_1 E_5 - E_2 E_3}{2E_1} \quad , \tag{3.30b}$$

$$C_3 = \frac{4E_1 E_6 - E_3^2}{4E_1} \quad . \tag{3.30c}$$

Thus we are led to solve a single Euler equation for x_2:

$$(2C_1 r^3 x_2' + C_2 r^2 x_2)' - (C_2 r^2 x_2' + 2C_3 r x_2) = 0 . \tag{3.31}$$

Note that the C_i's depend on the eigenvalue $\hat{\gamma}$ through the E_i's.

At this point we can address the high-beta stability of the mode. For this purpose it is sufficient to work with the potential energy W alone, thus we set $\hat{\gamma} = 0$ when evaluating the C_i's. We consider the $\epsilon\beta_p \gg 1$ limit where α approaches unity within most of the plasma domain. Noting that in this limit σ tends to zero, we see from the expressions (3.20a-f) that there are singular terms which should dominate in the integral (3.29). Now if we expand the C_i coefficients in powers of σ we find that the leading $O(\sigma^{-5})$ terms exactly cancel. From the terms in the next order, $O(\sigma^{-3})$, we find after an integration by parts:

$$W[x_2; \epsilon\beta_p \gg 1] = \frac{\pi B_0^2}{4R_0} \int_0^a dr \left[\left(\frac{r^3}{2q^2\sigma^3}\right) x_2'^2 + \frac{3}{r}\left(\frac{r^3}{2q^2\sigma^3}\right)' x_2^2 \right] . \tag{3.32}$$

Finally, if we recall the equilibrium relationship (3.11),
and the definition of β_p (2.11) we have[11]:

$$W[x_2; \ \varepsilon\beta_p \gg 1] = -\pi^2 \int_0^a dr \left\{ \left[\int_0^r d\hat{r} \ \hat{r}^2 p'(\hat{r}) \right] x_2'(r)^2 \right.$$

$$\left. + 3rp'(r)x_2(r)^2 \right\} . \tag{3.33}$$

Hence a sufficient condition for stability in the high-beta
limit is that the pressure be a monotonically decreasing func-
tion of the radius. This is due to the enhanced magnetic
tension induced by the pressure gradient through the equili-
brium shift of the magnetic surfaces[9]. Moreover Eq.(3.33)
is independent of n, so this stabilization occurs for all
toroidal modes.

The high-beta stabilization of the mode can be verified
by a numerical solution of the eigenvalue equation (3.31).
As a typical example, we consider the class of equilibria
determined by the profiles:

$$p(r) = p_0(1 - r^2/a^2) \exp(-2r^2/a^2) \quad , \tag{3.34a}$$

$$q(r) = q_0(1 + r^2/a^2 + r^4/a^4) \quad . \tag{3.34b}$$

The magnetic axis pressure p_0 can be used to scale $\varepsilon\beta_p$ within
a flux conserving sequence characterized by a fixed value of
q_0. Given the profiles (3.34), the equilibrium equation (3.11)

must be solved for $\alpha(r)$. Then $x_2(r)$ and $\hat{\gamma}$ are determined from
Eq. (3.31) together with the boundary conditions for x_2. The
coefficient function C_1 never vanishes, so there is no problem
with regularity of x_2 at the $\mu = 1/2$ magnetic surface r_2.
This is due to the inclusion of a finite coupling between $m = 1$
and $m = 2$ harmonics as well as finite inertial effects in the
theory. In Fig. 2a - c, we plot the eigenfunctions x_1 and x_2
as well as their derivatives for $q_0 = 0.75$ and $\varepsilon\beta_p \equiv \varepsilon\beta_p(a) = 0.13$,
0.62 and 0.95 respectively. For this q-profile we consider
the $n = 1$ mode. Figure 2a is a low-beta case which exhibits
the step function behaviour of x_1 and the piecewise continuous
nature of x_2 that we should expect from the analysis of Chapter
2. As $\varepsilon\beta_p$ increases towards the peak growth rate case displayed
in Fig. 2b , we see that the eigenfunctions become smoother,
although x_1' is still strongly peaked at r_1. As $\varepsilon\beta_p$ is further
increased towards the "second" marginal point in Fig. 2c,
the eigenfunctions again become sharper at r_1 but x_2 continues
to get smoother at r_2. In all cases we see that x_2 is signi-
ficantly smaller in magnitude than x_1. Finally in Fig. 3
we plot the eigenvalue $\hat{\gamma}$ as a function of $\varepsilon\beta_p$. For this
choice of profiles the mode is stable above $\varepsilon\beta_p = 0.99$. In the
$\varepsilon\beta_p \ll 1$ limit, $\hat{\gamma}$ tends to zero as $(\varepsilon\beta_p)^2$ so that the mode
appears marginally stable. This will be resolved by an asymp-
totic matching to the low-beta theory. Also indicated in
Fig. 3 is the result of the variational calculation which we
describe next.
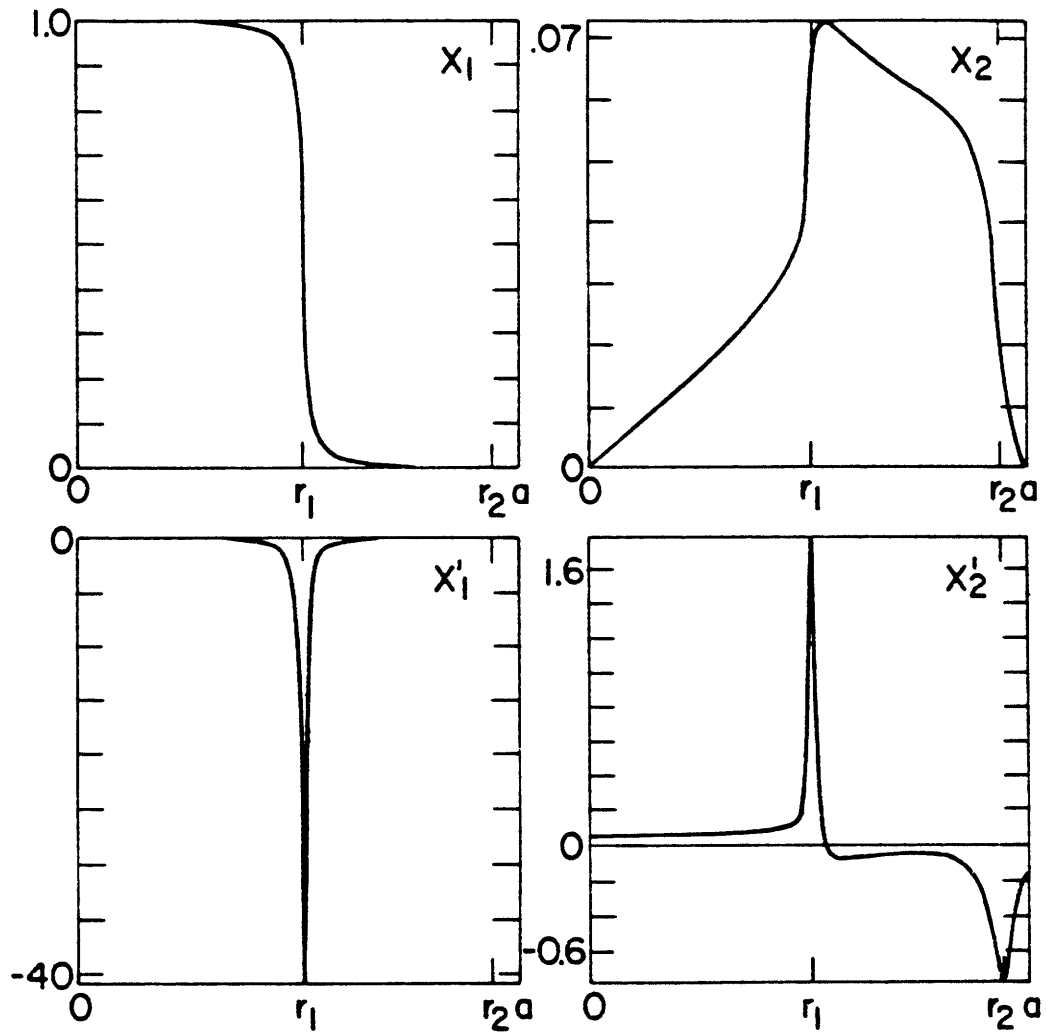
Figure 2a: Eigenfunctions $x_1(r)$, $x_2(r)$ and their derivatives
which give the $m = 1$ and $m = 2$ components of the
internal kink displacement in the radial direction.
Here $\varepsilon\beta_p = 0.13$, and r_1 and r_2 are the positions
of the mode rational surfaces. The vertical axes
are not drawn to scale.
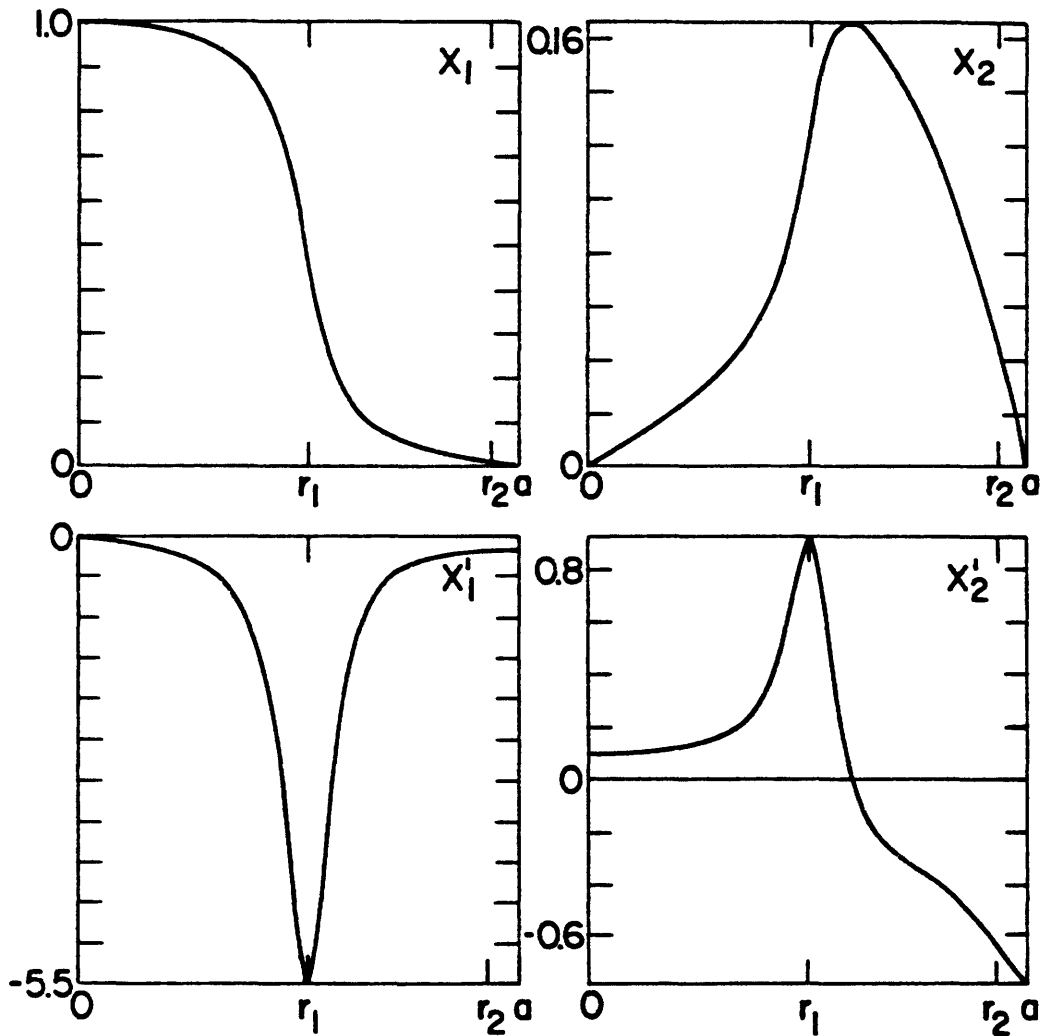
Figure 2b: Eigenfunctions $x_1(r)$, $x_2(r)$ and their derivatives for $\varepsilon\beta_p = 0.62$, which corresponds to the peak growth rate.
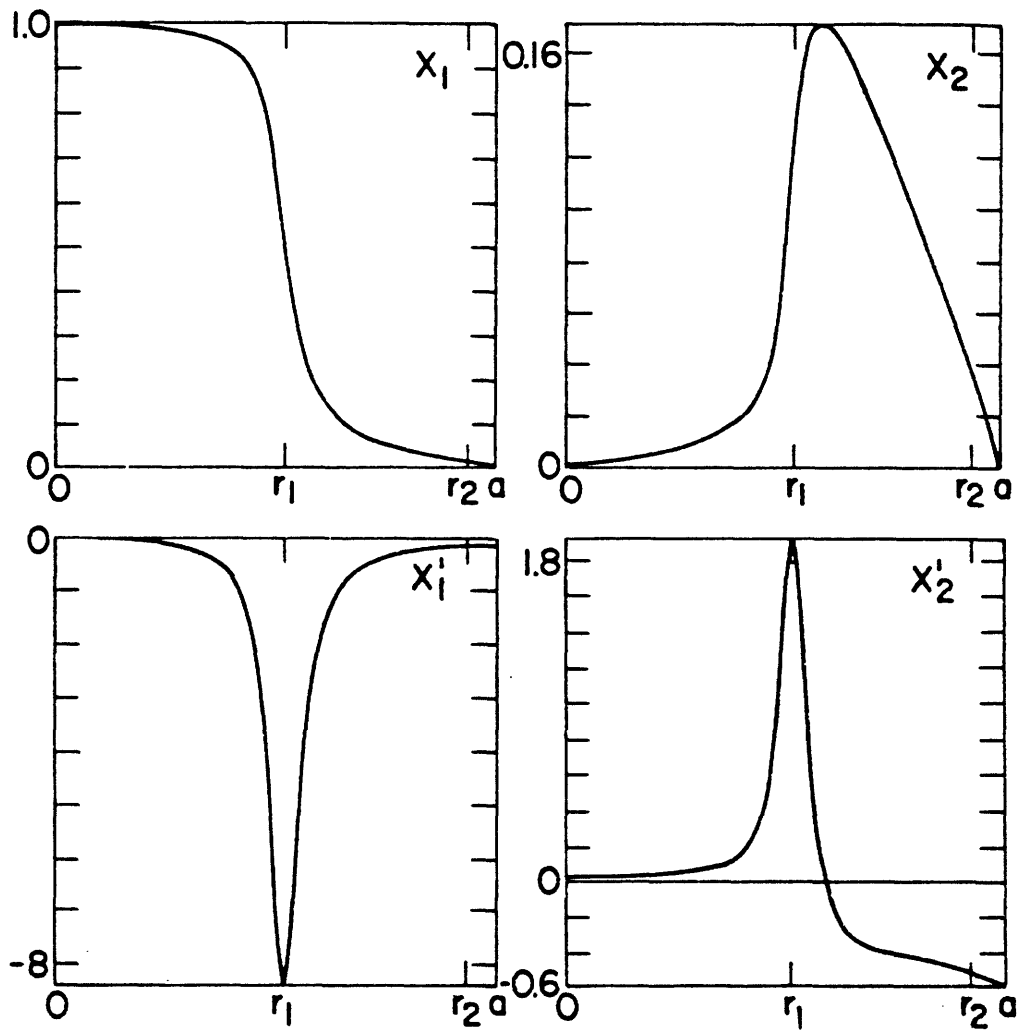
Figure 2c: Eigenfunctions $x_1(r)$, $x_2(r)$ and their derivatives for $\varepsilon\beta_p = 0.95$, which is near the second point of marginal stability.
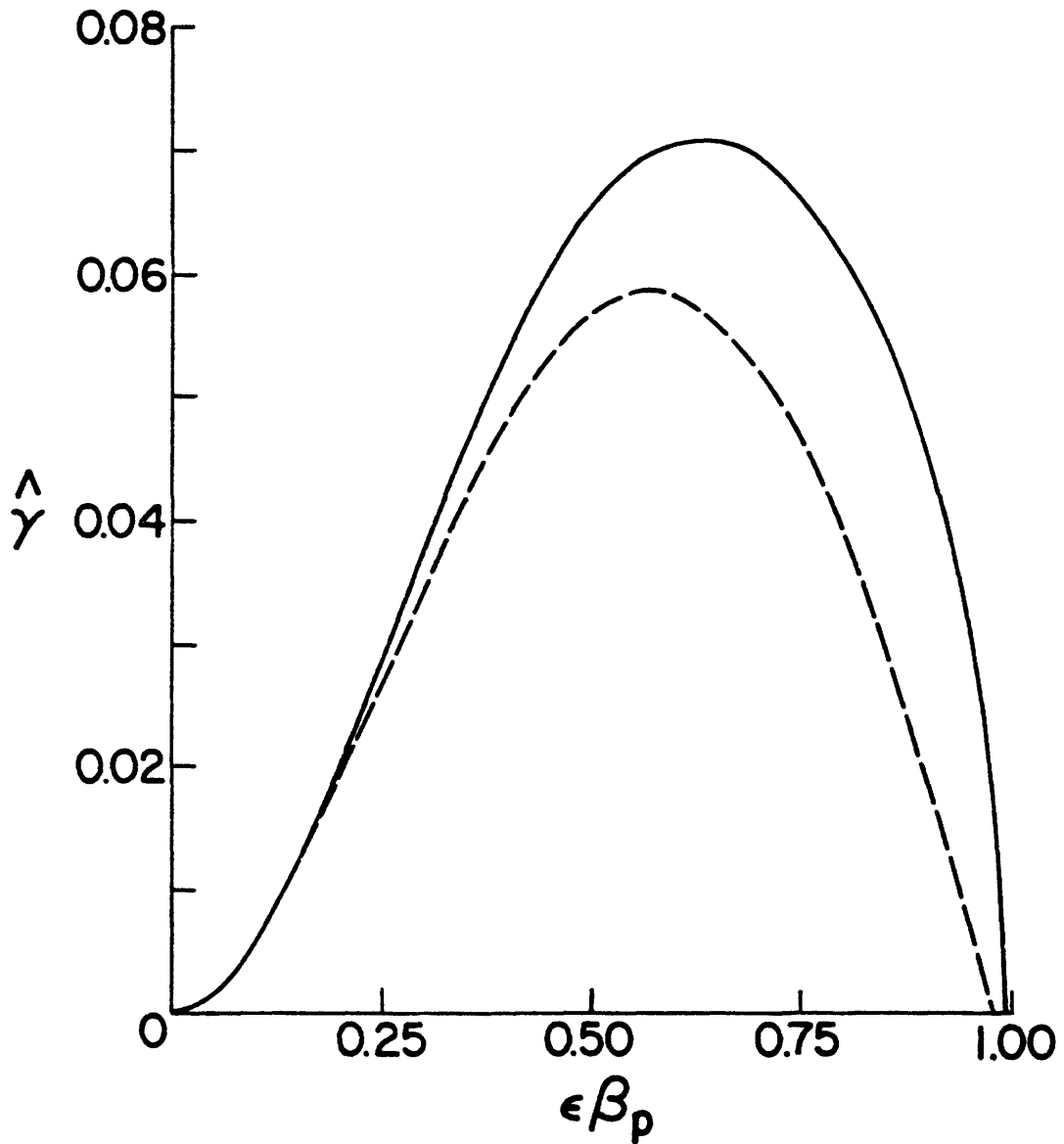
Figure 3: Normalized growth rate $\hat{\gamma}$ of Eq.(2.35) as a function of $\varepsilon\beta_p \equiv aR_0^{-1}\beta_p(a)$ in the finite-beta regime for $nq_0 = 0.75$. For comparison the variational estimate (dashed curve) of Eqs.(3.42,48) is plotted together with the numerical solution (solid curve) of the one-dimensional eigenvalue problem (3.31).

We begin the variational calculation by expressing the solution of the Euler equation (3.27) for x_2 in terms of a Green's function. Since Eq. (3.27) has the same form as its analogue (2.38) in the low-beta theory, the solution is formally the same, i.e., Eq. (2.41), and the Green's function is determined via the same procedure detailed in Appendix A. Taking this solution to Eq. (3.26), we are left with a single integral equation to solve for x_1':

$$\left[\frac{4E_1(r)E_4(r) - E_2(r)^2}{4E_4(r)} \right] r^3 x_1'(r) =$$

$$4r_1^2 E_4(r_1)(b+1-c) \int_0^a d\hat{r}\, x_1'(\hat{r}) \sum_{+,-} G_\pm(\hat{r}) G_-(r) \theta(\pm r_+^- \hat{r}), \qquad (3.35)$$

where the functions $G_\pm(r)$ as well as the parameters b and c are obtained from Eqs. (A.11, A.12) of Appendix A using the coefficient functions $E_i(r)$ of the finite-beta theory (3.20, 24). Now we define

$$\chi(r) \equiv x_1'(r) \left[\frac{4rE_1(r)E_4(r) - rE_2(r)^2}{16(b+1-c)E_4(r_1)E_4(r)} \right]^{1/2}, \qquad (3.36)$$

$$k_\pm(r) \equiv G_\pm(r) \left[\frac{4rE_1(r)E_4(r) - rE_2(r)^2}{16(b+1-c)E_4(r_1)E_4(r)} \right]^{-1/2}, \qquad (3.37)$$

and express Eq. (3.35) as a homogeneous Fredholm equation of the second kind:

$$\chi(r) = \kappa \int_0^a d\hat{r} \, K(r,\hat{r}) \, \chi(\hat{r}) \quad , \tag{3.38}$$

with a split kernel:

$$K(r,\hat{r}) = \begin{cases} k_+(r) \, k_-(\hat{r}) & \text{for } r > \hat{r} \\[2mm] k_-(r) \, k_+(\hat{r}) & \text{for } r < \hat{r} \end{cases} \tag{3.39}$$

We have introduced an eigenvalue κ which is equal to unity for a solution of the original equation (3.35). If we now multiply Eq. (3.38) by $\chi(r)$ and integrate, we find:

$$\kappa = \frac{\displaystyle\int_0^a dr \, \chi(r)^2}{\displaystyle\int_0^a dr \int_0^a d\hat{r} \, \chi(r) \, K(r,\hat{r}) \, \chi(r)} \quad , \tag{3.40}$$

which is a variational form for the original equation.

In order to proceed we must simplify the functional form of the kernel $K(r,\hat{r})$. To do this we begin by noting that the combination $4W_1W_4 - W_2^2$ has a minimum near r_1 where it is roughly equal to $(1-\mu)^2$. This behavior is responsible for the maximum of x_1' at r_1 seen in Fig. 2a-c. Thus the largest contribution to $k_\pm$ comes from $r \sim r_1$, and so we set $r = r_1$ everywhere except for the combination $(1-\mu)^2 \simeq s_1^2 (r-r_1)^2/r_1^2$.

Secondly, recalling that in the low-beta theory it was suffi-
cient to retain the growth rate only in the coefficient
function E_1, we likewise neglect $\hat{\gamma}$ except in E_1 now, as we
expect this eigenvalue to still be numerically small. Thus
we adopt the approximation:

$$\frac{4E_1E_4 - E_2^2}{4E_4} \simeq \frac{4E_1W_4 - W_2^2}{4W_4} \simeq s_1^2 \left[\left(\frac{r - r_1}{r_1}\right)^2 + \lambda_H^2 \right] . \quad (3.41)$$

Here we have introduced a parameter λ_H, analogous to that of
the low-beta theory, defined by the relation:

$$\hat{\gamma} = \frac{s_1 \lambda_H}{N_{11}^{1/2} \sigma_1^{5/2}} , \quad (3.42)$$

where $\sigma_1 \equiv \sigma(r_1)$ and $N_{11} \equiv N_1(r_1)$. Then we may write:

$$k_\pm(r) \simeq k_{0\pm} \left[\left(\frac{r - r_1}{r_1}\right)^2 + \lambda_H^2 \right]^{-1/2} , \quad (3.43)$$

where

$$k_{0+} = -W_{21}(b+1+d) [r_1 s_1^{-2} \sigma_1^{-5} W_{41}(b+1-c)]^{-1/2} , \quad (3.44a)$$

$$k_{0-} = -W_{21}(c+d) [r_1 s_1^{-2} \sigma_1^{-5} W_{41}(b+1-c)]^{-1/2} , \quad (3.44b)$$

are constants, and we have written $W_{i1} \equiv W_i(r_1)$ and introduced

$$d \equiv \frac{W_{31} - 3W_{21}}{4W_{21}} \quad . \tag{3.45}$$

Now, if we take a trial function of the form

$$\chi(r) = \left[\left(\frac{r - r_1}{r_1} \right)^2 + \nu^2 \right]^{-1/2} \tag{3.46}$$

where ν is a variational parameter, the integrals in Eq. (3.40) can be performed to give:

$$\kappa(\lambda_H < \nu) = \frac{\pi}{4r_1 k_{0+} k_{0-} \nu} \left(\frac{\nu}{K(1-\lambda_H^2/\nu^2)} \right)^2 , \tag{3.47a}$$

$$\kappa(\lambda_H > \nu) = \frac{\pi}{4r_1 k_{0+} k_{0-} \nu} \left(\frac{\lambda_H}{K(1-\nu^2/\lambda_H^2)} \right)^2 . \tag{3.47b}$$

Here $K(z)$ is the complete elliptic integral of the first kind and we have assumed λ_H, $\nu \ll 1$. Now if we set $d\kappa/d\nu = 0$ we get $\nu = \lambda_H$. Finally, from the condition $\kappa = 1$ we find

$$\lambda_H = \frac{\pi \, W_{21}^2 \sigma_1^5 \, (b+1+d) \, (c+d)}{s_1^2 \, W_{41} \, (b+1-c)} , \tag{3.48}$$

and then the growth rate is given by Eq. (3.42). This growth rate estimate is plotted in Fig. 3 for comparison with the numerical result. As expected, the approximate variational

calculation underestimates $\hat{\gamma}$, although not significantly, and provides a lower bound for the "second" point of marginal stability.

CHAPTER 4

Ideal MHD stability results

In the preceding sections we have analyzed the internal kink mode in two distinct beta regimes. We now consider the question of the asymptotic matching that exists between them. In both cases we assumed a large aspect ratio, $\varepsilon \ll 1$, but in the low-beta theory we assumed $\beta_p \sim 1$ while in the finite-beta theory we took $\varepsilon \beta_p \sim 1$. Thus we are interested in the agreement between the low-beta theory in the limit $\beta_p \gg 1$, and the finite-beta theory in the limit $\varepsilon \beta_p \ll 1$. For this purpose we consider a common or matching regime where the ordering $\varepsilon \ll \varepsilon \beta_p \sim \alpha \ll 1$ holds. Comparing the equilibrium relations (2.7,8,9) and (3.9,10,11), we see that in this matching regime they have a common limit to leading order in α and ε:

$$\frac{rT}{R_0 \psi} = q \ [1 + O(\alpha\varepsilon)] \quad , \tag{4.1}$$

$$T = R_0 B_0 \left[1 + \frac{4\pi(p_0 - p)}{B_0^2} + O(\varepsilon^2) \right] \quad , \tag{4.2}$$

$$\alpha = \frac{r}{R_0} \beta_p(r) + O(\alpha^3) + O(\varepsilon) \quad . \tag{4.3}$$

Minimization of W in the matching regime follows the same lines of either the low-beta or the finite-beta case. In the trial function for $X(r,\theta)$ we now have $x_2 \sim \alpha x_1$, and calculations need to be carried out only to order α^2. The resulting radial

functional $W[x_1, x_2]$ equals that obtained by taking the $\beta_p \gg 1$ limit of the low-beta result (2.31,32), i.e., by neglecting there terms of order ε^2 and $\alpha\varepsilon$ compared to those of order α^2:

$$W_0 = 0 \quad , \tag{4.4a}$$

$$W_1 = (1-\mu)^2 + (\tfrac{1}{4} - 2\mu + 2\mu^2)\alpha^2 \quad , \tag{4.4b}$$

$$W_2 = (\tfrac{1}{2} - 3\mu + 3\mu^2)\alpha \quad , \tag{4.4c}$$

$$W_3 = 3(\tfrac{1}{2} - \mu + \mu^2)\alpha \quad , \tag{4.4d}$$

$$W_4 = (\tfrac{1}{2} - \mu)^2 \quad , \tag{4.4e}$$

$$W_5 = 0 \quad , \tag{4.4f}$$

$$W_6 = 3(\tfrac{1}{2} - \mu)^2 \quad . \tag{4.4g}$$

Identical W_i coefficient functions are obtained by taking the $\varepsilon\beta_p \sim \alpha \ll 1$ limit of the finite-beta result (3.19,20). To verify this, we only have to expand Eqs. (3.19) and (3.20) in powers of α to order α^2 and integrate by parts the $W_5\ r^2 x_2 x_2'$ term. Likewise, the coefficient functions of the normalizing functional in the matching regime are:

$$N_1 = 1 \quad , \tag{4.5a}$$

$$N_2 = \alpha/2 \quad , \tag{4.5b}$$

$$N_3 = 3\alpha/2 \quad , \tag{4.5c}$$

$$N_4 = 1/4 \quad , \tag{4.5d}$$

$$N_5 = 1/2 \quad , \tag{4.5e}$$

$$N_6 = 5/4 \quad . \tag{4.5f}$$

Since $x_2 \sim \alpha x_1$ and $\hat{\gamma} \sim \alpha^2$, only the N_1 term needs to be retained in this regime, as in the low-beta theory.

Consider now the eigenfunctions $x_1(r)$ and $x_2(r)$ obtained in the minimization of the radial functional $W[x_1, x_2]$. In the finite-beta theory x_1 and x_2 are continuous functions of r as in Fig. (2a), the resonant surfaces r_1 and r_2 are easily identified by abrupt changes in x_1 and x_2. Viewed as a progression, x_1' and x_2' develop δ-function singularities as $\epsilon\beta_p$ tends to zero. This is in agreement with their behavior in the low-beta regime where

$$x_1(r) \simeq x_{10} \; \theta(r_1 - r) \quad , \tag{4.6a}$$

$$x_2(r) \simeq -x_{10} \; G(r, r_1) \quad , \tag{4.6b}$$

and the Green's function $G(r, r_1)$ has discontinuities at $r = r_1$ and $r = r_2$, as shown in Appendix A.

Given these considerations, the mode growth rate in the matching regime is easily obtained as the $\beta_p \gg 1$ limit of Eqs. (2.53,57):

$$\hat{\gamma} = \hat{\gamma}_{match} = \frac{\pi r_1^2 \beta_{p1}^2 (b+1) c}{R_0^2 s_1 (b+1-c)} \quad . \tag{4.7}$$

This expression is also the $\alpha \ll 1$ limit of our variational result at finite-beta (3.42,48). In this matching regime, the α-dependent terms drop out of the linear differential operator L defined in Eqs. (2.38) or (3.27). As a consequence the parameters b and c are independent of β_p and are determined by the q-profile alone. Also, d is of order α^2 and is therefore neglected compared to either b or c. We show in Appendix B that $b > 0$ and $c < 3/4$. Thus, in the matching regime, the stability is entirely determined by the sign of c, which is usually positive unless r_1 is sufficiently close to the conducting wall a. The $(\varepsilon\beta_p)^2$ dependence of $\hat{\gamma}_{match}$ is responsible for the parabolic shape of both the variational and the numerical growth rate curves of Fig. 3 in the $\varepsilon\beta_p \ll 1$ region. As shown in Fig. 3 and more clearly in Fig. 4, the numerical result for $\hat{\gamma}_{finite}$ also agrees with Eq. (4.7) in the matching regime. In Fig. 4 we have plotted, on logarithmic scales, the growth rates predicted by the low-beta and finite-beta theories of Chapters 2 and 3 as well as the result (4.7) for the matching regime, as functions of $\varepsilon\beta_p$. We have used the same equilibrium sequence of Figs. 2 and 3, and set $\varepsilon = 0.1$ when evaluating
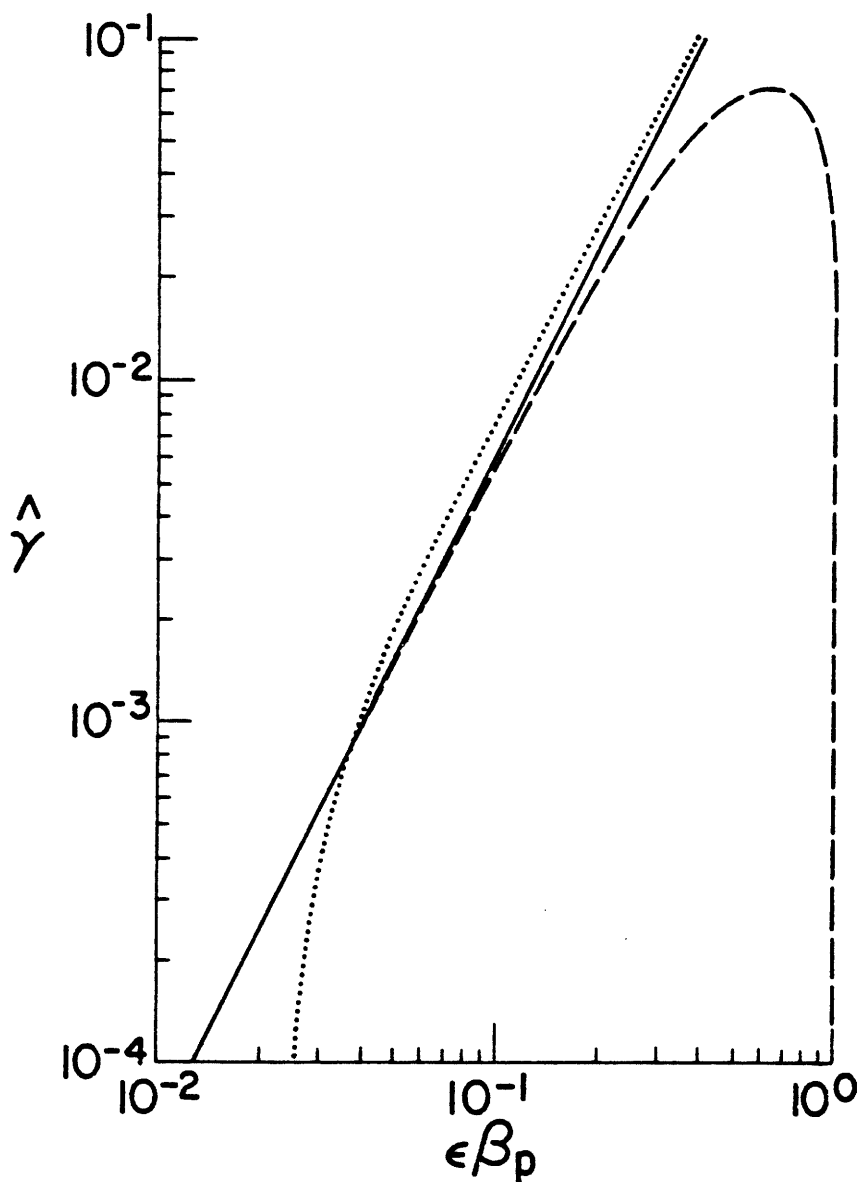
Figure 4: Asymptotic matching of $\hat{\gamma}$ for an n = 1 internal
kink mode in different beta regimes. The finite-
beta result (dashed curve) agrees with $\hat{\gamma}_{match}$
(solid line) as $\varepsilon\beta_p \to 0$, while the low-beta result
(dotted curve) agrees with $\hat{\gamma}_{match}$ as $\varepsilon\beta_p \to \infty$.

$\hat{\gamma}_{low}$ from Eqs. (2.53,57) for the sake of clarity. In this logarithmic plot, $\hat{\gamma}_{match}$ appears as a straight line of slope 2 that asymptotically approaches $\hat{\gamma}_{low}$ for large $\epsilon\beta_p$ and $\hat{\gamma}_{finite}$ for small $\epsilon\beta_p$. In short, there is an asymptotic match between the low-beta and finite-beta theories. We are therefore at liberty to construct an asymptotically matched growth rate:

$$\hat{\gamma} = \hat{\gamma}_{finite} + \hat{\gamma}_{low} - \hat{\gamma}_{match} \quad , \tag{4.8}$$

and use it to discuss the stability of the internal kink mode for arbitrary beta.

We present a complete stability diagram against $m = 1$ dominated internal kink modes in Fig. 5. The marginal stability curves correspond to the zeros of the matched growth rate defined in Eq. (4.8). Here we have taken the p and q profiles given by Eq. (3.34) and set $\epsilon = 0.25$ when evaluating $\hat{\gamma}_{low}$. Since for this choice of q profile, $q(a) = 3 \, q_0$, the $m = 1$ mode resonant surface will lie within the plasma for $n < 1/q_0 < 3n$. The cases $n = 1$ and $n \overset{>}{=} 2$ are distinguished at low-beta due to the second term in Eq. (2.57), whereas we have already noted that at finite-beta all n modes are equivalent.

At low-beta, $n \overset{>}{=} 2$ modes are unstable if the $\mu = 1$ surface lies within the plasma, because the second term of Eq. (2.57), which equals $(1-n^{-2})$ times the cylindrical value, makes a large positive contribution to λ_H. On the other hand, this term vanishes for $n = 1$ and so the stability of this mode at low-beta is entirely determined by b, c, ℓ_{i1} and β_{p1}. We recall
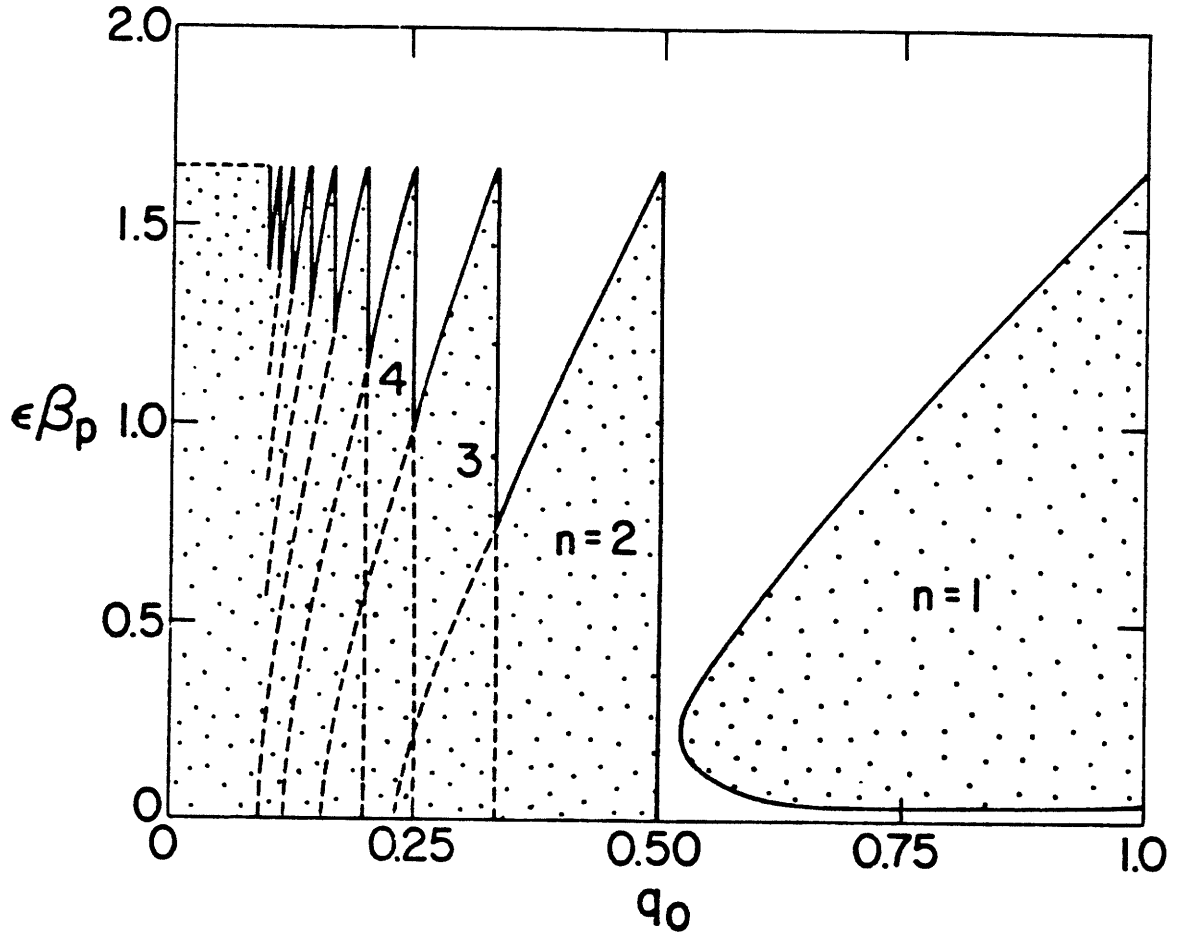
Figure 5: Stability diagram against ideal internal kink modes for the profiles of Eq.(3.34) and inverse aspect ratio $\varepsilon = 0.25$. The plasma is stable for values of $\varepsilon\beta_p$ and q_0 outside the stippled region. For the profiles chosen, the safety factor $q(a) = 3q_0$.

that, for $\varepsilon\beta_p \ll 1$ and monotonically increasing $q(r)$ profiles, $b > 0$ and $c < 3/4$; also $\ell_{i1} > 1/2$. If r_1 is sufficiently close to a, c becomes negative and large in magnitude so that λ_H is negative and the plasma is stable. This stabilization is due to the proximity of the conducting wall to the mode resonant surface, and causes the stability window for $0.5 < q_0 \stackrel{<}{\sim} 0.6$ in Fig. 5. Otherwise the plasma is stable against the $n = 1$ mode only for β_{p1} less than some critical value.[6]

As β_{p1} exceeds this threshold, the internal kink mode becomes unstable. Its growth rate increases parabolically with β_p into the finite-beta regime. Here the indirect stabilizing effect of the pressure gradient discussed in Chapter 3 comes into play, and acts to suppress the instability. We can also observe this from our variational expression for λ_H (3.48). In the very high-beta limit ($\sigma \to 0$), $W_{41}\sigma_1^5 = 1/2$, $d = -3/4$ and we prove in Appendix B that $b > -1/4$ and $c < 3/4$. Thus $\lambda_H < 0$ and the mode is stable. For the considered class of equilibria, all n modes are stable above $\varepsilon\beta_p = 1.6$. Again, the improved stability towards lower values of q_0 is due to wall stabilization. Finally, the jagged appearance of the stability boundaries for low values of q_0 is due to the onset of the individual n modes at $q_0 = 1/n$. For $q_0 > 1$ no internal kink instability exists because there are no $m = 1$ mode rational surfaces within the plasma.

Let us now return to the question of the validity of our results which arises due to the approximate nature of our finite-beta equilibrium model. We recall that with our model

we were able to balance only the first two moments of the
Grad-Shafranov equation, leaving unbalanced terms proportional
to $\alpha^m \cos m\theta$ for $m \geq 2$. As pointed out earlier, we expect reliable
results if α is not too large. For the profiles (3.34) used
in generating Fig. 5, the maximum equilibrium value of α at
the second marginal point is $\alpha(a) \simeq 0.65$ for $\varepsilon \beta_p \simeq 1.6$, when
nq_0 approaches 1. At this moderate value of α, the flux sur-
faces obtained from a consistent solution of the equilibrium
equations are no longer circular in cross section. For a
circular conducting wall, the flux surfaces near the magnetic
axis have developed a noticeable vertical elongation. However,
the most significant feature of these equilibria, namely the
way the flux surfaces are squeezed towards the outer wall,
is well represented by our model. Another point worthy of
note is that even near the second marginal point, e.g. in
Fig. 2c, the amplitude of the x_2 sideband is still rather small
when compared to x_1. This suggests that our truncation of the
trial function (3.16) at the first poloidal harmonics is a
reasonable approximation. Thus, although our results should
not be taken as quantitatively exact given the approximate
nature of our analytical model, we do not expect any signifi-
cant change in the topology of the stability diagram. Recently,
this has been confirmed numerically by means of large 2-dimen-
sional equilibrium and stability codes.[12]

CHAPTER 5

In the preceding three chapters we have examined the stability properties of internal kink modes within the framework of the ideal MHD theory. However, the behavior of these modes can be significantly affected when other effects which lie outside the scope of the ideal MHD theory are taken into consideration. In particular the "frozen-in law" Eq. (1.4) has been assumed valid throughout the plasma, and this need not be the case. In fact the singular behavior of the radial displacement given in Eq. (2.51) and (3.46) near the mode resonant surface is due precisely to this restriction. The addition of the slightest resistivity, or any other effects which cause the electric field to have a component parallel to the magnetic field, removes the singularity. Recalling that the growth rate of the ideal mode was determined from a boundary layer analysis at the mode resonant surface, it is clear that the introduction of non-ideal effects within this layer will affect the growth of these modes, and may enable the excitation of other modes as well. Qualitatively, these effects are most important near marginal stability points. In this chapter and its successors, we shall examine the behavior of these non-ideal modes. We adopt a kinetic description to describe these effects. In particular we shall assume that the temperatures are sufficiently high that we may neglect collisions.

5.1 External boundary conditions

Our approach shall take the form of a boundary layer analysis. That is, we shall assume the MHD description of $\underline{\xi}(r,\theta,\zeta)$ is adequate throughout the plasma, except for a narrow layer in the vicinity of the mode resonant surface. Within the layer we adopt a kinetic description. Here the mode structure is best described in terms of electromagnetic potentials ϕ, A. Finally an asymptotic matching is performed between the solutions in the two regions which determines the eigenfrequency ω of the mode.

In order to make analytic progress, certain assumptions must be made. We recall that the amplitude of the $m = 1$ harmonic of $\underline{\xi}$ is larger than that of the $m = 2$ harmonic. Thus we would expect the most significant effect to be on the $m = 1$ component. Accordingly we work with its radial component

$$\tilde{\xi}(r,\theta,\zeta,t) = \xi(r)e^{i\theta - in\zeta - i\omega t} \qquad (5.1)$$

As we saw in Chapters 2 and 3, $\xi(r)$ is singular near $r = r_1$, that is,

$$\frac{r_1}{\xi} \frac{d\xi}{dr} \simeq - \frac{\lambda_H r_1^2}{\pi (r-r_1)^2} . \qquad (5.2)$$

The quantity λ_H is given by an asymptotic matching of the expressions (2.57) and (3.48)
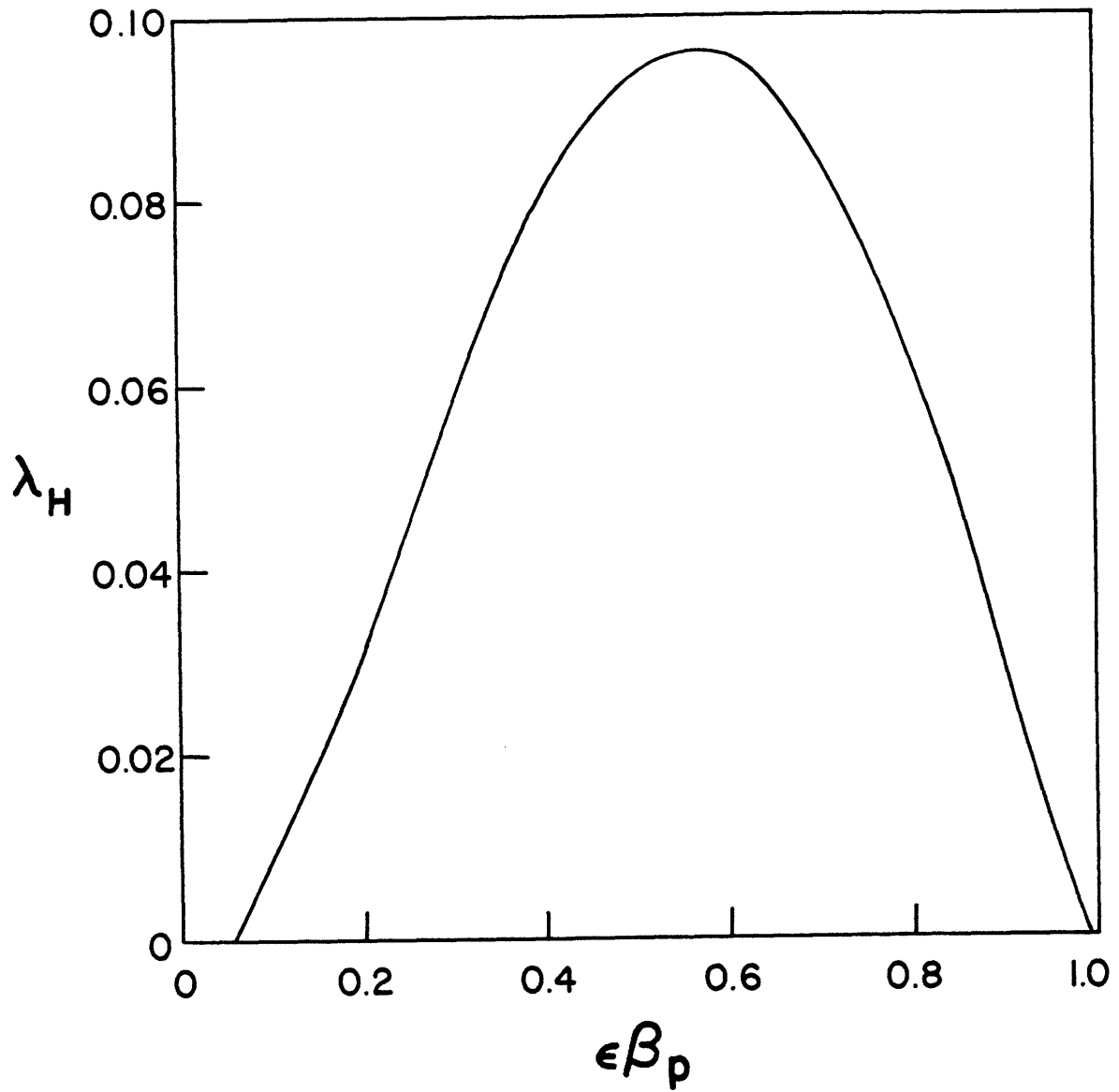
Figure 6: The MHD stability parameter $\lambda_H(\varepsilon\beta_p)$ for the profiles of Eq.(3.34) with $\varepsilon = 0.25$, $q_0 = 0.75$ and $n = 1$.

$$\lambda_H = \lambda_H^{\text{low}} + \lambda_H^{\text{finite}} - \lambda_H^{\text{match}} \qquad (5.3)$$

to handle arbitrary $\varepsilon\beta_p$ regimes. This function has been plotted in Fig. 6 for the case of the profiles (3.34). This approach is analogous to that adopted for the determination of the ideal growth rate, where an inner layer was required in order to determine the function $x_1(r)$.

In the second place, we are primarily interested in the radial structure of the mode, $\xi(r)$ defined by expression (5.1). If the inner layer is sufficiently narrow, we may perform the analysis using a simple slab model equilibrium. We note that this approximation neglects many of the toroidal effects studied in previous chapters, but this is consistent with our decision to work with the $m = 1$ component alone. The inclusion of these effects could be extremely difficult.

Thus within the layer we choose a cartesian coordinate system (with unit vectors $\underset{\sim}{e}_x$, $\underset{\sim}{e}_y$, $\underset{\sim}{e}_z$) whose x coordinate represents the radial variable $r - r_1$. If the y-axis is chosen to lie in the direction of the transformed wave vector $\underset{\sim}{k} = k_y \underset{\sim}{e}_y$ ($k_y = -1/r_1$ to $O(\varepsilon^2)$), then the magnetic field will lie along the z axis at the resonant surface and will have a slight shear:

$$\underset{\sim}{B} \simeq B_o(\underset{\sim}{e}_z + \frac{x}{L_s} \underset{\sim}{e}_y) , \qquad (5.4)$$

where the magnetic shear length

$$L_s \equiv R_0/ns \ , \tag{5.5}$$

B_0 is the toroidal magnetic field, R_0 is the major radius, and the shear, s, was defined in (2.13). Finally other equilibrium quantities, such as density and temperature , will depend on x alone.

As noted, within the layer the mode can be described as an electromagnetic perturbation

$$\tilde{\underline{E}} = - \underline{\nabla}\tilde{\phi} - \frac{1}{c}\frac{\partial\tilde{\underline{A}}}{\partial t} \tag{5.6a}$$

$$\tilde{\underline{B}} = \underline{\nabla} \times \tilde{\underline{A}} \ . \tag{5.6b}$$

Here we use the notation

$$\tilde{\phi} = \phi(x) \ e^{ik_y y - i\omega t} \tag{5.7}$$

for perturbed quantities. We shall assume that $\tilde{\underline{A}} = \tilde{A} \ \underline{e}_z$. Equivalently, we assume that the perturbed current lies parallel to the equilibrium magnetic field. This assumption requires[20,21] $\beta_j \ll 1$, where

$$\beta_j \equiv \frac{8\pi n T_j}{B_0^{\ 2}} \tag{5.8}$$

is the ratio of the jth species plasma pressure to the magnetic field energy. To relate these potentials to the displacement

$\tilde{\xi}$, we note that in the external (MHD) region, the "frozen-in law" (1.4) is valid. From its y and z components,

$$\tilde{\phi} = \frac{\omega B_o}{k_y c} \tilde{\xi} \tag{5.9a}$$

$$\tilde{A} = \frac{x B_o}{L_s} \tilde{\xi} \quad . \tag{5.9b}$$

Taken together, it is no surprise that these equations require that the parallel electric field

$$\tilde{E}_{||} = -ik_{||} \ (\tilde{\phi} - \frac{\omega}{k_{||} c} \tilde{A}) = 0 \tag{5.10}$$

in the MHD region, where we have introduced an effective parallel wavenumber $k_{||} = k_y x/L_s$. Finally, we recall that $\tilde{\xi}$, and therefore $\tilde{\phi}$, has an overall step function discontinuity in the vicinity of the layer. Using Eqs. (5.9) and (5.2) we can then summarize the MHD boundary conditions by

$$\phi(x) \simeq \phi_\infty \ [\ \Theta(-x) + \frac{r_1 \lambda_H}{\pi x}] \tag{5.11a}$$

$$A(x) \simeq \frac{k_{||} c}{\omega} \ \phi(x) \tag{5.11b}$$

as $x \to 0$, where ϕ_∞ is an arbitrary constant.

5.2 Field equations within reconnection layer

Within the layer, the potentials are governed by the constituentive Maxwell equations

$$-\nabla^2 \tilde{\phi} = 4\pi \sum_j e_j \tilde{n}_j \qquad (5.12a)$$

$$-\nabla^2 \tilde{A} = \frac{4\pi}{c} \sum_j \tilde{J}_{\parallel j} \qquad (5.12b)$$

where the summation is over plasma species of charge e_j, having perturbed densities $\tilde{n}_j$ and parallel currents $\tilde{J}_{\parallel j}$. We shall consider a two component plasma of electrons and positive ions. As indicated in Chapter 1, we shall assume the temperatures are sufficiently high that $\tilde{n}_j$ and $\tilde{J}_{\parallel j}$ must be calculated from a kinetic, collisionless description of both plasma species.

It is useful to bear in mind that there are several scale distances which are of interest in the analysis. For example the boundary conditions (5.11) scale x with a distance $x \sim r_1 \lambda_H$. On the other hand ion dynamics occur on a scale $x \sim \rho_i$, the ion gyro-radius. Finally electron inertia is important on a scale

$$x \sim \delta_e \equiv \frac{\omega L_s}{k_y v_e} , \qquad (5.13)$$

where v_e is the electron thermal speed. This distance arises because the parallel wavevector $k_{\parallel}$ depends on x. Thus an electron with parallel velocity $v_{\parallel}$ is resonant with the mode at $x = \delta_e \, v_{\parallel}/v_e$. It is customary at this point in the analysis of a boundary layer problem to introduce an inner variable scaled to the width of the layer, $\hat{x} \equiv x/\delta$. For the problem

at hand, this turns out to be more of a liability than an asset: we would introduce an additional scale distance δ to scale finite functions which are already scaled for small x (e.g. $P_e(\delta_e/|x|)$ in Eq. (5.41) below). For the sake of simplicity, we shall refrain from making δ explicit. However, when we refer to the limit $x \to \infty$, we really mean $x/\delta \to \infty$.

We shall first calculate the electron response to the perturbed potentials $\tilde{\phi}$, $\tilde{A}$. Anticipating that the electron gyro-radius ρ_e is negligibly smaller than other scales of interest, we shall average over their gyro-motion, and then identify particles with their guiding centers. This procedure is discussed in Appendix C; the result is that the electron distribution function $f_e(r, v_{||})$ satisfies[32]

$$\frac{\partial f_e}{\partial t} + v_{||} \; \underset{\sim}{b} \cdot \frac{\partial f_e}{\partial \underset{\sim}{r}} + \underset{\sim}{v}_E \cdot \frac{\partial f_e}{\partial \underset{\sim}{r}} - \frac{e}{m_e} \underset{\sim}{E} \cdot \underset{\sim}{b} \frac{\partial f_e}{\partial v_{||}} = 0 \; , \quad (5.14)$$

where $\underset{\sim}{v}_E = c \, \underset{\sim}{E} \times \underset{\sim}{b}/B$ is the drift velocity. To solve this equation we linearize in $\tilde{\phi}, \tilde{A}$. Thus we decompose f_e into an equilibrium piece and a perturbed piece

$$f_e = f_{Me} + \tilde{f}_e \qquad (5.15)$$

and note that in our geometry

$$\underset{\sim}{b} = (\underset{\sim}{e}_z + \frac{x}{L_s} \underset{\sim}{e}_y) + \frac{ik_y}{B_o} \tilde{A} \, \underset{\sim}{e}_x \; . \qquad (5.16)$$

Then f_{Me} must satisfy

$$\frac{\partial f_{Me}}{\partial t} + v_{||} \left(\frac{\partial f_{Me}}{\partial z} + \frac{x}{L_s} \frac{\partial f_{Me}}{\partial y} \right) = 0 \; , \tag{5.17}$$

which is accomplished with a Maxwellian distribution

$$f_{Me}(x, v_{||}) = \frac{n(x)}{\sqrt{\pi} \, v_e} e^{-v_{||}^2/v_e^2} \; , \tag{5.18}$$

where $v_e \equiv [2T_e(x)/m_e]^{1/2}$ is the electron thermal speed, and

$$n(x) = \int_{-\infty}^{\infty} dv_{||} \; f_{Me} \tag{5.19}$$

is the electron density. The linearized form of Eq.(5.14) is satisfied by

$$\tilde{f}_e = (k_{||} v_{||} - \omega)^{-1} \left\{ \left[\tilde{\phi} - \frac{v_{||}}{c} \tilde{A} \right] \frac{k_y c}{B_o} \frac{\partial f_{Me}}{\partial x} - \left[\tilde{\phi} - \frac{\omega}{k_{||}} \frac{\tilde{A}}{c} \right] \frac{ek}{m_e} \frac{\partial f_{Me}}{\partial v_{||}} \right\} \; . \tag{5.20}$$

The induced density and parallel current are then given by

$$\tilde{n}_e = \int_{-\infty}^{\infty} dv_{||} \; \tilde{f}_e \tag{5.21}$$

$$\tilde{J}_{\|e} = -e \int_{-\infty}^{\infty} dv_{\|} \; v_{\|} \; \tilde{f}_e \quad . \tag{5.22}$$

These two quantities are related by a continuity equation obtained by integrating (5.14) over $v_{\|}$, which gives

$$\frac{\partial n}{\partial t} + \nabla_{\|} \int_{-\infty}^{\infty} dv_{\|} \; (v_{\|} \; f_e) + v_E \cdot \nabla n = 0 \quad . \tag{5.23}$$

Inserting (5.15) in this equation, we find

$$\tilde{J}_{\|e} = \frac{en\omega}{k_{\|}} \left(\frac{\omega_{*e}}{\omega} \frac{e\tilde{\phi}}{T_e} - \frac{\tilde{n}_e}{n} \right) \tag{5.24}$$

where $\omega_{*e} \equiv k_y c T_e / eB r_n$ is the electron drift frequency, and $r_n^{-1} \equiv -d\ell n n/dx$. The integral (5.21) may be expressed in terms of the function

$$W(\lambda) \equiv \frac{1}{\sqrt{\pi}} \int_{-\infty}^{\infty} du \; \frac{ue^{-u^2}}{\lambda - u} \; , \quad \mathrm{Im}(\lambda) > 0 \tag{5.25}$$

which is related to the plasma dispersion function[33] $Z(\lambda)$ by $W(\lambda) = -[1 + \lambda Z(\lambda)]$. Thus Eq. (5.21) becomes

$$\tilde{n}_e = -\frac{ne}{T_e} (\tilde{\phi} - \frac{\omega}{k_{\|}c}\tilde{A}) \left\{ \frac{1}{2}\eta_e \frac{\omega_{*e}}{\omega} + W(\lambda_e) \left[1 - \frac{\omega_{*e}}{\omega} + \eta_e \frac{\omega_{*e}}{\omega}(\frac{1}{2} - \lambda_e^2) \right] \right\}$$
$$+ \frac{\omega_{*e}}{\omega} \frac{ne}{T_e} \tilde{\phi} \tag{5.26}$$

where $\lambda_e \equiv \delta_e/|x|$, and $\eta_e \equiv r_n \, d\ell n T_e/dx$. Then from (5.24) we find

$$\tilde{J}_{\parallel e} = \frac{ne^2\omega}{T_e k_{\parallel}} \left(\tilde{\phi} - \frac{\omega}{k_{\parallel}c}\tilde{A}\right) \left\{\frac{1}{2}\eta_e \frac{\omega*e}{\omega} + W(\lambda_e)\left[1 - \frac{\omega*e}{\omega} + \eta_e \frac{\omega*e}{\omega}(\frac{1}{2} - \lambda_e^2)\right]\right\}$$

(5.27)

As noted previously, these equations scale x with δ_e. Assuming $\omega \gtrsim \omega*e$, our neglect of ρ_e is justified since

$$\frac{\rho_e}{\delta_e} \lesssim \frac{v_e m_e c}{\delta* eB_o} = \frac{2r_n}{L_s} \sim \varepsilon \ll 1$$

(5.28a)

where we have introduced a convenient parameter

$$\delta* \equiv \omega*e \, L_s/k_y v_e \quad .$$

(5.28b)

In treating the ion terms, we cannot neglect ρ_i, although we shall still assume $\omega \ll \Omega_i \equiv eB_o/m_i c$. Furthermore, provided the ion temperature $T_i \lesssim T_e$, the wave ion resonances occur at distances $\delta_i \equiv \omega L_s/k_y v_i$, where v_i is the ion thermal speed, which are greater than either δ_e or ρ_i, that is, outside the layer. Thus we can safely assume $\omega \gg k_{\parallel} v_i$, which results in a considerable simplification.

We solve the Vlasov equation for the ion distribution function f_i,

$$\frac{\partial f_i}{\partial t} + \underset{\sim}{v} \cdot \frac{\partial f_i}{\partial \underset{\sim}{r}} + \frac{e}{m_i}\left(\underset{\sim}{E} + \frac{1}{c}\underset{\sim}{v} \times \underset{\sim}{B}\right) \cdot \frac{\partial f_i}{\partial \underset{\sim}{v}} = 0$$

(5.29)

by the method of characteristics[34], as detailed in Appendix D. The solution is of the form

$$f_i = f_{Mi} + \tilde{f}_i \quad , \tag{5.30}$$

where the first term gives the equilibrium ion distribution function as a Maxwellian with a slow spatial variation,

$$f_{Mi}(x, \underline{v}) = \frac{n(x)}{\pi^{3/2} v_i^2} e^{-v^2/v_i^2} \quad , \tag{5.31}$$

where $v_i = [2T_i(x)/m_i]^{1/2}$.

The perturbed ion density and parallel current are given by expressions analogous to Eqs. (5.21-22),

$$\tilde{n}_i = \int d^3v \, \tilde{f}_i \tag{5.32}$$

$$\tilde{J}_{\parallel i} = e \int d^3v \, v_z \, \tilde{f}_i \quad . \tag{5.33}$$

The ion response is best treated with the introduction of a Fourier representation for the rapid variation of the potentials. Thus we define a Fourier transform functional $\mathfrak{F}$, defined by

$$\mathfrak{F}[\phi](k) \equiv \int_{-\infty}^{\infty} dx \, e^{-ikx} \, \phi(x) \quad , \tag{5.34a}$$

with an inverse given by

$$\mathfrak{J}^{-1}[\phi](x) = \int_{-\infty}^{\infty} \frac{dk}{2\pi} e^{ikx} \phi(k) , \qquad (5.34b)$$

and in performing the integral (5.34a), the slow variation of $\phi(x)$ is taken to be constant. Also note that the limits of integration in (5.34a) treat x as an inner variable.

The integrals (5.32,33) are performed in Appendix D. If we define

$$\Phi(k) \equiv \mathfrak{J}[\phi](k) , \quad \Psi(k) \equiv \mathfrak{J}[A](k) \qquad (5.35)$$

the result can be written

$$\mathfrak{J}[\tilde{n}_i] = \frac{ne}{T_i} \tilde{\Phi} \left\{ S_0 (1 - \frac{\omega_{*i}}{\omega}) - 1 + \frac{\omega_{*i}}{\omega} \eta_i b (S_0 - S_1) \right\}$$

$$- \frac{nev_i}{T_i c} \tilde{\Psi} \frac{k_{||} v_i}{\omega} \left\{ S_0 [1 - \frac{\omega_{*i}}{\omega} (1 + \eta_i)] + \frac{\omega_{*i}}{\omega} \eta_i b (S_0 - S_1) \right\}$$

$$(5.36)$$

and

$$\mathfrak{J}[\tilde{J}_{||i}] = \frac{e^2 n\omega}{T_i k_{||}} (\tilde{\Phi} - \frac{\omega}{k_{||} c} \tilde{\Psi}) \frac{k_{||}^2 v_i^2}{\omega^2} \left\{ S_0 [1 - \frac{\omega_{*i}}{\omega} (1 + \eta_i)] \right.$$

$$\left. + \frac{\omega_{*i}}{\omega} \eta_i b (S_0 - S_1) \right\} , \qquad (5.37)$$

where $\omega_{*i} = -k_y c T_i / e B_o r_n$, $\eta_i = r_n \, d\ell n T_i / dx$, $b = \frac{1}{2} k^2 \rho_i^2$
and $S_{o,1}(b) = \exp(-b) I_{o,1}(b)$, where $I_{o,1}$ are modified Bessel
functions. Note that Eqs. (5.36,37) still retain slow equi-
librium x-dependence through $n(x)$, $T_i(x)$, $k_{||}(x)$. Now as
long as $\phi \gtrsim (\omega/k_{||} c) A$, the assumption $\omega >> k_{||} v_i$ renders the
second term of (5.36) negligible. Thus the ions couple only
to the electrostatic potential.

Now we may return to Poisson's equation (5.12a) with
the expressions (5.26,36). For the identified scales
$\delta \sim \delta_e, \rho_i$, $\nabla^2 \phi$ is negligible, so we are left with the quasi-
neutrality condition

$$\tilde{n}_e = \tilde{n}_i . \tag{5.38}$$

If we compare the currents (5.27,37), we note that

$$\frac{\tilde{J}_{||i}}{\tilde{J}_{||e}} \sim \frac{T_e}{T_i} \frac{k_{||}^2 v_i^2}{\omega^2} << 1 , \tag{5.39}$$

hence the parallel conductivity is due primarily to finite
electron inertia, and $\tilde{J}_{||i}$ may be ignored. We also note that
$d^2/dx^2 >> k_y^2$. Thus Ampère's law becomes

$$\frac{d^2 \tilde{A}}{dx^2} = - \frac{4\pi}{c} \tilde{J}_{||e} . \tag{5.40}$$

After factoring out the common exponential factors in (5.38,40),
we arrive at a pair of equations for $\phi(x)$, $A(x)$:

$$\phi(1+\hat{\omega}\tau) - (\phi - \frac{\delta_e v_e}{xc}A)P_e(\frac{\delta_e}{|x|}) = \mathcal{F}^{-1}\left[\mathcal{F}[\phi]G\right](x) \tag{5.41a}$$

$$\frac{d^2A}{dx^2} = -\frac{2\omega_{pe}^2}{v_e c}\frac{\delta_*}{x}(\phi - \frac{\delta_e v_e}{xc}A)P_e(\frac{\delta_e}{|x|}) \ , \tag{5.41b}$$

where $\hat{\omega} = \omega/\omega_{*e}$, $\tau = T_e/T_i$, $\omega_{pe}^2 = 4\pi ne^2/m_e$. The conductivity function P_e is defined

$$P_e(\lambda_e) = \frac{1}{2}\eta_e + W(\lambda_e)[\hat{\omega} - 1 + \eta_e(\frac{1}{2} - \lambda_e^2)] \ . \tag{5.42}$$

Noting that $\omega_{*i} = -\omega_{*e}/\tau$, we may write

$$G(k) = S_o(1 + \hat{\omega}\tau) - \eta_i b(S_o - S_1) \ , \tag{5.43}$$

which is the non-adiabatic ion response function. The right hand side of (5.41a) gives this ion response to ϕ correct to all orders of ρ_i. This term is an integral operator which is in fact a convolution

$$\mathcal{F}^{-1}\left[\mathcal{F}[\phi]G\right](x) = \int_{-\infty}^{\infty}d\hat{x}\phi(x-\hat{x})g(\hat{x}) = (g \circ \phi)(x) \ , \tag{5.44}$$

where $g \equiv \mathcal{F}^{-1}[G]$. Manifest in (5.44) is the fact that the ion response to ϕ is nonlocal.

Finally we note that it is possible to transform to a pair of potentials with definite parity. In fact

$$\phi \rightarrow \phi - \frac{1}{2} \phi_\infty \qquad (5.45a)$$

$$A \rightarrow A - \frac{x}{2} \frac{c}{\delta_e v_e} \phi_\infty \qquad (5.45b)$$

leaves (5.41) invariant and makes ϕ odd, A even in x. In terms
of these new potentials, the boundary conditions for matching
to the MHD region are

$$\phi(x) \sim \phi_\infty \left(\frac{r_1 \lambda_H}{\pi x} - \frac{x}{2|x|} \right) \qquad (5.46a)$$

$$A(x) \sim \frac{c}{\delta_e v_e} x\phi(x) \qquad (5.46b)$$

as $|x| \rightarrow \infty$. In the next two chapters we shall examine solutions
to the system (5.41) with (5.46).

CHAPTER 6

In this chapter we examine the stability properties of modes that owe their existence to the decoupling of plasma motion from that of the field lines. Thus we look for these modes in regimes of ideal MHD stability, that is, where $\lambda_H < 0$. Referring to Fig. 6, we identify two such $\varepsilon\beta_p$ regimes. However, in this analysis we must assume $\hat{\beta} \ll 1$, where

$$\hat{\beta} \equiv \frac{\beta_e}{2} \left(\frac{L_s}{r_n}\right)^2 = \frac{4\pi n T_e}{B_o^2} \left(\frac{L_s}{r_n}\right)^2 \quad , \tag{6.1}$$

so that our results are directly applicable only to the low-beta regime. We shall also restrict our attention to the realistic case $T_e \sim T_i$ and $\eta_e \gtrsim 1$ which was not covered by previous treatments[16]. For simplicity we shall assume $\delta_e \ll \rho_i$, in which case the solution of Eqs. (4.51,46) can be given in terms of certain integral expressions[17]. Finally a numerical approach may be used to study these expressions and complete the analysis of these modes[23].

The analysis presented in this chapter was originally developed for the treatment of $m \geq 2$ reconnecting modes[17,23]. When $|\lambda_H|$ is fairly large, the boundary conditions (5.46) for the $m = 1$ case are essentially the same as in the $m \geq 2$ case, and so the same analysis may be applied[21]. However, for the sake of definiteness, the original analysis took

$k_y > 0$, while we have $k_y < 0$. Rather than redo the analysis
making the change of signs explicit, we shall instead repeat
the analysis with $k_y > 0$ and note that the physical results
$\text{Re}(\omega)/k_y$ and growth rate $\text{Im}(\omega)$ should be independent of the
sign of k_y. (Since the boundary conditions are real, working
with either (5.7) or its complex conjugate should produce
the same results.)

6.1 Integral formulation of collisionless reconnecting modes

In the analysis of reconnecting modes, it is conventional
to asymptotically match solutions of Eq. (5.41) to the boundary
conditions via the discontinuity Δ' in the derivative of the
perturbed vector potential

$$A \simeq A_o \left(1 + \frac{1}{2} \Delta' |x|\right) , \tag{6.2}$$

where comparison with (5.46) gives the constant $A_o = cr_1 \lambda_H \phi_\infty / (v_e \delta_e \pi)$ and

$$\Delta' = - \frac{\pi}{r_1 \lambda_H} , \tag{6.3}$$

which is positive for $\lambda_H < 0$. Referring to Ampère's law (5.41b),
we find (6.2) remains valid across the region provided $\hat{\beta} \ll 1$.
Adopting this "constant A approximation", the integral of
Ampère's law across the reconnecting region gives

$$\Delta' = \frac{2\delta_*}{d^2} \int_{-\infty}^{\infty} dx \, \frac{1}{x} \, P_e \left(\frac{\delta_e}{|x|}\right) \left(\frac{\delta_e}{x} - \hat{\phi}\right) \tag{6.4}$$

where $\hat{\phi}(x) = c\phi(x)/(v_e A_o)$, $d^2 = c^2/\omega_{pe}^2$ is the electron skin depth, and δ_* was defined in Eq. (5.28b). In this approximation the quasi-neutrality equation (5.41a) becomes

$$g \circ \hat{\phi} - (1 + \hat{\omega}\tau)\hat{\phi} = P_e \left(\frac{\delta_e}{|x|}\right)\left(\frac{\delta_e}{x} - \hat{\phi}\right) . \tag{6.5}$$

A slight rearrangement gives

$$\hat{\phi} = \frac{-(\delta_e/x)P_e}{1 + \hat{\omega}\tau - P_e} + \frac{g \circ \hat{\phi}}{1 + \hat{\omega}\tau - P_e} , \tag{6.6}$$

which allows us to rewrite (6.4) as

$$\Delta' = \frac{4\delta_*}{d^2}(\Delta_o - \Delta_1) \tag{6.7}$$

where

$$\Delta_o = (1 + \hat{\omega}\tau) \int_0^\infty \frac{dx}{x} \frac{(\delta_e/x)\, P_e\, (\delta_e/|x|)}{1 + \hat{\omega}\tau - P_e(\delta_e/|x|)} , \tag{6.8}$$

and

$$\Delta_1 = \frac{1}{2} \int_{-\infty}^\infty \frac{dx}{x} \frac{g \circ \hat{\phi}\, P_e(\delta_e/|x|)}{1 + \hat{\omega}\tau - P_e(\delta_e/|x|)} . \tag{6.9}$$

Now for $\delta_e \ll \rho_i$, $\Delta_1/\Delta_o \sim \delta_e/\rho_i$. Thus, for $d^2\Delta'/(4\delta_*) \ll 1$, the mode frequencies are determined by $\Delta_o(\hat{\omega}_o) = 0$. Stability

properties are then determined by Δ' and $\Delta_1(\hat{\omega}_0)$.

6.2 Evaluation of Δ_0

The function $\Delta_0(\hat{\omega})$ is defined by a contour integral which lies along the positive real x-axis when $\text{Im}(\hat{\omega})$ is sufficiently large. Since we require Δ_0 to be an analytic function of $\hat{\omega}$, we must deform the contour of integration C so that it is crossed by no poles of the integrand. Changing variables, $\lambda \equiv \delta_e/x$, Eq. (6.8) becomes

$$\Delta_0 = (1 + \hat{\omega}\tau) \int_C d\lambda \, \frac{P_e(\lambda)}{D_e(\lambda)} \tag{6.10}$$

where the denominator is

$$D_e(\lambda) = 1 + \hat{\omega}\tau - P_e(\lambda) \quad . \tag{6.11}$$

The contour C must be deformed from the positive real λ-axis so as to avoid the zeros of $D_e(\lambda)$. Since the integrand is zero along $|\lambda| = \infty$, any ray emanating from the origin and satisfying this criterion may be chosen.

The behavior of the zeros of $D_e(\lambda)$ are determined from several observations. First, for $|\hat{\omega}| \to \infty$, no zeros of $D_e(\lambda)$ exist in the upper half λ-plane. To determine if zeros of $D_e(\lambda)$ pass into the upper half λ-plane, we look for zeros of $D_e(\lambda)$ for real values of λ as a function of real $\hat{\omega}$. We find that for $\hat{\omega} \to -1/\tau$, $D_e(\infty) \to 0$ while as $\hat{\omega} \to 0$, $D_e(0) \to 0$. If in addition $\eta_e > 2$, then $D(\lambda_\pm) = 0$ when $\hat{\omega} = \hat{\omega}_+ \equiv (\eta_e/2-1)/\tau$, where
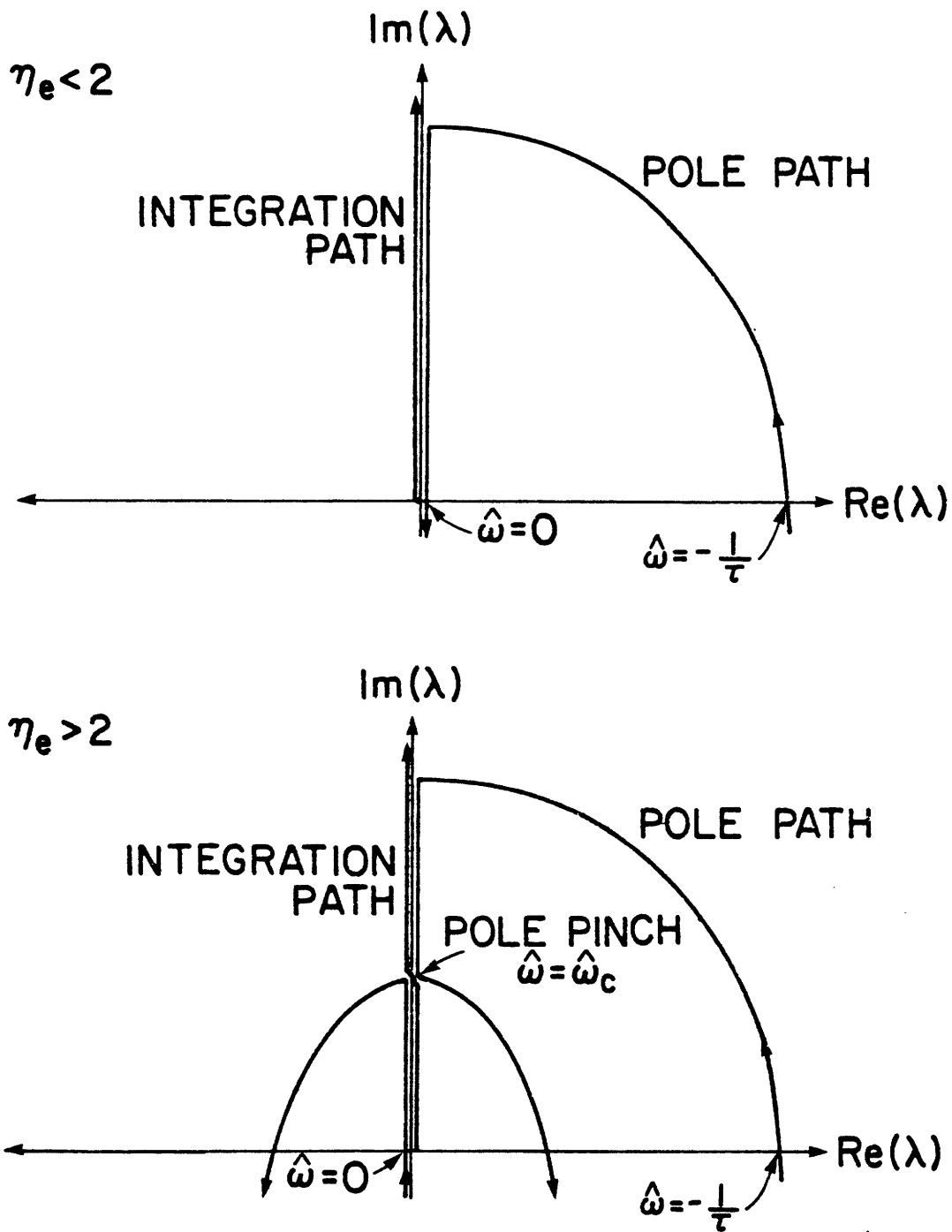
Figure 7: Poles of the integrand and integration contour for $\Delta_o(\hat{\omega})$.

$\lambda_{\pm}^2 = (\hat{\omega} - 1)/\eta_e + 1/2$. Thus the number of poles in the upper

half λ-plane will depend on whether η_e is greater or less than

2. Pole plots for the integrand are shown in Fig. 7.

For $\eta_e < 2$, there is only one pole in the upper half

plane, which is present for $-1/\tau < \hat{\omega} < 0$. This pole is found on

the imaginary λ-axis since $W(\lambda)$ is then real. In this case, we

integrate along the negative real axis, thereby avoiding the

pole. The resulting value of $\Delta_o(\hat{\omega})$ is complex for $\hat{\omega}$ in this

range. For other values of $\hat{\omega}$ (i.e. $\hat{\omega} < -1/\tau$, $\hat{\omega} > 0$), it is

convenient to integrate along the imaginary axis; for these

cases Δ_o is purely imaginary.

For $\eta_e > 2$, two poles may cross into the upper half

λ-plane. When $\hat{\omega} < 0$, only one of these poles is present,

and the evaluation of Δ_o proceeds as in the $\eta_e < 2$ case. As

$\hat{\omega}$ is increased through zero, a second pole crosses the real

λ-axis (at $\lambda = 0^-$) and moves up the imaginary axis. At some

critical frequency $\hat{\omega} = \hat{\omega}_c$, the two poles meet at $\lambda = \lambda_c$. For

larger values of $\hat{\omega}$, the two poles split off the axis and move

towards the lower half plane, eventually crossing the real

axis when $\hat{\omega} = \hat{\omega}_+$ at $\lambda = \lambda_+$ and λ_-. For $\hat{\omega} > \hat{\omega}_c$, Δ_o can be evalu-

ated with an integral along the imaginary axis. In the range

$0 < \hat{\omega} < \hat{\omega}_c$, we must choose a contour which snakes between the

poles. In practice this is accomplished with a contour along

the real axis and a residue from a pole on the imaginary axis,

$$R_e(\hat{\omega}) = \mp 2\pi i \frac{P_e(\lambda_p(\hat{\omega}))}{D_e'(\lambda_p(\hat{\omega}))} \qquad (6.12)$$

where λ_p is the location of the pole ($|\lambda_p| \gtrless |\lambda_c|$), and the prime denotes a derivative with respect to λ.

At the critical frequency $\hat{\omega}_c$, there is a double pole at λ_c, thus $D_e(\lambda_c) = D_e'(\lambda_c) = 0$. Introducing a frequency-independent function

$$B_e(\lambda) = 1 - \frac{1}{2} \eta_e + W(\lambda) [1 + \eta_e (\lambda^2 - \frac{1}{2})] \ , \tag{6.13}$$

we find $\hat{\omega}_c$ and λ_c are a solution of the system

$$\hat{\omega}_c [\tau - W(\lambda_c)] + B_e(\lambda_c) = 0 \tag{6.14a}$$

$$- \hat{\omega}_c W'(\lambda_c) + B_e'(\lambda_c) = 0 \ . \tag{6.14b}$$

On the imaginary axis these equations are real; eliminating $\hat{\omega}_c$ between them yields a single equation which may be solved numerically for λ_c and, therefore, $\hat{\omega}_c$.

Finally, the asymptotic approximation to the W-function

$$W(\lambda) \quad \frac{1}{2\lambda^2} + \frac{3}{4\lambda^4} + \frac{15}{8\lambda^6} + \ldots \tag{6.15}$$

as $|\lambda| \to \infty$, may be used to approximate the integrand to order λ^{-4}. Thus for the integral from λ_m to ∞, we have, to order λ_m^{-3},

$$I_O(\lambda_m, \hat{\omega}) = \frac{\hat{\omega} - 1 - \eta_e}{2\lambda_m} + \frac{\hat{\omega}(\hat{\omega}+1-2\eta_e)+\eta_e^2 - 4\eta_e-2}{12\lambda_m^3(1 + \hat{\omega}\tau)} \qquad (6.16)$$

Combining Eqs. (6.10, 12, 16), we find

$$\Delta_O(\hat{\omega}) = (1 + \hat{\omega}\tau) \int_O^{\lambda_m} d\lambda \frac{\hat{\omega}W(\lambda) + 1 - B_e(\lambda)}{\hat{\omega}[\tau - W(\lambda)] + B_e(\lambda)}$$

$$+ I_O(\lambda_m, \hat{\omega}) + R_e(\hat{\omega}) \quad . \qquad (6.17)$$

To calculate $\Delta_O(\hat{\omega})$ we first store values of $W(\lambda)$, $B_e(\lambda)$ along the required axes from $|\lambda| = 0$ to $|\lambda_m|$. Then Simpson's rule may be applied to the first term of Eq. (6.17) for all $\hat{\omega}$; additional evaluations of $W(\lambda)$, $B_e(\lambda)$ are made only for $0 < \hat{\omega} < \hat{\omega}_c$, when $R_e(\hat{\omega})$ is required.

Nyquist plots of $\Delta_O(\hat{\omega})$ are readily obtained by evaluating Eq. (6.17) for real values of $\hat{\omega}$. Typical plots for $\eta_e < 2$ and $\eta_e > 2$ are shown in Figs. 8 and 9, respectively. In addition to the poles at $\hat{\omega} = 0$, $\hat{\omega}_c$, ∞, we note that there are two zeros. One of these, at $\hat{\omega} = -1/\tau$, occurs at a branch point of Δ_O and has a phase velocity $\omega/k_y = -cT_i/(eB_o r_n)$. The other zero occurs for $\hat{\omega} = \hat{\omega}_o > 0$, and therefore has a phase velocity in the opposite direction. This frequency is primarily a function of η_e and is only weakly dependent on T_e/T_i. We may obtain a good estimate[16] for ω_o by neglecting $\hat{\phi}$ altogether in Eq. (6.4), and rewriting
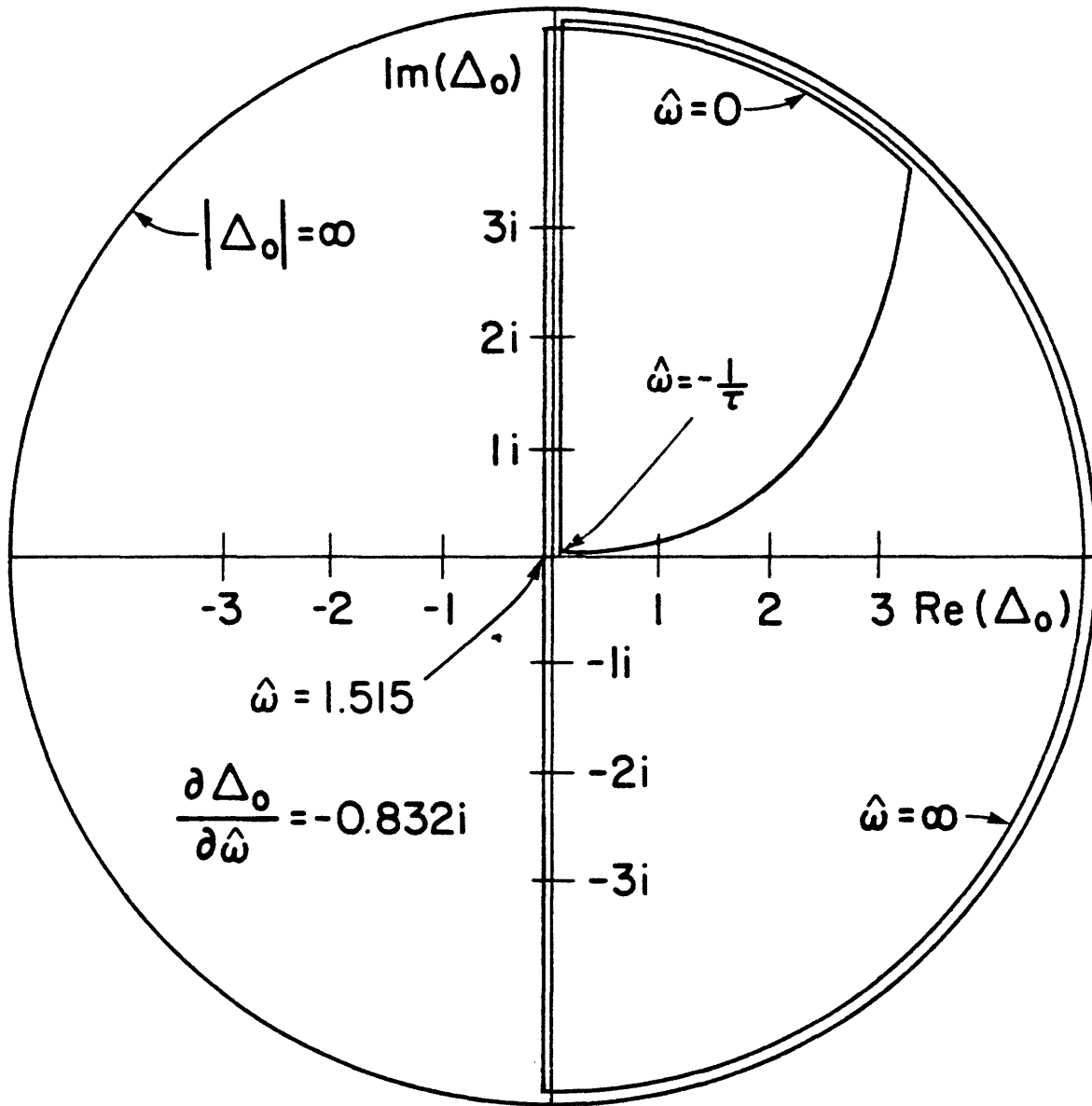
Figure 8: Nyquist plot of $\Delta_o(\hat{\omega})$ for $\eta_e = 1.0$, $\tau = 1$.
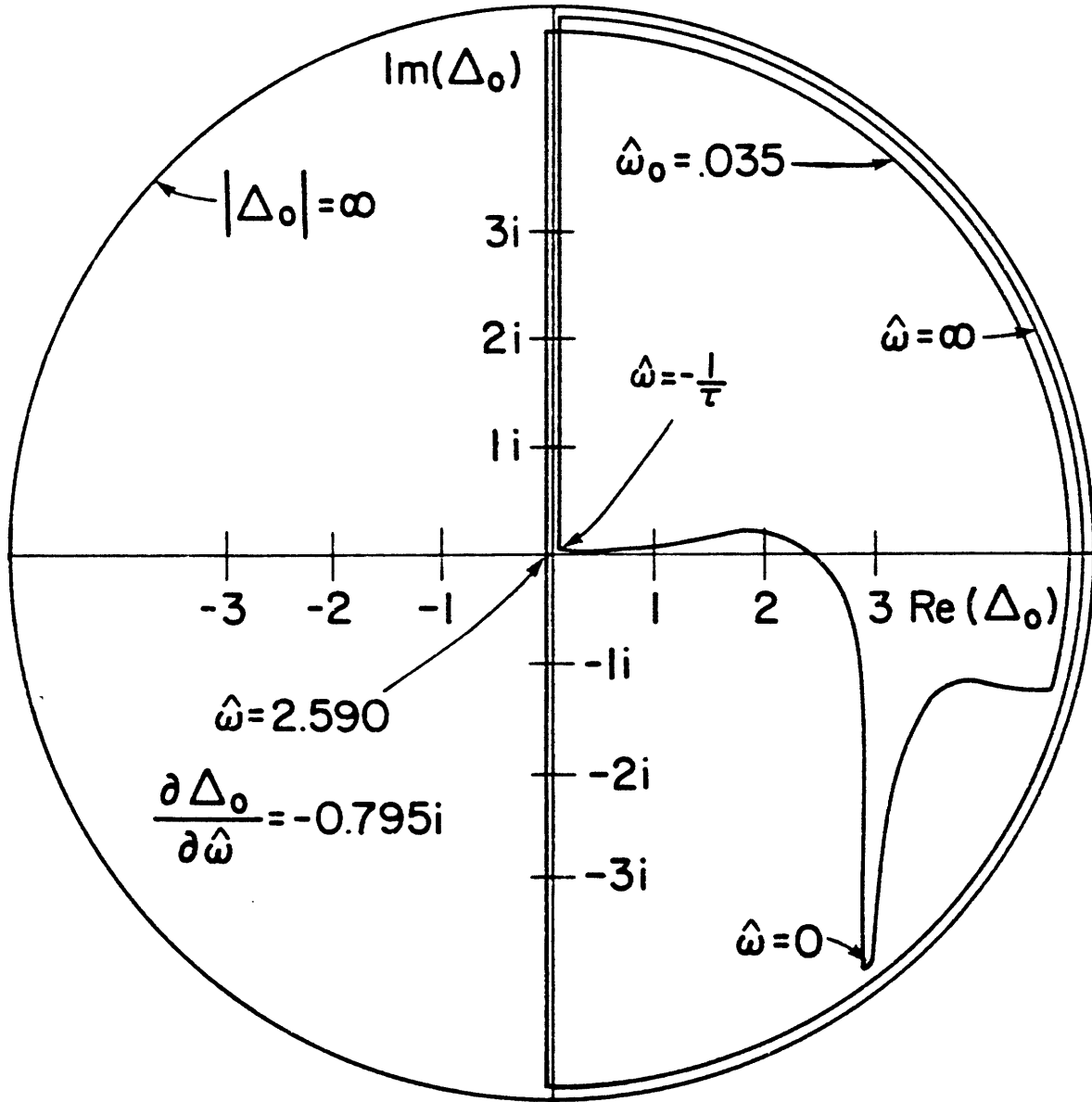
Figure 9: Nyquist plot of $\Delta_o(\hat{\omega})$ for $\eta_e = 3.0$, $\tau = 1$.

$$P_e(\lambda) = W(\lambda) [\hat{\omega} - (1 + \frac{1}{2}\eta_e)] + \frac{1}{2}\eta_e \frac{d}{d\lambda} [\lambda W(\lambda)] \quad . \tag{6.18}$$

Then we have

$$\Delta_0 = [\hat{\omega} - (1 + \frac{1}{2}\eta_e)] \int_0^\infty d\lambda \ W(\lambda) \tag{6.19}$$

so that

$$\hat{\omega}_0 \simeq 1 + \frac{1}{2}\eta_e \quad . \tag{6.20}$$

Both of these functions are displayed in Fig. 10.

Recalling Eq. (6.7), the mode with $\hat{\omega} = \hat{\omega}_c$ is unstable when $R_e(\Delta' d^2/(4\delta_*) + \Delta_1) > 0$. The growth rate can be estimated from a Taylor series expansion of $\Delta_0(\hat{\omega})$ around $\hat{\omega}_0$:

$$\gamma = \frac{R_e[\Delta' d^2/(4\delta_*) + \Delta_1(\hat{\omega}_0)]}{\left| \partial \Delta_0(\hat{\omega})/\partial\hat{\omega} \right|_{\hat{\omega} = \hat{\omega}_0}} \ |\omega_*| \tag{6.21}$$

The mode with $\hat{\omega} = -1/\tau$ requires $Im\Delta_1 > 0$ in addition for instability. Thus to assess the stability properties of these modes, we need to examine Δ_1.

6.3 Stability properties

The integral expression for Δ_1 can be greatly simplified by the introduction of Fourier transforms. The main advantage is that the convolution factor $g \circ \hat{\phi}$ reduces to a product of transforms $G\hat{\phi}$. Our remaining task will be to find a suitable expression for the unknown $\hat{\phi}$.
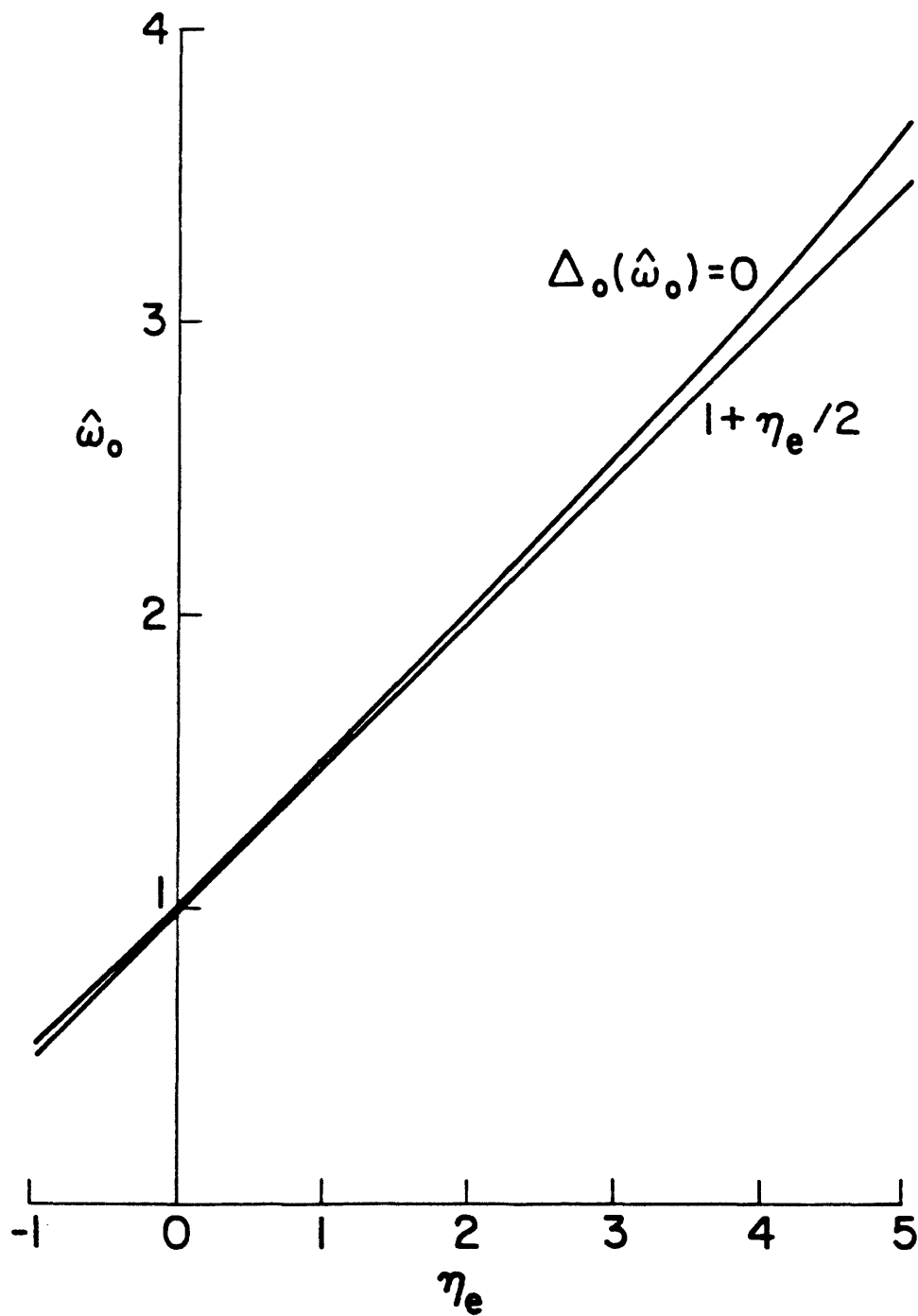
Figure 10: Plot of $\hat{\omega}_o(\eta_e)$ defined by $\Delta_o(\hat{\omega}_o) = 0$, and the approximation $\hat{\omega}_o \approx 1 + \eta_e/2$.

Recalling Eqs. (5.33a,44), we note

$$(g \ast \hat{\phi})(x) = \int_{-\infty}^{\infty} \frac{dk}{2\pi} \hat{\phi}(k) G(k) e^{ikx} \tag{6.22}$$

where $\hat{\phi} = \Im[\phi]$, and G is given by Eq. (5.43). Then if we define a function

$$s_e(x) = \frac{(\delta_e/x) P_e(\delta_e/|x|)}{1 + \hat{\omega}\tau - P_e(\delta_e/|x|)} \quad , \tag{6.23}$$

introduce Eqs. (6.22,23) in the expression (6.9) for Δ_1, and interchange the order of k- and x-integration, we find

$$\Delta_1 = \frac{1}{\delta_e} \int_0^{\infty} \frac{dk}{2\pi} S_e(-k) \hat{\phi}(k) G(k) \tag{6.24}$$

where $S_e = \Im[s_e]$, and we have used the fact that S_e, $\hat{\phi}$ and G are odd, odd and even functions of k.

To proceed, we need to determine $\hat{\phi}(k)$. We cannot solve Eq. (6.5) for $\hat{\phi}(k)$ exactly, but we can construct an approximate solution when $\delta_e \ll \rho_i$. Note that (6.20) implies

$$\frac{\delta_e}{\rho_i} \sim \frac{\delta_*}{\rho_i} = \frac{1}{2} \frac{L_s}{r_n} \left(\frac{m_e}{m_i} \frac{T_e}{T_i} \right)^{1/2} \quad . \tag{6.25}$$

The most rapid variations in $\hat{\phi}(x)$ occur for $x \sim \delta_e$. In this regime the ion response is mostly adiabatic[17], so the second

term of Eq. (6.6) is negligible. Taking the Fourier transform
we find

$$\hat{\phi}(k) \simeq - S_e(k) \qquad (6.26)$$

for $k \gtrsim 1/\delta_e$. Conversely, the long-wavelength limit is deter-
mined by $x \sim \rho_i$ for which $P_e \simeq 1 - \hat{\omega}$. The Fourier transform
of Eq. (6.6) then gives

$$\hat{\phi}(k) \simeq i\pi\delta_e \, \text{sign}(k) \, \frac{1 - \hat{\omega}}{\hat{\omega}(1 + \tau) - G(k)} \qquad (6.27)$$

which is valid for $k \lesssim 1/\rho_i$.

These expressions are asymptotically matched. Noting
that $G(k \to \infty) = 0$, and

$$S_e(k \to 0) = i\pi\delta_e \, \frac{\hat{\omega} - 1}{\hat{\omega}(1 + \tau)} \quad , \qquad (6.28)$$

we see that the $k \to 0$ limit of (6.26) is equal to the $k \to \infty$
limit of Eq. (6.27). An asymptotically matched expression is

$$\hat{\phi}(k) = - S_e(k) \, \frac{\hat{\omega}(1 + \tau)}{\hat{\omega}(1 + \tau) - G(k)} \quad . \qquad (6.29)$$

which is valid for all k to leading order in δ_e/ρ_i.

Numerical evaluation of $S_e(k)$ is complicated by the $1/x$
decay of $s_e(x)$, which leads to a discontinuity in $S_e(k)$ at

$k = 0$. The discontinuity is removed from the numerical procedure by introducing

$$t_o(x) = \frac{S_e(k \to 0)}{-i\pi} \frac{x \, \delta_e}{x^2 + x_o^2} \tag{6.30a}$$

$$t_1(x) = s_e(x) - t_o(x). \tag{6.30b}$$

We then find $(T_{o,1} \equiv \mathfrak{F}[t_{o,1}])$

$$T_1(k) = S_e(k \to 0) \, \text{sign}(k) \, e^{-|kx_o|} \tag{6.31}$$

so that $T_1(k)$ is continuous as $k \to 0$. The choice of a value for the parameter x_o is quite arbitrary; in practice it was chosen to minimize the importance of $T_1(k)$ near $k = 0$. (Typically $x_o \simeq 10\delta_e$.)

Since $t_1(x)$ decays as $1/x^2$, we approximate its Fourier transform as an integral over a finite domain approximated by a summation,

$$T_1(k) \simeq h \sum_{n=1}^{N} e^{-ikx_n} t_1(x_n) \tag{6.32a}$$

$$x_n = h \left(\frac{N-1}{2} - n\right) \tag{6.32b}$$

to leading order in the small step size h. Note that Eq. (6.32) is only valid for $k \ll 2\pi/h$; however, the integral (6.24) converges before large k-values are reached. Finally,

if we restrict attention to a discrete set of k-values,

$k_\ell = 2\pi\ell/hN$, $\ell = 0,1, \ldots,$ Eq. (6.32a) becomes

$$T_1(k_\ell) = e^{-2\pi i(\frac{1}{2} - \frac{1}{N})} \sum_{n=1}^{N} e^{2\pi i n\ell/N} t_1(x_n) . \qquad (6.33)$$

This summation can be economically performed by using the fast Fourier transform technique[35]. Satisfactory results were obtained for $h \lesssim 0.1\delta_e$ and $N = 2^m$, $m \gtrsim 11$.

We can now calculate $\hat{\Phi}(k)$; a typical case is shown in Fig. 11. The sharp peak in $\text{Im}\hat{\Phi}$ occurs when Eq. (6.27) is valid and reflects the variation of G on the scale $k \sim 1/\rho_i$. For $k \sim 1/\delta_e$, Eq. (6.26) is valid; the oscillatory behavior of $\hat{\Phi}$ is due to δ_e, since G decays as $1/k$.

Numerical values of $\Delta_1(\eta_e)$ are plotted in Fig. 12 for several values of L_s/r_n. A deuterium plasma with $T_e = T_i$ was assumed, hence $\eta_e = \eta_i$, and $\delta_*/\rho_i \simeq (L_s/r_n)/120$. If we rewrite Eq. (6.24), using Eq. (6.29),

$$\Delta_1 = \int_0^\infty \frac{dk}{2\pi} S_e(k)^2 \left[\frac{\hat{\omega}(1+\tau)G(k)}{\hat{\omega}(1+\tau) - G(k)} \right] , \qquad (6.34)$$

we can explain some of the qualitative features of these plots. Comparison of Eq. (6.29) with Fig. 11 shows that as $k \to 0$, $\text{Im}S_e^2$, $\text{Re}S_e^2 < 0$. Since the quantity in brackets in Eq. (6.34) is sharply peaked at $k = 0$, we find that most of the contribution to the integral comes from the range $0 < k \lesssim 1/\rho_i$, thus $\Delta_1 \sim \delta_e/\rho_i$, and $\text{Im}\Delta_1$, $\text{Re}\Delta_1 < 0$.
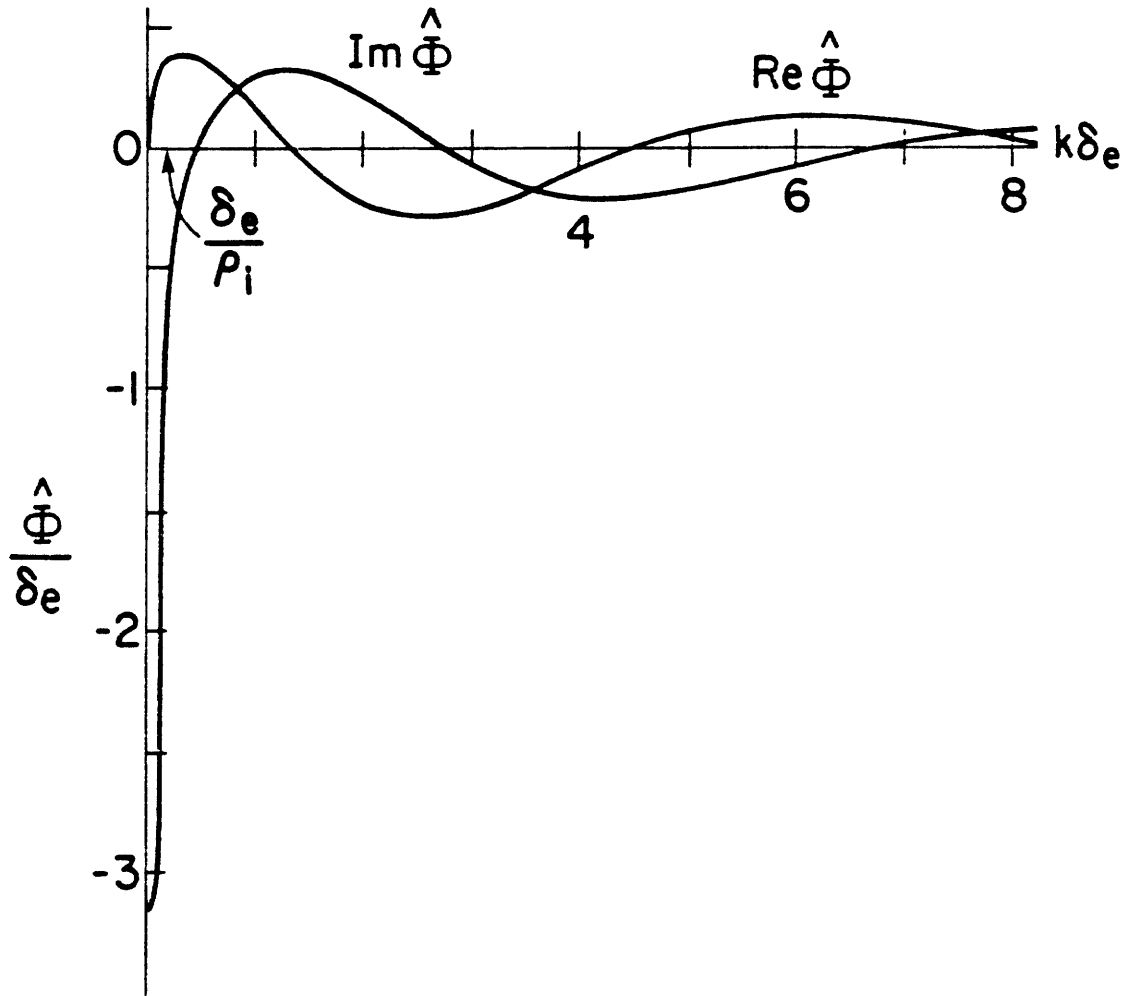
Figure 11: Plot of $\hat{\Phi}(k)$ for $\eta_e = \eta_i = 1.0$, $\tau = 1$, $\hat{\omega} = 1.5$, $\rho_i/\delta_e = 8$.
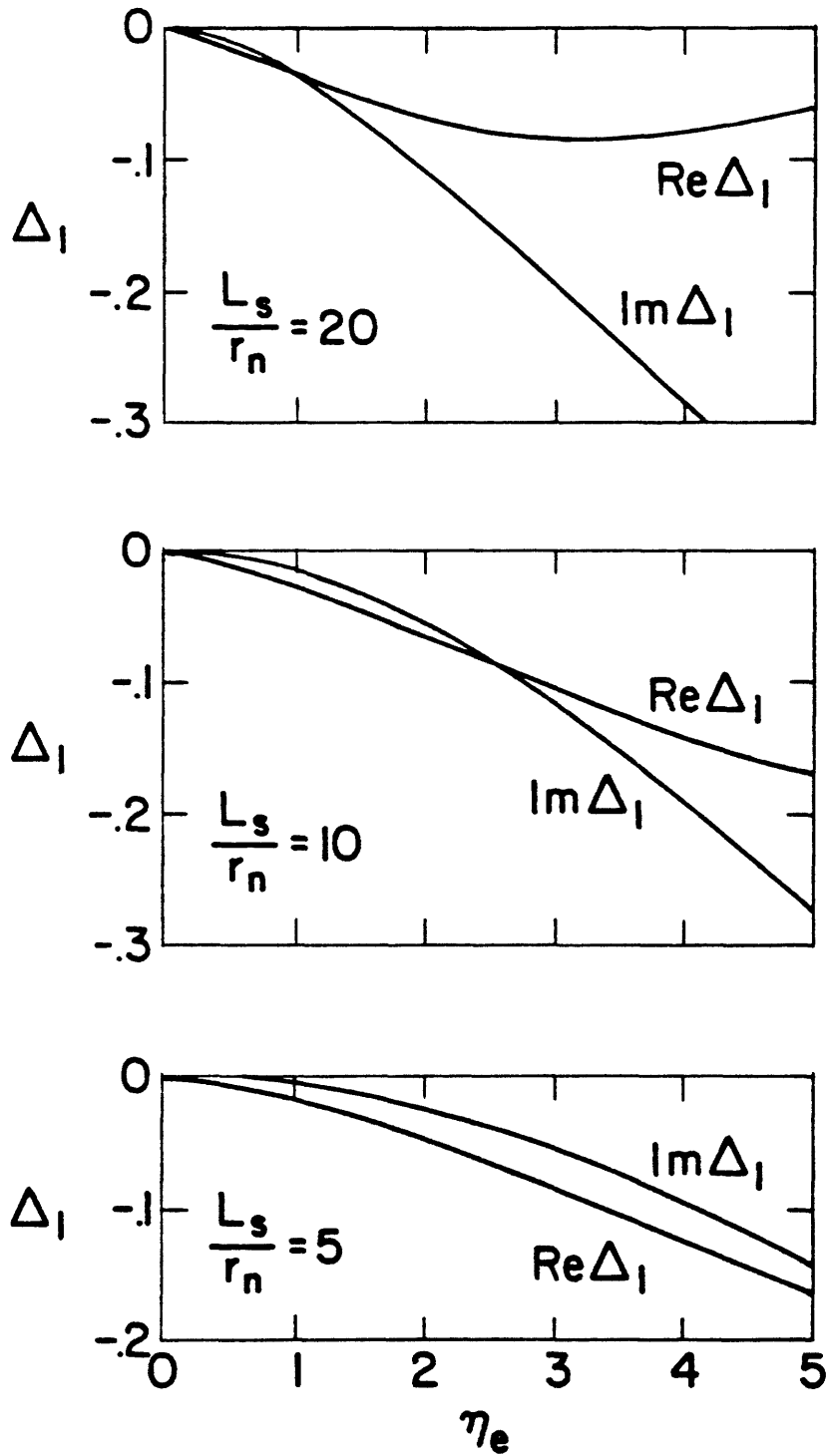
Figure 12: Plots of $\Delta_1(\eta_e)$ for $L_s/r_n = 20$, 10, 5.

Referring to Figs. 8 and 9, this means that the mode with $\hat{\omega} = -1/\tau$ is stable. The stability criterion for the other mode is expressed in terms of Δ', or recalling Eq. (6.2), λ_H. The mode is unstable for

$$0 > \frac{r_1 \lambda_H}{\rho_i} > \frac{d^2}{\rho_i \delta_*} \frac{\pi}{4} \left[\text{Re } \Delta_1 \left(\frac{\delta_e}{\rho_i}, \frac{L_s}{r_n}, \eta_e, \eta_i, \tau \right) \right]^{-1} \qquad (6.35)$$

which for the paramters of Fig. 12 gives

$$0 > \frac{r_1 \lambda_H}{\rho_i} > \frac{\pi}{240} \left(\frac{L_s}{r_n} \right) \frac{1}{\hat{\beta} \ \text{Re} \Delta_1} \qquad . \qquad (6.36)$$

These results are in general agreement with those of Ref. (16) where the case $\eta_e \sim 1$ and $T_e \sim T_i$ was excluded from the analytic treatment, but was considered in a purely numerical solution. We find the same roughly linear dependence of the stability boundary on η_e. Our treatment of the ion gyro-radius effects results, however, in instability at slightly smaller values of Δ' (larger values of $|\lambda_H|$).

In conclusion we note that the non-adiabatic ion response exerts a strong stabilizing effect on these collisionless reconnecting modes. This stabilization increases with both η_e and L_s/r_n.

CHAPTER 7

7.1 Collisionless internal kink modes

In the previous chapter we saw that the non-adiabatic
ion response to the electrostatic potential was responsible
for a strong stabilizing effect on collisionless reconnecting
modes. In this chapter we shall examine what role this ion
response plays in modifying the behavior of the internal kink
modes that exist when $\lambda_H > 0$. We note, however, that the
approach of the preceding chapter is limited by the need to
adopt the "constant A" approximation, which imposes a low-beta
restriction, $\hat{\beta} \ll 1$. Since it is our desire to investigate
higher beta regimes, we shall take a different approach in our
analysis.

A related difficulty arises from the fact that near
marginal stability the vector potential is far from being
constant (although for $\hat{\beta} \ll 1$ it may not depart significantly
from the MHD result (5.46)). At the same time the electro-
static potential does not decay towards the boundaries of
the layer, but rather it approaches a constant. Consequently
it does not have a Fourier transform in the usual sense, which
makes the analysis of the previous chapter inappropriate.
These problems are resolve by the formulation of the problem
presented below.

The system of equations (5.41) may be rewritten

$$ x \, \frac{d^2 \hat{A}}{dx^2} = \hat{\beta} \, \hat{\omega} \, (h \circ \hat{\phi}) \qquad\qquad (7.1a) $$

$$\frac{x}{\hat{\beta} \, \hat{\omega} \, P_e} \frac{d^2 \hat{A}}{dx^2} = \frac{1}{x} \hat{A} - \hat{\phi} \tag{7.1b}$$

where we have written $\hat{\phi} = \phi/\phi_\infty$, $\hat{A} = A\delta_e v_e/(c\phi_\infty)$, and $\hat{\beta} = (\beta_e/2)(L_s/r_n)^2$ was defined in Eq. (6.1). We have introduced a new convolution kernel

$$h(x) = g(x) - (1 + \hat{\omega}\tau) \, \delta(x) \tag{7.2}$$

where $\delta(x)$ is the Dirac delta function. The Fourier transform of h is

$$H(k) = (1 + \hat{\omega}\tau)(S_o - 1) - \eta_i b(S_o - S_1) \tag{7.3}$$

where we recall $b = k^2 \rho_i^2/2$, $S_{o,1}(b) = \exp(-b) \, I_{o,1}(b)$ and $I_{o,1}$ are modified Bessel functions. Now we introduce a function

$$\chi \equiv x \frac{d\hat{A}}{dx} - \hat{A} + \frac{r_1 \lambda_H}{\pi} \tag{7.4}$$

whose virtue lies in its derivative

$$\frac{d\chi}{dx} = x \frac{d^2 \hat{A}}{dx^2} \, . \tag{7.5}$$

Then if we differentiate (7.1b), $\hat{A}$ can be replaced by χ:

$$\frac{d}{dx} \left(\frac{1}{\hat{\beta}\hat{\omega}P_e} \frac{d\chi}{dx} \right) - \frac{\chi}{x^2} + \frac{d\hat{\phi}}{dx} + \frac{r_1 \lambda_H}{\pi x^2} = 0 \, . \tag{7.6}$$

Now if we make the replacement (7.5) in Eq. (7.1a) and differentiate,

$$\frac{d^2\chi}{dx^2} = \hat{\beta}\hat{\omega}[h \circ (\frac{d\hat{\phi}}{dx})]$$ (7.7)

we obtain a pair of equations in which only the derivative of $\hat{\phi}$ appears. Thus when we Fourier transform Eq. (7.7), we obtain an algebraic relationship between $X \equiv \mathfrak{F}[\chi]$ and $\Xi \equiv \mathfrak{F}[d\hat{\phi}/dx]$,

$$k^2 X(k) + \hat{\beta}\hat{\omega}H(k)\Xi(k) = 0 \quad .$$ (7.8)

Boundary conditions on χ for the differential equation (7.6) may be obtained from those on $\hat{A}$ and Eq. (7.4). In the first place, since $\hat{A}$ is even, χ is as well. Eq. (7.4) may be inverted:

$$\hat{A}(x) = -\frac{x}{2} + \frac{r_1\lambda_H}{\pi} - \chi(x) - x\int_x^\infty d\hat{x}\, \frac{1}{\hat{x}}\, \frac{d\chi(\hat{x})}{dx} \quad ,$$ (7.9)

where the constant of integration was chosen to agree with Eq. (5.46) in the limit $x \to +\infty$. For consistency in the limit $x \to -\infty$, we require

$$\int_{-\infty}^{\infty} dx \; \frac{1}{x} \; \frac{d\chi(x)}{dx} \; = \; -1 \; , \tag{7.10}$$

and of course $\chi(x \to \pm\infty) = 0$. This condition may be expressed in terms of $d\hat{\phi}/dx$, since Eq. (5.46a) implies

$$\int_{-\infty}^{\infty} dx \; \frac{d\hat{\phi}}{dx} \; = \; -1 \; , \tag{7.11a}$$

or equivalently

$$\Xi(0) \; = \; -1 \; . \tag{7.11b}$$

To summarize, we have reformulated the original integro-differential system of equations (5.41) in A and ϕ into a new system (7.6,8) in χ and $d\hat{\phi}/dx$, which is, in fact, applicable at arbitrary λ_H and $\hat{\beta}$. The new system has an advantage in that the integral relation between χ and $d\hat{\phi}/dx$ take the simple form Eq. (7.8). We can exploit this to construct a quadratic form for χ alone. If we multiply Eq. (7.6) by χ and integrate, then

$$\mathcal{P} \int_{-\infty}^{\infty} dx \; \left[\chi\frac{d}{dx}\left(\frac{1}{\hat{\beta}\hat{\omega}P_e} \; \frac{d\chi}{dx}\right) - \frac{\chi^2}{x^2} + \frac{r_1\lambda_H}{\pi x^2} \chi \right] + \int_{-\infty}^{\infty} dx \; \chi\frac{d\hat{\phi}}{dx} = 0 \tag{7.12}$$

where the first integral is a principle value integral because of the $1/x^2$ singularity of the integrand. Integrating the first term by parts, and expressing the second in terms of Fourier transforms, we have

$$- \int_{-\infty}^{\infty} dx \left[\frac{1}{\hat{\beta}\hat{\omega}P_e} \left(\frac{d\chi}{dx}\right)^2 + \frac{1}{x}\frac{d}{dx}(\chi^2) - \frac{r_1\lambda_H}{\pi x}\frac{d\chi}{dx} \right]$$

$$- \lim_{\eta \to 0} 2\chi(\eta)\left[\frac{1}{\hat{\beta}\hat{\omega}P_e(\delta_e/\eta)}\frac{d\chi(\eta)}{dx} + \frac{\chi(\eta)}{\eta} - \frac{r_1\lambda_H}{\pi\eta} \right]$$

$$+ \int_{-\infty}^{\infty} \frac{dk}{2\pi} \Xi(k)\, X(k) = 0 \quad, \tag{7.13}$$

where we have used the fact that χ and X are even. The second term vanishes provided χ satisfies Eq. (7.6). We can eliminate $\Xi(k)$ in the last term using Eq. (7.8). Using the normalization (7.10) in the first term we finally have

$$\mathcal{I}[\chi] \equiv \int_{-\infty}^{\infty} dx \left[\frac{1}{\hat{\beta}\hat{\omega}P_e}\left(\frac{d\chi}{dx}\right)^2 + \frac{1}{x}\frac{d}{dx}(\chi^2) \right] + \frac{r_1\lambda_H}{\pi}$$

$$+ \int_{-\infty}^{\infty} \frac{dk}{2\pi}\frac{k^2}{\hat{\beta}\hat{\omega}H}\, X^2 = 0 \tag{7.14}$$

This quadratic form $\mathfrak{I}$ may then be used in conjunction with trial functions χ to provide estimates of the eigenvalue $\hat{\omega}$. That is, we require

$$\mathfrak{I}[\chi] \; (\hat{\beta}, \; r_1\lambda_H, \; \rho_i, \; \delta_*, \; \tau, \; \eta_e, \; \eta_i; \; \hat{\omega}) = 0 \tag{7.15}$$

where we have explicitly indicated the parameters that appear in Eq. (7.14). We note that the trial function must be normalized according to Eq. (7.10). As a further condition, we note that although for an eigenfunction Eqs. (7.10) and (7.11) are equivalent, for a trial function this is generally not the case. Thus we require Eq. (7.11) to be explicitly satisfied, that is

$$X(0) = - \lim_{k \to 0} \frac{\hat{\beta}\hat{\omega}H(k)}{k^2} \; \Xi(k)$$

$$= - \frac{1}{2} \hat{\beta}\hat{\omega} (1 + \hat{\omega}\tau) \; \rho_i^2 \; . \tag{7.16}$$

Finally, we note that although the form (7.14) is self-adjoint, the function $P_e(\delta_e/|x|)$ is in general complex. The eigenvalue $\hat{\omega}$ is then complex, and so the estimates of $\hat{\omega}$ made by Eq. (7.15) are not extremal. In particular, we will not be able to place lower or upper bounds on the growth rate $\hat{\gamma}$. However, we note that insofar as the conductivity term is concerned, this quadratic form is the same as one discussed by other authors[36,37] who found excellent agreement between variational estimates and numerical results.

7.2 Model problem

The system of equations developed in the previous section is still too complicated to solve directly, primarily due to the complexity of the functions P_e and H. In this section we shall therefore look for solutions to a simplified problem, in which the effects of temperature gradients are neglected. That is, we set

$$\eta_e = \eta_i = 0 \ , \qquad\qquad (7.17)$$

and for convenience we equate T_e and T_i. In addition we shall approximate the functional forms of $P_e \propto W(\delta_e/|x|)$ and $H \propto [1 - S_o(b)]$. Noting that $W(\lambda \to 0) = -1$ and $W(\lambda \to \infty) \simeq 1/2\lambda^2$ we take

$$\frac{1}{\hat\beta\hat\omega P_e(\delta_e/|x|)} \simeq \frac{1}{\hat\beta\hat\omega(\hat\omega - 1)} \frac{2\delta_e^2 - x^2}{x^2} \ . \qquad\qquad (7.18)$$

Since $S_o(b \to 0) \simeq 1 - b$ and $S_o(b \to \infty) \simeq (2\pi b)^{-1/2}$, we approximate

$$\frac{k^2}{\hat\beta\hat\omega H(k)} \simeq - \frac{1}{\hat\beta\hat\omega(\hat\omega + 1)} (\frac{2}{\rho_i^2} + k^2) \ . \qquad\qquad (7.19)$$

We shall use the quadratic form (7.14) to examine the gross stability properties of these modes. For this model problem, we have

$$\mathfrak{s}[\chi] \ (\hat{\beta}, \ \hat{\lambda}, \ \delta_*/\rho_i; \ \hat{\omega}) \ = \ 0 \ , \tag{7.20}$$

that is, the behavior of these modes can be discussed in terms of a parameter space in $\hat{\beta}$ and

$$\hat{\lambda} \equiv r_1 \lambda_H/\rho_i \ , \tag{7.21}$$

which for the purpose of this chapter we take non-negative. The parameter

$$\frac{\delta_*}{\rho_i} \ = \ \frac{L_s}{2r_n} \left(\frac{m_e}{m_i}\right)^{1/2} \tag{7.22}$$

shall be viewed as being held fixed. A convenient choice for the trial function is

$$\chi(x) \ = \ \frac{\delta^3}{\pi(x^2 + \delta^2)} \tag{7.23}$$

whose Fourier transform is

$$X(k) \ = \ \delta^2 \ e^{-|k|\delta} \ , \tag{7.24}$$

and these expressions make sense while $\mathrm{Re}(\delta^2) > 0$ and $\mathrm{Re}(\delta) > 0$. The motivation for the functional form of (7.23) lies in the fact that the MHD solution (2.54, 3.46) when expressed in terms of χ is expression (7.23) with $\delta = \lambda_H$. Evaluating $\mathfrak{s}[\chi]$ using

the model functions (7.18, 19), we find

$$\frac{1}{\hat{\beta}\hat{\omega}(\hat{\omega}-1)}\left(\frac{5}{2}\frac{\delta_e^2}{\delta^2} - \frac{1}{4}\right) - 1 + \frac{1}{8}\frac{\rho_i^2}{\delta^2} + \hat{\lambda}\frac{\rho_i}{\delta} = 0 \quad , \qquad (7.25)$$

where the condition (7.16) gives

$$\delta^2 = -\frac{1}{2}\hat{\beta}\hat{\omega}(\hat{\omega}+1)\rho_i^2 \quad . \qquad (7.26)$$

Solutions of Eq. (7.25) in a few limiting cases are of interest. When $\hat{\gamma} \equiv -i\hat{\omega} \gg 1$, a balance of the third and fifth terms (all others being negligible) yields

$$|\hat{\gamma}| = \sqrt{2}\,\hat{\lambda}/\hat{\beta}^{1/2} \qquad (7.27a)$$

which in fact gives the ideal MHD internal kink growth rate (2.53,3.42),

$$\gamma = \lambda_H v_A/L_s \quad , \qquad (7.27b)$$

where v_A is the Alfvén speed $B_o/(4\pi nm_i)^{1/2}$. Another possibility is a balance between the first and third terms. This gives a low-$\hat{\beta}$ unstable mode,

$$|\hat{\gamma}| = \sqrt{5}\,\delta_*/\hat{\beta}\rho_i \quad , \qquad (7.28a)$$

whose growth rate may be written

$$\gamma = \left| \sqrt{5} \, dv_A k_y / 2L_s \right| \quad . \tag{7.28b}$$

This mode has been noted by other authors[20,21] and can exist even for $\lambda_H = 0$.

An important question is the fate of these modes in high-$\hat{\beta}$ regimes. Taking the limit $\hat{\beta} \gg 1$, the last three terms may be balanced to find

$$\hat{\omega} = -1 + O(\hat{\beta})^{-1} \tag{7.29}$$

which implies a stabilization at high $\hat{\beta}$. In fact for $\lambda_H = 0$, Eqs. (7.25) and (7.26) may be combined to give

$$\frac{4\hat{\beta}^2 \hat{\omega}^2 - 4\hat{\beta}^2 + 2\hat{\beta} + 20\delta_*^2/\rho_i^2}{4\hat{\beta}^2 (\hat{\omega}^2 - 1)} = 0 \tag{7.30}$$

Marginal stability then occurs at

$$\hat{\beta}_c = \frac{1}{4} + \left(\frac{1}{16} + \frac{5\delta_*^2}{\rho_i^2} \right)^{1/2} \quad . \tag{7.31}$$

For deuterium, and $L_s/r_n = 10$, $\hat{\beta}_c = 0.56$. These results are summarized in Fig. 13 which illustrates the different instability regimes in the $(\hat{\lambda}, \hat{\beta})$ parameter space.

When $\lambda_H = 0$ the analysis simplifies, because with the approximation (7.19), we may rewrite Eq. (7.8) as
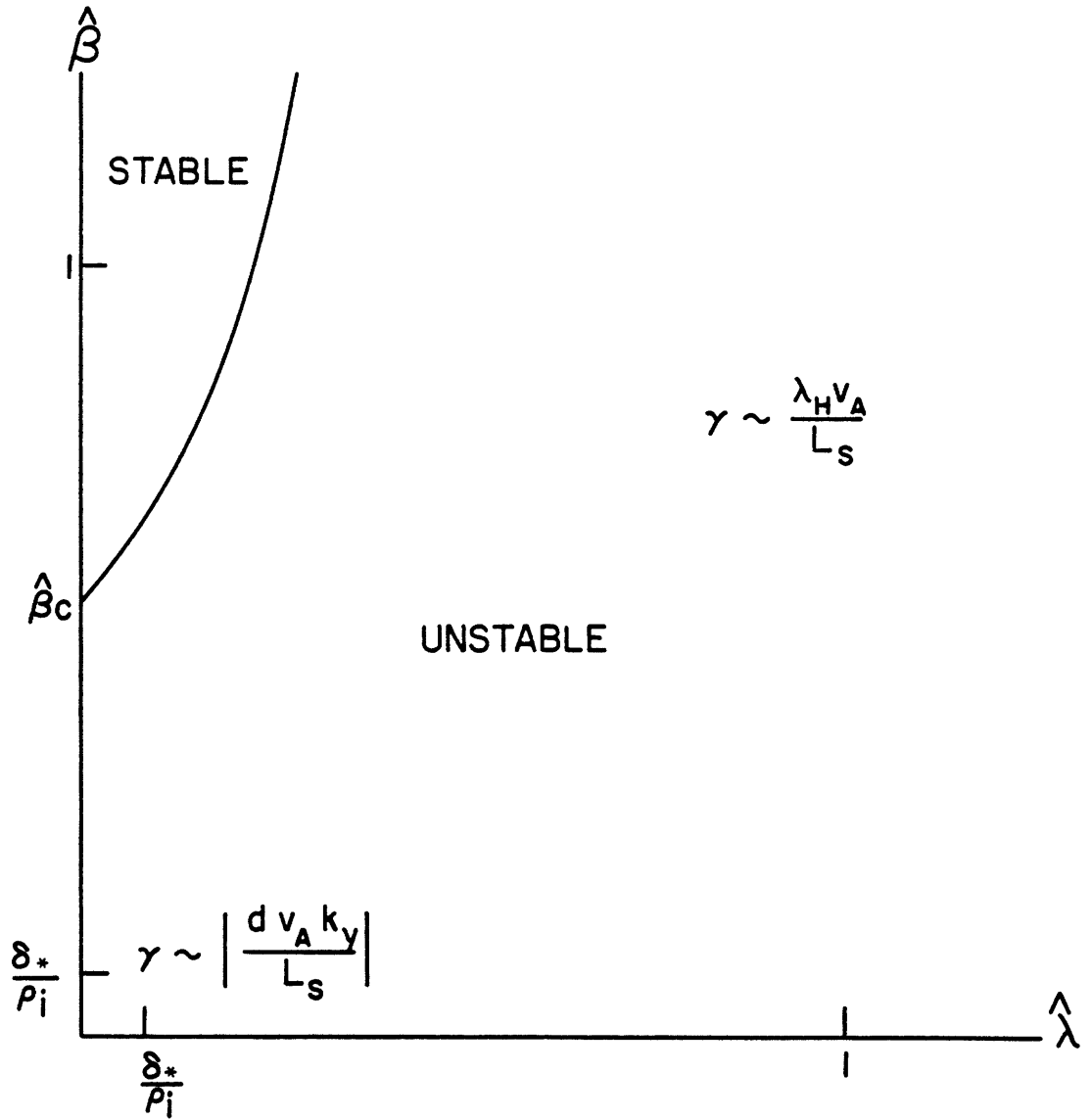
Figure 13: Stability diagram for collisionless modes.

$$\frac{d\hat{\phi}}{dx} = \frac{1}{\hat{\beta}\hat{\omega}(\hat{\omega}+1)} \left(\frac{2}{\rho_i^2} \chi - \frac{d^2\chi}{dx^2} \right) \quad . \tag{7.32}$$

Using this equation to eliminate $d\hat{\phi}/dx$ in Eq. (7.6) gives a single homogeneous second order differential equation for χ,

$$\frac{d}{dx} \left[\left(\frac{2\delta_*^2}{\hat{\beta}(\hat{\omega}^2-1)x^2} - \frac{2}{\hat{\beta}(\hat{\omega}^2-1)} \right) \frac{d\chi}{dx} \right] - \left[\frac{1}{x^2} - \frac{2}{\hat{\beta}\hat{\omega}(\hat{\omega}+1)\rho_i^2} \right] \chi = 0$$

$$\tag{7.33}$$

Now as $x \to \infty$, we find

$$\chi \sim e^{-\kappa x} , \qquad \kappa^2 \equiv \frac{\hat{\omega}-1}{\hat{\omega}\rho_i^2} . \tag{7.34}$$

If we define a new variable $\hat{x} = x\kappa(\hat{\beta}\rho_i^2/2\delta_*^2)^{1/2}$ then Eq. (7.33) takes the simple form

$$\frac{d}{d\hat{x}} \left[\left(\frac{1}{\hat{x}^2} + \frac{\hat{\beta}\rho_i^2}{2\delta_*^2} \frac{1}{\Gamma^2} \right) \frac{d\chi}{d\hat{x}} \right] - \left[\frac{1}{\hat{x}^2} + \frac{1}{\Gamma^2} \right] \chi = 0 \tag{7.35}$$

where

$$\Gamma^2 = \frac{\hat{\beta}^2\rho_i^2}{4\delta_*^2} (1 - \hat{\omega}^2) \quad . \tag{7.36}$$

As long as $\hat{\omega} \notin [0,1]$, we may solve Eq. (7.35) on a contour for which $\hat{x}$ is real; a solution decaying in $\hat{x}$ also decays in x.

Eq. (7.35) has a single solution. In the limit as $\hat{\beta} \to 0$, the solution is simply

$$\chi(\hat{x}) = e^{-\hat{x}^2/2} \ , \qquad \Gamma^2 = 1 \tag{7.37}$$

which has a growth rate that scales as Eq. (7.28),

$$\gamma = \left| d \ v_A \ k_y/L_s \right| \ . \tag{7.38}$$

At high values of $\hat{\beta}$, the solution develops the exponential tail (7.34), while retaining the Gaussian shape near $\hat{x} = 0$. This is in fact guaranteed by the singular nature of Eq. (7.35) at $\hat{x} = 0$. Numerical solutions of this equation with the proper asymptotic behavior are obtained by a shooting procedure. That is, a differential equation solver[38] is initialized at large $\hat{x}$ using Eq. (7.34) and used to integrate inwards to $\hat{x} = 0$. The eigenvalue Γ^2 is obtained by the requirement that χ be even. In practice we require $d^3\chi/d\hat{x}^3 = 0$ at $\hat{x} = 0$, since the singularity at the origin demands $d\chi/d\hat{x} = 0$ for any Γ^2. The growth rate is then computed from Γ^2 via Eq. (7.36); these results are displayed in Fig. 14 as functions of $\hat{\beta}$. The eigenfunction χ at the marginal point $\hat{\beta}_c = 0.41$ is plotted in Fig. 15.
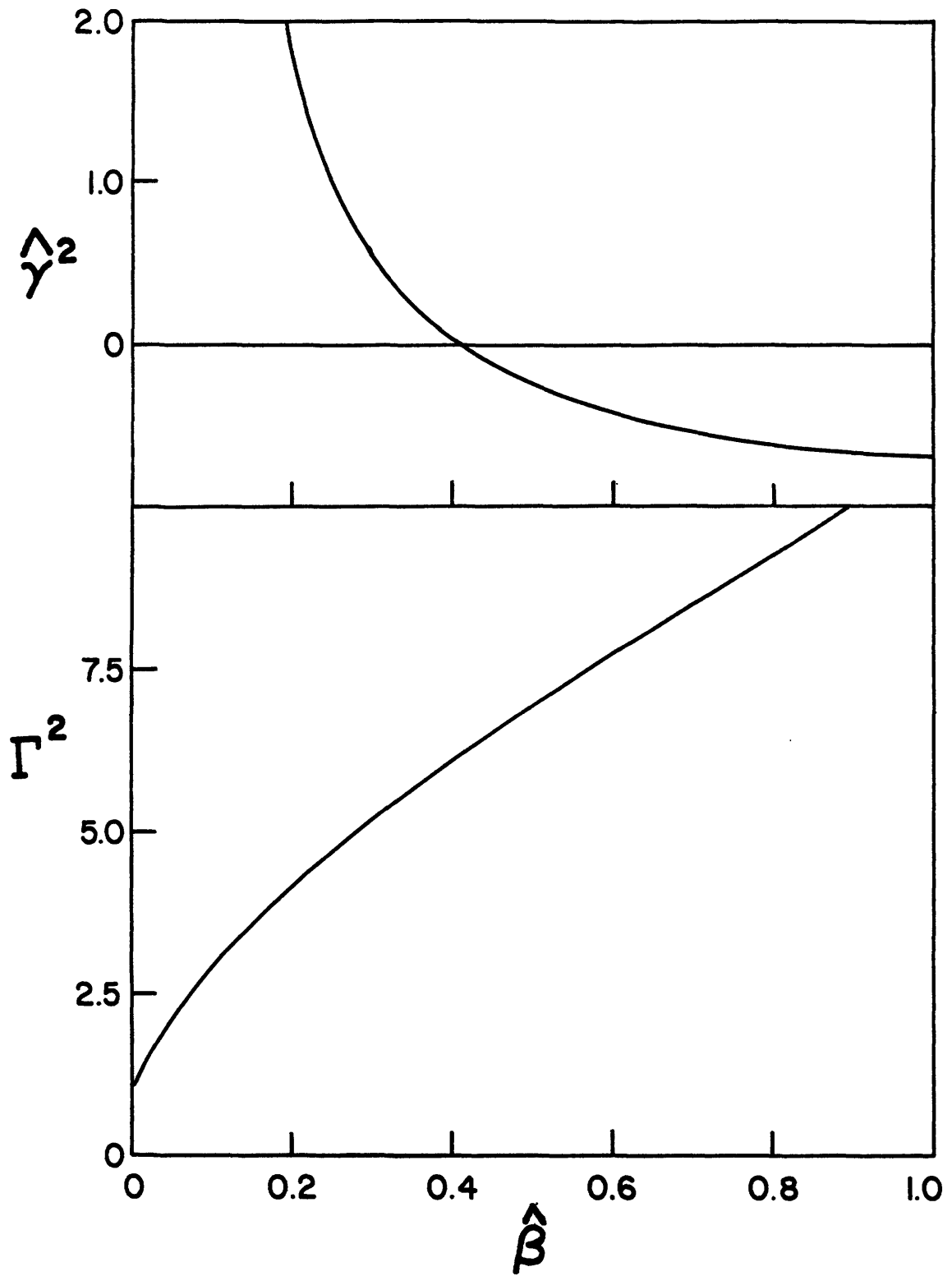
Figure 14: Variation of eigenvalues Γ^2, $\hat{\gamma}^2$ with $\hat{\beta}$ for the solution of Eqs.(7.35,36).
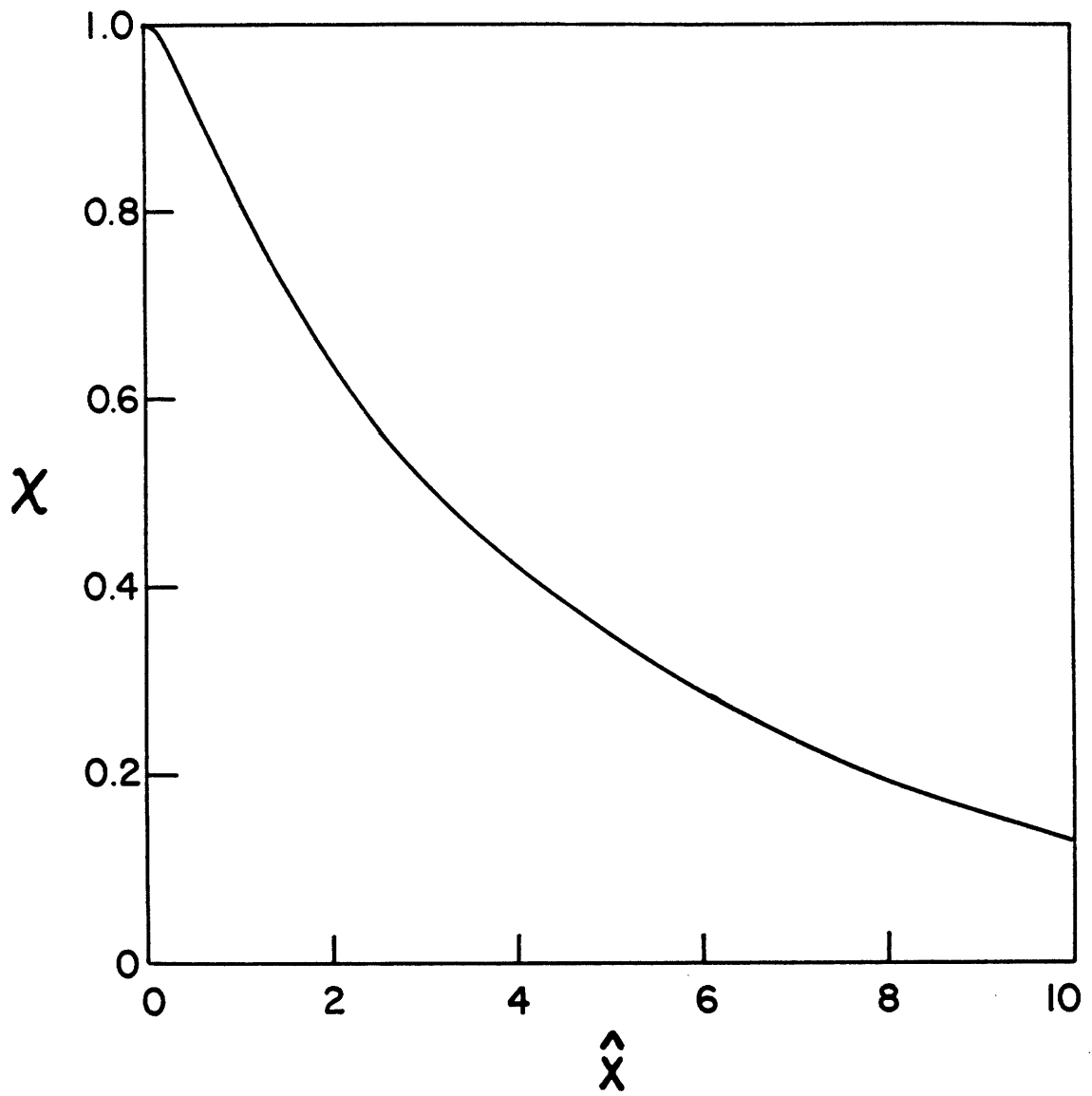
Figure 15: Eigenfunction $\chi(\hat{x})$ for Eq.(7.35) with $\hat{\beta} \simeq 0.4$.

This stabilization at $\lambda_H = 0$ can be demonstrated simply from a quadratic form that we can construct for Eq. (7.35). When solved for Γ^2 it gives

$$\Gamma^2 = \frac{\int_{-\infty}^{\infty} d\hat{x}\; \chi^2 + (\hat{\beta}\rho_i^2/2\delta_*^2) \int_{-\infty}^{\infty} d\hat{x}\; (d\chi/d\hat{x})^2}{\int_{-\infty}^{\infty} d\hat{x}\; \chi^2 - \int_{-\infty}^{\infty} d\hat{x}\; [(1/\hat{x})(d\chi/d\hat{x}) + \chi]^2} \qquad (7.39)$$

Thus as $\hat{\beta} \to \infty$, Γ^2 increases at most linearly with $\hat{\beta}$. However Eq. (7.36) implies

$$\Gamma^2 \sim \hat{\beta}^2 (1 - \hat{\omega}^2) \qquad (7.40)$$

so that $\hat{\omega} \to -1 + O(\hat{\beta}^{-1})$. Note also that Γ^2 is real, so the marginal point is $\hat{\omega} = 0$.

To summarize the results of this chapter, we have reformulated the collisionless reconnection equations into a form suitable for treating reconnecting modes for arbitrary values of $\hat{\beta}$. Restricting attention to modes with $\lambda_H \geq 0$ and neglecting the effects of temperature gradients, we found that these modes are stable at high beta. For small λ_H, the stability threshold was found at $\hat{\beta}_c \lesssim 1/2$. Recalling that when $\lambda_H < 0$ there was extra stabilization for $\eta_e > 0$, we would expect stability to improve in a more exact treatment of these modes.

CHAPTER 8

Summary and conclusions

In this thesis we have examined the linear stability of high temperature plasmas against the onset of internal kink modes. For the sake of definiteness we have assumed a large aspect ratio toroidal geometry with an axisymmetric confinement configuration typical of tokamak experiments. These instabilities are kinks in the sense that they involve a macroscopic outward displacement of the center of the plasma column, and internal modes in the sense that the amplitude of the plasma displacement falls to zero at the plasma boundary.

These modes were analyzed within the framework of the ideal MHD theory in the first half of this thesis. There we were able to identify two general $\varepsilon\beta_p$ regimes of stability. In the low-beta, $\varepsilon\beta_p \sim \varepsilon$ regime, the plasma is stable provided $\varepsilon\beta_p$ is less than some critical value and $q_0 > 1/2$, where q_0 is the value of the inverse rotational transform at the magnetic axis. Above this threshold, the plasma remains unstable until finite-beta, $\varepsilon\beta_p \sim 1$ regimes are reached. There we found a second point of marginal stability against internal kinks, which exists regardless of the value of q_0. Above this point the plasma is completely stable. This stabilization was attributed to the enhanced magnetic tension induced by the plasma pressure gradient which results from the equilibrium crowding of the magnetic flux surfaces towards the outside of the plasma.

Recognizing that the ideal MHD solution changes rapidly across a narrow radial layer, we considered the possibility that non-ideal effects could play a major role in this layer and thereby alter the stability properties of the plasma. To address this question we assumed that the temperatures were sufficiently high that collisions could be neglected. Recalling from Chapters 7 and 8 that $\omega \sim \omega_{*e}$, the assumption $\omega > \nu_e$, or equivalently $k_{||} \lambda_e > 1$, places the restriction on the temperature

$$(\frac{T_e}{1\ keV})^{5/2} > 1.38\ (\frac{\ln\Lambda}{15})\ (\frac{B}{10kG})\ (\frac{n}{10^{14}\ cm^{-3}})\ (\frac{r_1 r_n}{10^2\ cm^2}) \qquad (8.1)$$

where ν_e is the electron-electron collision frequency, λ_e is the electron mean free path, and $\ln\Lambda$ is the Coulomb logarithm. Then from a kinetic description of the plasma constituents, we were able to derive a set of equations for the electromagnetic potentials within the layer. In conjunction with boundary conditions imposed by the external MHD solution, these equations are sufficient for a solution of the problem. This description was then reformulated in terms of a new function χ, which allowed us to consider arbitrary regimes of $\hat{\beta}$ and $\hat{\lambda}$, where

$$\hat{\beta} \equiv \frac{\beta_e}{2}\ (\frac{L_s}{r_n})^2 \qquad (8.2)$$

provides a measure of the plasma beta, and

$$\hat{\lambda} \equiv \frac{r_1 \lambda_H}{\rho_i} , \qquad (8.3)$$

where λ_H is the MHD stability parameter.

The results of our analysis of these modes are indicated schematically in Fig. 16, where we identify stable and unstable regimes in $(\hat{\lambda}, \hat{\beta})$ space. For $\hat{\lambda} < 0$, the ideal MHD theory predicts stability. However the low-beta analysis of Chapter 7 shows that a collisionless mode, the reconnecting mode, is unstable below a $\hat{\beta}$ threshold. At $\hat{\lambda} = 0$, which is the ideal MHD marginal stability curve, we find what we have called the collisionless internal kink instability. This mode is in fact the collisionless analog of the resistive internal kink mode. In Chapter 8 we found that this mode was stable for $\hat{\beta} \gtrsim 1$. As $\hat{\lambda}$ increases, the significance of non-ideal effects decreases, until we recover what is essentially the ideal internal kink mode, at $\hat{\lambda} \gtrsim 1$. Finally the MHD boundary conditions on the reconnecting layer imply a relation between $\hat{\beta}$ and $\hat{\lambda}$, since $\lambda_H(\epsilon \beta_p)$. We have indicated this schematically by the dashed curve in Fig. 16 (assuming $q_0 > 1/2$). Then we can consider a flux-conserving sequence of equilibria starting at low-beta and progressing towards finite-beta regimes. We would expect the plasma to be unstable to the reconnecting mode, the collisionless kink, and finally the ideal internal kink, before finally stabilizing at finite-beta regimes.
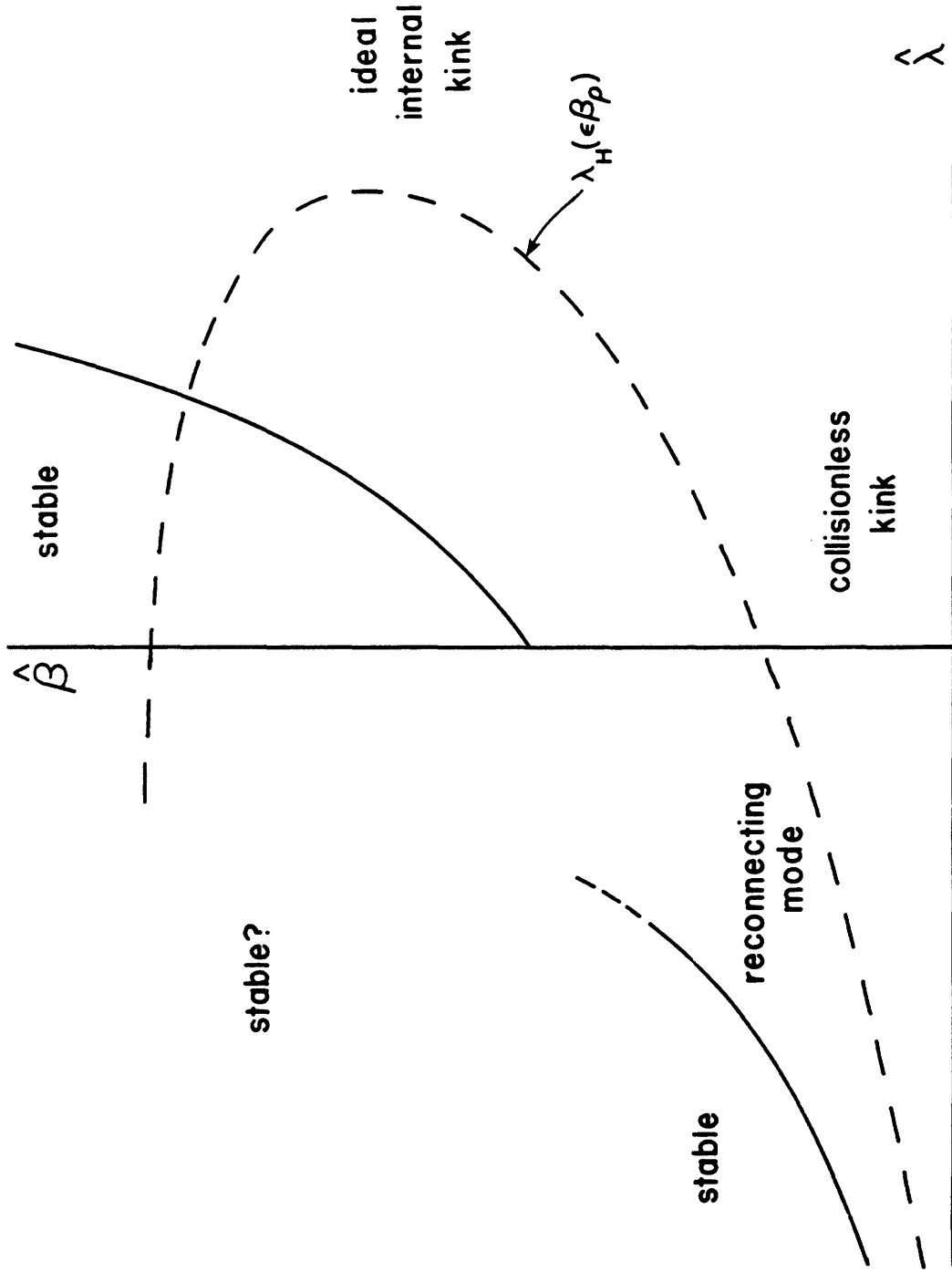
Figure 16: Summary of stability in $(\hat{\lambda}, \hat{\beta})$ space for all modes discussed in this thesis.

This picture is, however, incomplete to the extent that we have not been able to analyze the reconnecting modes for $\hat{\beta} \sim 1$. On the other hand, the topology of Fig. 16 suggests that this is a regime of stability for the reconnecting modes. In addition, recent work on tearing modes, the resistive counterpart of collisionless reconnecting modes, shows that these modes are stable at $\hat{\beta} \sim 1$ in the limit of low collisionality.[39] Furthermore, the effects of temperature gradients on the collisionless kinks were completely neglected. On the basis of the analysis for the reconnecting modes, we would expect additional stabilization to result from their inclusion in the analysis. Aside from these noted exceptions, our description of these collisionless modes can be considered complete.

Improvements and extensions to this theory might be made in several ways. We recall that the MHD calculation of λ_H was performed using circular cross-section flux surfaces. Ideally we would like to include small amounts of ellipticity and triangularity in order to make a better approximation to experimental configurations. Realistically, however, this could prove an intractable analytic problem; the better prospects for results probably lie with the fully numerical approach using equilibrium and stability codes.

As far as the collisionless calculation is concerned, we note that we proceeded on the fairly strong assumption that the perpendicular component of the vector potential could be neglected. Although this assumption is a priori

reasonable at low-beta, it is probably not valid when $\hat{\beta} \sim 1$.
In this case we should redo the calculation of Chapter 5 to
derive a set of three coupled equations in ϕ, $A_{\parallel}$, $A_{\perp}$. We
should also note that the matching between MHD and slab regions
was made with the leading $1/(r - r_1)^2$ singularity in $d\xi/dr$
given by Eqs. (2.51) and (3.41). This allowed us to perform
the analysis within the collisionless layer using definite
parity functions. The next order corrections to Eqs. (2.51)
and (3.41) can be calculated, and in fact introduce a small
antisymmetric component to the boundary conditions (5.46),
thereby breaking the symmetry within the layer. Collisionless
equations retaining this asymmetry within the layer have
been derived[40], but their analysis is extremely difficult.

A more serious difficulty resides in our choice of a
slab geometry for the reconnecting layer. In a full toroidal
geometry, we recall that the local value of the inverse
rotational transform

$$q_\ell \equiv \frac{rB_t}{RB_p} = \frac{rTD}{R\psi'}$$

(8.4)

depends on the poloidal angle through D. Thus the resonant
surface is not in fact coincident with the $q(r) = 1/n$ surface.
Thus we should consider abandoning the slab layer as presently
formulated, and instead consider a fully toroidal treatment.
At the same time, retention of the $m = 2$ harmonic in the mode
resonant layer may be necessary.

Finally there is the question of the non-linear evolution of these modes. The importance of the ideal internal kink has often been underrated due to the fact that it seems to saturate non-linearly at a relatively small amplitude[25]. This non-linear evolution should be investigated in finite-beta regimes.

On the other hand, there are indications that the internal kink has been observed in recent experimental work. High-frequency oscillations without sawtooth oscillations were observed in the JFT-2 tokamak, and a possible explanation in terms of the ideal internal kink, or perhaps the $m = 1$ resistive internal kink, was proposed[41]. (The temperatures in this experiment are still too low for a collisionless kink.) More recently the PDX group has reported MHD "fish-bone" activity at high neutral beam injection power, which they interpret in terms of an ideal internal kink[42]. Clearly there are many prospects for future work on these internal modes.

REFERENCES

[1] J.A. Wesson, Nucl. Fusion 18, 87 (1978).

[2] V.D. Shafranov, Zh. Tek. Fiz. 40, 241 (1970) [Sov. Phys. -- Tech. Phys. 15, 175 (1970)].

[3] G. Bateman, MHD Instabilities (MIT Press, Cambridge, Ma., 1978), p. 105.

[4] V.D. Shafranov, At. Energ. 13, 521 (1962) [Plasma Phys. 5, 251 (1963)].

[5] J.M. Greene, J.L. Johnson and K.E. Weimer, Phys. Fluids 14, 671 (1971).

[6] M.N. Bussac, R. Pellat, D. Edery and J.L. Soule, Phys. Rev. Lett. 35, 1638 (1975).

[7] A. Sykes and J.A. Wesson, Nucl. Fusion 14, 645 (1974).

[8] W. Kerner, R. Gruber and F. Troyon, Phys. Rev. Lett. 44, 536 (1980).

[9] B. Coppi, A. Ferreira and J.J. Ramos, Phys. Rev. Lett. 44, 990 (1980).

[10] A.M. Krymskii and A.B. Mikhailovskii, Fiz. Plazmy 5, 501 (1979) [Sov. J. Plasma Phys. 5, 279 (1979)].

[11] G.B. Crew and J.J. Ramos, Phys. Rev. A26, 1149 (1982).

[12] S. Tokuda, T. Tsunematsu, M. Azumi, T. Takizuka and T. Takeda, Nucl. Fusion 22, 661 (1982).

[13] H.P. Furth, J. Killeen and M.N. Rosenbluth, Phys. Fluids 6, 459 (1963).

[14] B. Coppi, Phys. Fluids 8, 2273 (1965).

[15] G. Laval, R. Pellat and M. Vuillemin, in Plasma Physics and Controlled Nuclear Fusion Research, 1965 (International Atomic Energy Agency, Vienna, 1966) Vol. II, p. 259.

[16] B. Coppi, J. W.-K. Mark, L. Sugiyama and G. Bertin, Phys. Rev. Lett. 42, 1058 (1979), and Ann. Phys. 119, 370 (1979).

[17] T.M. Antonsen, Jr. and B. Coppi, Phys. Lett. 81A, 335 (1981).

[18] B. Coppi, R. Galvão, R. Pellat, M. Rosenbluth and P. Rutherford, Fiz. Plazmy 2, 961 (1976) [Sov. J. Plasma Phys. 2, 533 (1976)].

[19] G. Ara, B. Basu, B. Coppi, G. Laval, M.N. Rosenbluth and B.V. Waddell, Ann. Phys. 112, 443 (1978).

[20] J.F. Drake, Phys. Fluids 21, 1777 (1978).

[21] B. Basu and B. Coppi, Phys. Fluids 24, 465 (1981).

[22] H.P. Furth, P.H. Rutherford and H. Selberg, Phys. Fluids 16, 1054 (1973).

[23] G.B. Crew, T.M. Antonsen, Jr. and B. Coppi, Nucl. Fusion 22, 41 (1982).

[24] L.E. Zakharov, Fiz. Plazmy 4, 898 (1978) [Sov. J. Plasma Phys. 4, 503 (1978)].

[25] M.N. Rosenbluth, R.Y. Dagazian and P.H. Rutherford, Phys. Fluids 16, 1894 (1973).

[26] I.B. Bernstein, E.A. Frieman, M.D. Kruskal and R.M. Kulsrud, Proc. R. Soc. A244, 17 (1958).

[27] W.A. Newcomb, Ann. Phys. 10, 232 (1960).

[28] V.D. Shafranov, Plasma Phys. 13, 757 (1971).

[29] J.F. Clarke and D.J. Sigmar, Phys. Rev. Lett. 38, 70 (1977).

[30] J.F. Clarke, ORNL/TM-5429 (1976).

[31] L. Sugiyama and J. W.-K. Mark, Phys. Lett. 84A, 123 (1981).

[32] P.H. Rutherford and E.A. Frieman, Phys. Fluids 11, 569 (1968).

[33] R.D. Fried and S.D. Conte, The Plasma Dispersion Function (Academic Press, New York, 1961).

[34] T.M. Antonsen, Jr., B. Coppi and R. Englade, Nucl. Fusion 19, 641 (1979).

[35] Using computer code FFT2 of I.M.S.L., Library 3, Edition 6, International Mathematics and Statistics Libraries, Inc. 1979.

[36] R.D. Hazeltine and H.R. Strauss, Phys. Fluids 21, 1007 (1978).

[37] S.M. Mahajan, R.D. Hazeltine, H.R. Strauss and D.W. Ross, Phys. Rev. Lett. 41, 1375 (1978).

[38] L.F. Shampine and M.K. Gordon, _Computer Solution of Ordinary Differential Equations_ (W.H. Freeman & Co., San Francisco, 1975).

[39] J.F. Drake, T.M. Antonsen, Jr., A.B. Hassam and N.T. Gladd, in _Plasma Physics and Controlled Nuclear Fusion Research, 1982_ (International Atomic Energy Agency, Vienna, to be published) paper CN-41/P-2-3.

[40] B. Chike-Obi, Ph.D. Thesis, Massachusetts Institute of Technology, Cambridge, MA, 1982.

[41] S. Yamamoto, _et.al._ Nucl. Fusion **21**, 993 (1981).

[42] K. McGuire, _et.al._, Princeton Plasma Physics Laboratory Report PPPL-1946 (1982).

[43] This deviation was suggested by T.M. Antonsen, Jr., private communication.

APPENDIX A

In this appendix we determine the Green's function $G(r,\hat{r})$ that is used in Chapters 2 and 3 to express x_2 in terms of x_1'. By definition $G(r,\hat{r})$ satisfies

$$L(r)\; G(r,\hat{r}) = -\hat{r}^3 E_2(\hat{r})\; \frac{\partial \delta(r-\hat{r})}{\partial r} + \hat{r}^2 E_3(\hat{r})\delta(r-\hat{r}), \qquad (A.1)$$

subject to the boundary conditions

$$G(0,\hat{r}) = G(a,\hat{r}) = 0 \quad \text{for} \quad 0 \le \hat{r} \le a \quad . \qquad (A.2)$$

The differential operator $L(r)$ is defined as

$$L(r)G(r,\hat{r}) \equiv \frac{\partial}{\partial r}\left[2r^2 E_4(r)\; \frac{\partial G(r,\hat{r})}{\partial r}\right]$$

$$+ \left[\left(r^2 E_5(r)\right)' - 2r E_6(r)\right] G(r,\hat{r}) \;, \qquad (A.3)$$

and the coefficient functions E_i are given in Chapter 2 for the low-beta case and in Chapter 3 for the finite-beta case. Except for $r = \hat{r}$, G satisfies $L(r)G(r,\hat{r}) = 0$. Thus we set:

$$G(r,\hat{r}) = \sum_{+,-} G_\pm(\hat{r}) x_\pm(r)\; \theta(\pm r \mp \hat{r}) \;, \qquad (A.4)$$

where x_+ and x_- are the solutions of the homogeneous equation

$$L(r) \ x_{\pm}(r) = 0 \ , \qquad\qquad (A.5)$$

that satisfy the boundary conditions

$$x_{-}(0) = 0 \ , \qquad\qquad (A.6a)$$

$$x_{+}(a) = 0 \ . \qquad\qquad (A.6b)$$

The $\pm$ subscripts refer to $r \lessgtr \hat{r}$, and the boundary conditions (A.6) are such that Eq. (A.2) holds. The normalization of $x_{\pm}$ is arbitrary. Next we must determine the coefficients $G_{\pm}(\hat{r})$ so that Eq. (A.1) is satisfied at $r = \hat{r}$. The inhomogeneous terms of Eq. (A.1) force both G and its r-derivative to be discontinuous at $r = \hat{r}$. The first of these two terms balances the discontinuity:

$$G(\hat{r}+0,\hat{r}) - G(\hat{r}-0,\hat{r}) = - \frac{E_2(\hat{r})}{2E_4(\hat{r})} \ . \qquad\qquad (A.7a)$$

In addition, if we integrate Eq. (A.1) across $r = \hat{r}$, we find:

$$\frac{\partial G(\hat{r}+0,\hat{r})}{\partial r} - \frac{\partial G(\hat{r}-0,\hat{r})}{\partial r} = \frac{E_3(\hat{r})}{2\hat{r}E_4(\hat{r})} \ . \qquad\qquad (A.7b)$$

Substituting our expression (A.4) for $G(r,\hat{r})$, we arrive at the pair of equations:

$$G_+(\hat{r})x_+(\hat{r}) - G_-(\hat{r})x_-(\hat{r}) = -\frac{E_2(\hat{r})}{2E_4(\hat{r})} \quad , \tag{A.8a}$$

$$G_+(\hat{r})\hat{r}\,x_+'(\hat{r}) - G_-(\hat{r})\hat{r}x_-'(\hat{r}) = \frac{E_3(\hat{r})}{2E_4(\hat{r})} \quad . \tag{A.8b}$$

The solution is:

$$G_\pm(r) = \frac{E_2(\hat{r})\hat{r}^3 x_\mp'(\hat{r}) + E_3(\hat{r})\hat{r}^2 x_\mp(\hat{r})}{2E_4(\hat{r})\hat{r}^3\,[x_+'(\hat{r})x_-(\hat{r}) - x_+(\hat{r})x_-'(\hat{r})]} \quad . \tag{A.9}$$

The denominator of this expression is $2\hat{r}^3 E_4$ times the Wronskian of x_+ and x_-, and is therefore a constant which we choose to evaluate at $\hat{r} = r_1$. Then if we normalize $x_\pm$ so that

$$x_\pm(r_1) = 1 \quad , \tag{A.10}$$

and define

$$b \equiv \frac{1}{4}\,[r_1\,x_-'(r_1) - 1] \quad , \tag{A.11a}$$

$$c \equiv \frac{1}{4}\,[r_1\,x_+'(r_1) + 3] \quad , \tag{A.11b}$$

we find

$$G_\pm(\hat{r}) = \frac{E_2(\hat{r})\hat{r}^3\,x_\mp'(\hat{r}) + E_3(\hat{r})\hat{r}^2\,x_\mp(\hat{r})}{8E_4(r_1)r_1^2(b+1-c)} \quad . \tag{A.12}$$

Again we point out that, although formally defined in the same way, these quantities are different for each beta regime, due to the different definitions of the coefficient functions E_i. In regimes where $\epsilon \beta_p \ll 1$ we have $E_4 = (1/2 - \mu)^2$. Thus, if $\mu(a) < 1/2$, Eq. (A.5) has a regular singular point at the $m = 2$ mode resonant surface r_2. In order for x_+ to represent a physical displacement and still satisfy the boundary condition at $r = a$ we must take in this case

$$x_+(r) = 0 \quad \text{for} \quad r_2 \leq r \leq a \ . \tag{A.13}$$

For $r \leq r_2$, x_+ is then taken to be the solution of (A.5) which is finite at $r = r_2$. No such problem arises in the finite-beta regime where E_4 never vanishes.

APPENDIX B

In this appendix we derive some useful bounds for the parameters b and c defined in Eq. (A.11). For the purpose of calculating these parameters it is convenient to transform Eq. (A.5) to a first order Ricatti equation:

$$r\, Z_{\pm}' + h_1\, Z_{\pm} + h_2 + (Z_{\pm} + 3)(Z_{\pm} - 1) = 0 , \qquad (B.1)$$

where

$$Z_{\pm} = \frac{r x'}{x_{\pm}} , \qquad (B.2)$$

$$h_1 = \frac{r E_4'}{E_4} , \qquad (B.3)$$

and

$$h_2 = 3 + \frac{r E_5' + 2E_5 - 2E_6}{2E_4} . \qquad (B.4)$$

The boundary conditions for $Z_{\pm}$ are now:

$$Z_-(r \to 0) = 1 , \qquad (B.5a)$$

$$Z_+(r \to a) = \frac{a}{r-a} , \qquad (B.5b)$$

with the exception that, when $\varepsilon \beta_p \ll 1$ and $r_2 < a$, the boundary condition for Z_+ is changed to:

$$Z_+(r \to r_2) = \frac{r-r_2}{r_2} , \qquad (B.5c)$$

as discussed in Appendix A. In terms of $Z_\pm$, the parameters b and c are:

$$b = \frac{1}{4} [Z_-(r_1) - 1] \quad , \tag{B.6a}$$

$$c = \frac{1}{4} [Z_+(r_1) + 3] \quad . \tag{B.6b}$$

In regimes where $\varepsilon \beta_p \ll 1$ we have:

$$h_1 = - \frac{2 \mu'}{1/2 - \mu} \quad , \tag{B.7}$$

$$h_2 = 0 \quad . \tag{B.8}$$

We consider $q(r)$ profiles that are monotonically increasing (and parabolic near $r = 0$). Then Eq. (B.7) implies $h_1 < 0$ for $0 < r < r_2$, and from Eq. (B.1) we see that $Z_\pm'$ must be positive wherever $Z_\pm$ should equal 0 or 1, and negative if $Z_\pm \leq -3$. In addition, as $r \to 0$, $Z_-(r)$ approaches 1 from above. Given this behavior of Z_- near $r = 0$ and the boundary condition (B.5b) or (B.5c) for Z_+, we conclude that $Z_-(r_1) > 1$ and $Z_+(r_1) < 0$, hence $b > 0$ and $c < 3/4$. Also if $r_2 < a$ and the boundary condition (B.5c) applies, then $Z_+(r_1) > -3$ and $c > 0$. When r_1 approaches a, Eq. (B.5b) applies and c tends to $-\infty$. On the other hand, when r_1 approaches 0, Eq. (B.1) forces $Z_+(r_1)$ to approach -3 from above and c becomes positive.

In finite-beta regimes it is convenient to transform Eq. (B.1) into the integral relation:

$$Z(r)^{-1} = r^2 E_4(r) \int_{r_0}^{r} \frac{1 + [h_2(\hat{r}) - 3] Z(\hat{r})^{-2}}{\hat{r}^3 E_4(\hat{r})} \, d\hat{r} \, , \qquad (B.9)$$

where r_0 is a constant of integration that should be fixed in such a way that Z satisfies its desired boundary condition. With $r_0 = a$, the solution of Eq. (B.9) satisfies the external boundary condition (B.5b) for Z_+. The solution Z_- is obtained as the (pointwise) limit of solutions of Eq. (B.9) when $r_0 \to 0$, so that the internal boundary condition (B.5a) is satisfied. Now, although we know that $E_4 > 0$, it is difficult to obtain bounds on Z_+ and Z_- due to the complexity of the $h_2 - 3$ term. However, in the very high-beta ($\varepsilon \beta_p \gg 1$) limit, where σ tends to zero except in a narrow region near the magnetic axis, this term makes a negligible contribution to the integral because $h_2 - 3$ is of order σ^2. Then, provided r_1 is not near zero, we find $Z_+(r_1) < 0$ and $Z_-(r_1) > 0$ so that $c < 3/4$ and $b > -1/4$.

APPENDIX C

Here we average over the Vlasov equation for electrons,

$$\frac{\partial f_e}{\partial t} + \underline{v} \cdot \frac{\partial f_e}{\partial \underline{r}} - \frac{e}{m_e}(\underline{E} + \frac{1}{c}\underline{v} \times \underline{B}) \cdot \frac{\partial f_e}{\partial \underline{v}} = 0 \qquad (C.1)$$

to eliminate their rapid gyro-motion.[43] We transform to guiding center coordinates

$$\underline{R} = \underline{r} + \frac{1}{\Omega_e}\underline{v} \times \underline{b} \qquad (C.2)$$

where $\underline{b} = \underline{B}/B$, $\Omega_e = -eB/m_e c$. Then we expand the distribution function in powers of Ω_e

$$f_e(\underline{R}, v_{||}, v_{\perp}, \alpha) = f_0 + f_1 + \ldots \qquad (C.3)$$

where $v_{||} = \underline{v} \cdot \underline{b}$, $v_{\perp} = |\underline{v} \times \underline{b}|$ and α is the gyro-angle. To leading order in Ω_e, the Vlasov equation becomes

$$\Omega_e (\underline{v} \times \underline{b}) \cdot \frac{\partial f_0}{\partial \underline{v}} \equiv \Omega_e \frac{\partial f_0}{\partial \alpha} = 0 \quad , \qquad (C.4)$$

and in the next,

$$\frac{\partial f_0}{\partial t} + \underline{v} \cdot \frac{\partial f_0}{\partial \underline{R}} - \frac{e}{m_e}\underline{E} \cdot (\frac{\partial f_0}{\partial \underline{v}} + \frac{\partial \underline{R}}{\partial \underline{v}} \cdot \frac{\partial f_0}{\partial \underline{R}})$$

$$+ \Omega_e \frac{\partial}{\partial \alpha}(f_1 + \underline{R} \cdot \frac{\partial f_0}{\partial \underline{R}}) = 0 \quad . \qquad (C.5)$$

From (C.4) we conclude $f_o(R, v_\parallel, v_\perp)$. Since f_1 must be periodic in α, we can eliminate the last term of (C.5) by averaging over α. Noting that

$$- \frac{e}{m_e} \underset{\sim}{E} \cdot \frac{\partial \underset{\sim}{R}}{\partial \underset{\sim}{v}} = \frac{c}{B} \underset{\sim}{E} \times \frac{\partial}{\partial \underset{\sim}{v}} (\underset{\sim}{v} \cdot \underset{\sim}{b}) = \frac{c \underset{\sim}{E} \times \underset{\sim}{b}}{B} \tag{C.6}$$

and

$$\oint d\alpha \; (\underset{\sim}{v}_\perp \cdot \frac{\partial}{\partial \underset{\sim}{R}_\perp}) \equiv 0, \quad \oint d\alpha \; (\underset{\sim}{E}_\perp \cdot \frac{\partial}{\partial \underset{\sim}{v}_\perp}) \equiv 0 \tag{C.7}$$

we find

$$\frac{\partial f_o}{\partial t} + v_\parallel \; \underset{\sim}{b} \cdot \frac{\partial f_o}{\partial \underset{\sim}{R}} + \frac{c \underset{\sim}{E} \times \underset{\sim}{b}}{B} \cdot \frac{\partial f_o}{\partial \underset{\sim}{R}} - \frac{e}{m_e} \underset{\sim}{E} \cdot \underset{\sim}{b} \frac{\partial f_o}{\partial v_\parallel} = 0 \tag{C.8}$$

Identifying the electron position r with R gives Eq. (5.14) of the main text.

APPENDIX D

In this appendix we solve the Vlasov equation (5.29) by the method of characteristics in order to calculate the ion response.[34] Writing the Vlasov equation

$$\frac{df_i}{dt} \equiv \frac{\partial f_i}{\partial t} + \underset{\sim}{v} \cdot \frac{\partial f_i}{\partial \underline{r}} + \underset{\sim}{a} \cdot \frac{\partial f_i}{\partial \underset{\sim}{v}} = 0 \; , \tag{D.1}$$

where

$$\underset{\sim}{a} = \frac{e}{m_i}(\underset{\sim}{E} + \frac{1}{c} \underset{\sim}{v} \times \underset{\sim}{B}) \; , \tag{D.2}$$

we see that the phase space density f_i is constant along the particle trajectories. Thus any function of the constants of motion gives us an equilibrium solution. We choose

$$f_{Mi}(H,P_y) = \frac{n}{\pi^{3/2} v_i^3} \; e^{-H/T_i} \; , \tag{D.3}$$

where in our x-dependent equilibrium the energy and y-component of canonical momentum are the only constants of motion

$$H = \frac{1}{2} m_i v^2 \tag{D.4a}$$

$$P_y = m_i v_y + m_i \Omega_i x \; , \tag{D.4b}$$

where $\Omega_i = eB_o/m_i c$. Note that the x-dependence of n, T_i and $v_i = (2T_i/m_i)^{1/2}$ must be expressed via P_y. In response to potentials

$$\tilde{\phi} \equiv \mathcal{F}[\tilde{\phi}](k_x) = \phi \; e^{i\underset{\sim}{k}\cdot\underset{\sim}{r}-i\omega t} \tag{D.5a}$$

$$\underset{\sim}{\tilde{\psi}} \equiv \mathcal{F}[\underset{\sim}{\tilde{A}}](k_x) = \psi \; e^{i\underset{\sim}{k}\cdot\underset{\sim}{r}-i\omega t} \underset{\sim}{e}_z \tag{D.5b}$$

we find a change $\tilde{F}$ in f_i determined by

$$\frac{d\tilde{F}}{dt} = - \underset{\sim}{\tilde{a}} \cdot \frac{\partial f_{Mi}}{\partial \underset{\sim}{v}} \quad . \tag{D.6}$$

But

$$\frac{\partial f_{Mi}}{\partial \underset{\sim}{v}} = m_i \underset{\sim}{v} \; \frac{\partial f_{Mi}}{\partial H} + m_i \; \frac{\partial f_{Mi}}{\partial P_y} \; \underset{\sim}{e}_y \tag{D.7}$$

and

$$\underset{\sim}{\tilde{a}} = - \frac{e}{m_i} \nabla\tilde{\phi} - \frac{e}{m_i c} \frac{\partial}{\partial t} \underset{\sim}{\tilde{\psi}} + \frac{e}{m_i c}\nabla(\underset{\sim}{v}\cdot\underset{\sim}{\tilde{\psi}}) - \frac{e}{m_i c}(\underset{\sim}{v}\cdot\underset{\sim}{\nabla})\underset{\sim}{\tilde{\psi}} \; , \tag{D.8}$$

so that

$$\frac{d\tilde{F}}{dt} = \frac{\partial f_{Mi}}{\partial H} \; [e \; \frac{d\tilde{\phi}}{dt} - e \; \frac{\partial}{\partial t}(\tilde{\phi} - \frac{1}{c} \; \underset{\sim}{v} \cdot \underset{\sim}{\tilde{\psi}})]$$

$$+ \frac{\partial f_{Mi}}{\partial P_y} \; [\frac{e}{c} \frac{d\tilde{\psi}_y}{dt} + e \; \frac{\partial}{\partial y} \; (\tilde{\phi} - \frac{1}{c} \; \underset{\sim}{v} \cdot \underset{\sim}{\tilde{\psi}})] \tag{D.9}$$

Thus

$$\tilde{F}(t) = [e\tilde{\Phi} + i\omega e(\tilde{\Phi} - \frac{1}{c} \underline{v} \cdot \underline{\tilde{\Psi}})I] \frac{\partial f_{Mi}}{\partial H}$$

$$+ [\frac{e}{c} \tilde{\Psi}_y + ik_y e(\tilde{\Phi} - \frac{1}{c} \underline{v} \cdot \underline{\tilde{\Psi}})I] \frac{\partial f_{Mi}}{\partial P_y} \qquad (D.10)$$

where

$$I = \int_{-\infty}^{t} d\hat{t} \ e^{i\underline{k} \cdot (\hat{\underline{r}} - \underline{r}) - i\omega(\hat{t} - t)} \qquad (D.11)$$

is an integral over the trajectory $\hat{\underline{r}}(\hat{t})$ of the particle which terminates at $\underline{r} = \hat{\underline{r}}(t)$. Since $\rho_i \ll L_s$ we shall neglect the effects of shear on the ion orbits, and take $\underline{v}_\perp \simeq v_x \underline{e}_x + v_y \underline{e}_y$, $v_{||} \simeq v_z$. The main effect of the shear is to introduce an effective $k_{||} = k_y x/L_s$. Also we shall neglect $k_y \sim 1/r_1$ compared to $k_x \sim 1/\delta$. Thus we may write

$$I = \int_{-\infty}^{0} dt \ \exp[\ \frac{ik_x v_x}{\Omega} \sin\Omega t - \frac{ik_x v_y}{\Omega} (\cos\Omega\tau - 1)$$

$$+ ik_{||}v_z t - i\omega t] \ , \qquad (D.12)$$

and noting that

$$\frac{\partial f_{Mi}}{\partial H} = - \frac{1}{T_i} f_{Mi} \ , \quad \frac{\partial f_{Mi}}{\partial P_y} = \frac{1}{m_i \Omega_i} \frac{\partial f_{Mi}}{\partial x} \qquad (D.13)$$

we find

$$\tilde{F}(t) = -\frac{e\tilde{\phi}}{T_i}\left(f_{Mi} + i\omega I f_{Mi} - \frac{ik_y T_i}{m_i \Omega_i} I \frac{\partial f_{Mi}}{\partial x}\right) ,$$

$$+ \frac{e\tilde{\psi}}{T_i}\left(\frac{i\omega}{c} v_z I f_{Mi} - \frac{ik_y T_i}{m_i c\Omega_i} v_z I \frac{\partial f_{Mi}}{\partial x}\right) . \qquad (D.14)$$

The perturbed ion density and parallel current are given by (5.32,33); noting $\tilde{F} = \mathfrak{F}[\tilde{f}]$

$$\mathfrak{F}[\tilde{n}_i] = \langle\tilde{F}\rangle \qquad (D.15a)$$

$$\mathfrak{F}[\tilde{J}_{\|i}] = e \langle v_z \tilde{F}\rangle \qquad (D.15b)$$

where

$$\langle\ldots\rangle \equiv \int d^3v \ (\ldots) \qquad (D.16)$$

Defining $\omega_{*i} = -k_y cT_i/eB_o r_n$, we then have

$$\mathfrak{F}[\tilde{n}_i] = -\frac{e\tilde{\phi}}{T_i}\left[\langle f_{Mi}\rangle + i\omega\langle I f_{Mi}\rangle + i\omega_{*i} r_n \frac{\partial'}{\partial x} \langle I f_{Mi}\rangle\right]$$

$$+ \frac{e\tilde{\psi}}{cT_i}\left[i\omega\langle v_z I f_{Mi}\rangle + i\omega_{*i} r_n \frac{\partial'}{\partial x} \langle v_z I f_{Mi}\rangle\right] \qquad (D.17a)$$

$$\mathfrak{F}[\tilde{J}_{\|i}] = -\frac{e^2\tilde{\phi}}{T_i}\left[\langle v_z f_{Mi}\rangle + i\omega\langle v_z I f_{Mi}\rangle + i\omega_{*i} r_n \frac{\partial'}{\partial x}\langle v_z I f_{Mi}\rangle\right]$$

$$+ \frac{e^2\tilde{\psi}}{cT_i}\left[i\omega\langle v_z^2 I f_{Mi}\rangle + i\omega_{*i} r_n \frac{\partial'}{\partial x} \langle v_z^2 I f_{Mi}\rangle\right] \qquad (D.17b)$$

where the notation $\partial'/\partial x$ reminds us not to differentiate $k_{\parallel}$ (cf. Eq. (D.14)). The velocity integrals may be performed to give

$$\langle f_{Mi} \rangle = n \tag{D.18a}$$

$$\langle If_{Mi} \rangle = n \int_{-\infty}^{0} dt \; \exp\left(b\cos\Omega t - b - \frac{k_{\parallel}^2 v_i^2 t^2}{4} - i\omega t\right) \tag{D.18b}$$

$$\langle v_z If_{Mi} \rangle = nv_i \int_{-\infty}^{0} dt \; \left(\frac{ik_{\parallel} v_i t}{2}\right) \exp\left(b\cos\Omega t - b - \frac{k_{\parallel}^2 v_i^2 t^2}{4} - i\omega t\right)$$

$$\tag{D.18c}$$

$$\langle v_z^2 If_{Mi} \rangle =$$

$$nv_i^2 \int_{-\infty}^{0} dt \left(\frac{1}{2} - \frac{k_{\parallel}^2 v_i^2 t^2}{4}\right) \cdot \exp\left(b\cos\Omega t - b - \frac{k_{\parallel}^2 v_i^2 t^2}{4} - i\omega t\right) \tag{D.18d}$$

where $b = k_x^2 \rho_i^2/2$. Using the identity

$$e^{b\cos\Omega t} = \sum_{\ell = -\infty}^{\infty} I_{\ell}(b) \; e^{i\ell\Omega t}$$

where I_{ℓ} is the ℓth modified Bessel function, and the conven- ient definition of the plasma dispersion function[33],

$$Z(\lambda) = 2ie^{-\lambda^2} \int_{-\infty}^{i\lambda} d\xi \; e^{-\xi^2} \quad , \tag{D.19}$$

the integrals (D.18) may be expressed

$$<If_{Mi}> = - \frac{ine^{-b}}{|k_{\parallel}v_i|} \sum_{\ell=-\infty}^{\infty} I_{\ell}(b) \; Z(\lambda_{\ell}) \qquad \text{(D.20a)}$$

$$<v_z If_{Mi}> = - \frac{inv_i e^{-b}}{|k_{\parallel}v_i|} \sum_{\ell=-\infty}^{\infty} I_{\ell}(b) [1 + \lambda_{\ell} Z(\lambda_{\ell})] \qquad \text{(D.20b)}$$

$$<v_z^2 If_{Mi}> = - \frac{inv_i^2 e^{-b}}{|k_{\parallel}v_i|} \sum_{\ell=-\infty}^{\infty} I_{\ell}(b) [\lambda_{\ell} + \lambda_{\ell}^2 Z(\lambda_{\ell})] \; . \quad \text{(D.20c)}$$

However in the limit $\omega \gg k_{\parallel} v_i$, $\omega \ll \Omega_i$, we have $\lambda_{\ell} \gg 1$ for all ℓ, so that we can approximate

$$<If_{Mi}> \simeq \frac{in}{\omega} e^{-b} I_0(b) \qquad \text{(D.21a)}$$

$$<v_z If_{Mi}> \simeq <If_{Mi}> \frac{k_{\parallel} v_i^2}{2\omega} \qquad \text{(D.21b)}$$

$$<v_z^2 If_{Mi}> \simeq <If_{Mi}> \frac{v_i^2}{2} \; . \qquad \text{(D.21c)}$$

Recalling that $dI_0/db = I_1(b)$, and defining $S_{\ell}(b) = e^{-b} I_{\ell}(b)$, we find for the derivatives

$$\frac{\partial'}{\partial x} <If_{Mi}> = - \frac{in}{\omega r_n} [S_0 + \eta_i b(S_1 - S_0)] \qquad \text{(D.22a)}$$

$$\frac{\partial'}{\partial x} <v_z If_{Mi}> = \frac{k_{\parallel} v_i^2}{2\omega} \left(\frac{\partial'}{\partial x} <If_{Mi}> - \frac{\eta_i}{r_n} <If_{Mi}> \right) \qquad \text{(D.22b)}$$

$$\frac{\partial'}{\partial x} <v_z^2 If_{Mi}> = \frac{v_i^2}{2} \left(\frac{\partial'}{\partial x} <If_{Mi}> - \frac{\eta_i}{r_n} <If_{Mi}> \right) , \qquad (D.22c)$$

where $\eta_i = d\ell n T_i / d\ell nn$. Inserting (D.21,22) into (D.17) and identifying k_x with k then gives the result (5.36,37) quoted in the text.

VITA

The author was born in Glen Ridge, NJ, in 1956, and raised in Brookside, NJ. After graduating from W.M. Mendham H.S. as valedictorian of the class of 1974, he attended Dartmouth College in Hanover, NH, where he double-majored in Physics and Mathematics. His research under Prof. John E. Walsh led to an honors thesis "Stimulated backscattering from relativistic electron beam in a dielectric medium." In June, 1978, he received his A.B. from Dartmouth, summa cum laude. The author was a National Science Foundation Graduate Fellow for 1979-1982 while studying physics at M.I.T. He received his PhD from M.I.T. in 1983 in the field of plasma physics.